(2)

POR-2040(EX)
(WT-2040)(EX)
EXTRACTED VERSION

OPERATION DOMINIC, FISH BOWL SERIES

Project Officer's Report—Project 9.1a

Atmospheric Properties

K. S. W. Champion, Project Officer
A. C. Faire
Air Force Cambridge Research Laboratories
L. G. Hanscom Field
Bedford, MA

26 March 1965

NOTICE:

This is an extract of POR-2040 (WT-2040), Operation DOMINIC, Fish Bowl Series, Project 9.1a.

Extracted version prepared for
Director
DEFENSE NUCLEAR AGENCY
Washington, DC 20305-1000

1 September 1985

UNCLASSIFIED
SECURITY CLASSIFICATION OF THIS PAGE

AD-A995430

REPORT DOCUMENTATION PAGE

1a. REPORT SECURITY CLASSIFICATION UNCLASSIFIED	1b. RESTRICTIVE MARKINGS
2a. SECURITY CLASSIFICATION AUTHORITY	3. DISTRIBUTION / AVAILABILITY OF REPORT Approved for public release; distribution is unlimited.
2b. DECLASSIFICATION / DOWNGRADING SCHEDULE	
4. PERFORMING ORGANIZATION REPORT NUMBER(S)	5. MONITORING ORGANIZATION REPORT NUMBER(S) POR-2040 (EX) (WT-2040) (EX)
6a. NAME OF PERFORMING ORGANIZATION Air Force Cambridge Research Laboratories 6b. OFFICE SYMBOL (If applicable)	7a. NAME OF MONITORING ORGANIZATION Defense Atomic Support Agency
6c. ADDRESS (City, State, and ZIP Code) Bedford, MA	7b. ADDRESS (City, State, and ZIP Code) Washington, DC
8a. NAME OF FUNDING / SPONSORING ORGANIZATION 8b. OFFICE SYMBOL (If applicable)	9. PROCUREMENT INSTRUMENT IDENTIFICATION NUMBER
8c. ADDRESS (City, State, and ZIP Code)	10. SOURCE OF FUNDING NUMBERS PROGRAM ELEMENT NO. / PROJECT NO. / TASK NO. / WORK UNIT ACCESSION NO.

11. TITLE (Include Security Classification) OPERATION DOMINIC, FISH BOWL SERIES; PROJECT OFFICER'S REPORT - PROJECT 9.1a - Atmospheric Properties, Extracted Version

12. PERSONAL AUTHOR(S)
K.S.W. Champion and A. C. Faire

13a. TYPE OF REPORT	13b. TIME COVERED FROM ____ TO ____	14. DATE OF REPORT (Year, Month, Day)	15. PAGE COUNT
		650326	256

16. SUPPLEMENTARY NOTATION This report has had sensitive military information removed in order to provide an unclassified version for unlimited distribution. The work was performed by the Defense Nuclear Agency in support of the DoD Nuclear Test Personnel Review Program.

17. COSATI CODES			18. SUBJECT TERMS (Continue on reverse if necessary and identify by block number)
FIELD	GROUP	SUB-GROUP	
18	3		Dominic
4	1		Fish Bowl
			Atmospheric Properties

19 ABSTRACT (Continue on reverse if necessary and identify by block number)

The first experimental objective in support of the Fish Bowl Series was to make accurate measurements of the physical properties of the normal atmosphere (1) to provide information required for an accurate analysis of blast and shock wave data, (2) to provide density data permitting a more precise determination of the Thor reentry trajectory and (3) to provide data required for accurate determination of the functional relationship between the ionization produced by the detonation and the radiation that produced it.

The second objective was to make measurements shortly after each nuclear detonation to measure heating and changes in atmospheric density and pressure in the vicinity of the fireball.

20. DISTRIBUTION / AVAILABILITY OF ABSTRACT	21. ABSTRACT SECURITY CLASSIFICATION
☒ UNCLASSIFIED/UNLIMITED ☐ SAME AS RPT. ☐ DTIC USERS	UNCLASSIFIED

22a. NAME OF RESPONSIBLE INDIVIDUAL	22b. TELEPHONE (Include Area Code)	22c. OFFICE SYMBOL
MARK D. FLOHR	202-325-7559	DNA/ISCM

DD FORM 1473, 84 MAR 83 APR edition may be used until exhausted. All other editions are obsolete.

SECURITY CLASSIFICATION OF THIS PAGE
UNCLASSIFIED

FOREWORD

Classified material has been removed in order to make the information available on an unclassified, open publication basis, to any interested parties. The effort to declassify this report has been accomplished specifically to support the Department of Defense Nuclear Test Personnel Review (NTPR) Program. The objective is to facilitate studies of the low levels of radiation received by some individuals during the atmospheric nuclear test program by making as much information as possible available to all interested parties.

The material which has been deleted is either currently classified as Restricted Data or Formerly Restricted Data under the provisions of the Atomic Energy Act of 1954 (as amended), or is National Security Information, or has been determined to be critical military information which could reveal system or equipment vulnerabilities and is, therefore, not appropriate for open publication.

The Defense Nuclear Agency (DNA) believes that though all classified material has been deleted, the report accurately portrays the contents of the original. DNA also believes that the deleted material is of little or no significance to studies into the amounts, or types, of radiation received by any individuals during the atmospheric nuclear test program.

OPERATION DOMINIC

FISH BOWL SERIES

PROJECT OFFICERS REPORT—PROJECT 9.1a

ATMOSPHERIC PROPERTIES

K.S.W. Champion, Project Officer
A.C. Faire

Air Force Cambridge Research
Laboratories
L.G. Hanscom Field
Bedford, Massachusetts

ABSTRACT

Atmospheric density profiles were measured on nine occasions during the Fish Bowl Series. Five of these measurements were of the normal atmosphere, at different times of day and seasons, and four were made following nuclear detonations. The measurements of the normal atmosphere were made at different times so that accurate information would be available on diurnal and other variations. This data was obtained: (1) to provide information for an accurate analysis of blast and shock wave data, (2) to provide density data that would permit a more precise determination of the Thor re-entry trajectory for Blue Gill and, (3) to provide data so that the ionization produced by a test can be accurately related to the radiation that produces it.

The technique used was to eject a sphere, instrumented with an accelerometer and telemetry transmitter, from the second stage of a Nike-Cajun rocket. The sphere was tracked by a ground station, and the recorded data gave drag acceleration as a function of time of flight. This yielded density, and with the use of additional theory, temperature and pressure were deduced. Excellent data was obtained from all rockets, and except in one case, it corresponded to altitudes between 30 and 110 km. The back-

ground data is in general agreement with the available models, but there are some important differences. In addition, it will make it possible to extend the present Tropical Atmosphere model from 90 to 110 km.

The measurements after the nuclear detonations were made to measure heating of the atmosphere and related pressure and density changes produced by the fireball. Rockets were launched at H + 10 minutes on Check Mate, H + 15 minutes on Blue Gill Triple Prime, H + 10 minutes on King Fish, and H + 4 minutes on Tight Rope. Pressure and density changes as large as 50 percent from normal were recorded. Maximum temperature increase observed was 40 degrees C., except following Tight Rope when the increase (relatively close to the fireball) may have been more than 300 degrees C.

PREFACE

The authors wish to state their gratitude to the personnel and organizations who made possible the success of all nine Falling Sphere payloads flown during the Fish Bowl Series. Special mention is due to the following for their dedicated assistance in developing and fabricating the payloads: Professor O.C. Haycock, Mr. E. Pound, and Professor R. Woolley of the University of Utah, Salt Lake City; Messrs. R.B.E. Moren, E. Murphy, and J. Gundal of Wentworth Institute, Boston; Mr. N. Smith of the AFCRL Machine Shop; Messrs. J. Bickford and H. Nelson, Raymond Engineering Laboratory, Middletown, Conn.; Mr. R.D. Mitchell, University of Oklahoma, Stillwater, Okla.; and Mr. Malcolm Beggs, Aero Geo Astro Corp., Alexandria, Va. Appreciation is also expressed for excellent field support services rendered by other members of the University of Utah team.

Sincere appreciation for valuable assistance in the preparation of reports and data reduction is expressed to Mrs. O.M. Harris, AFCRL; Miss R. Almasian, Tyco Inc., Waltham, Mass; and Miss C. Aharonian and Mr. R. Johnson, Wentworth Institute.

CONTENTS

TABLES

FIGURES

CHAPTER 1

INTRODUCTION

1.1 OBJECTIVES

The Falling Sphere experiment was used to determine profiles of ambient air density within the range 20 to 110 km. Pressure and temperature as a function of altitude have been deduced from the density data.

The first experimental objective in support of the Fish Bowl Series was to make accurate measurements of the physical properties of the normal atmosphere (1) to provide information required for an accurate analysis of blast and shock wave data, (2) to provide density data permitting a more precise determination of the Thor re-entry trajectory and, (3) to provide data required for accurate determination of the functional relationship between the ionization produced by the detonation and the radiation that produced it.

The second objective was to make measurements shortly after each nuclear detonation to measure heating and changes in atmospheric density and pressure in the vicinity of the fireball. This data is not only of interest as an effect due to the detonation, but is also necessary to analyze accurately data

obtained by several other projects.

1.2 BACKGROUND

For several reasons it is desirable to measure the physical properties of the upper atmosphere before and after high-altitude nuclear tests. Alphatron and other ionization gauges are not suitable, since the radiation and resulting ionization from the detonation and debris would invalidate their readings. The Falling Sphere is not affected by radiation or increased ionization and is an ideal instrument to use under these conditions. One of the applications of the data obtained with the Falling Sphere is to relate radiation fluxes to ionization produced. This will make it possible to determine whether the test data is consistent with theoretical calculations based, in part, on laboratory ionization measurements.

Details of the theory of operation, earlier development and results of previous firings are contained in References 1, 2, 3, 4, 5, and 6.

In the Falling Sphere experiment, air density is calculated from the equation for aerodynamic drag applied to a free-falling

7-inch rigid aluminum sphere containing a transit-time accelerometer with omni-directional characteristics. The sphere contains its own telemetry system and is ejected from a Nike-Cajun rocket at an altitude of about 60 km during the up-leg portion of the trajectory. It continues in a trajectory similar to that of the rocket and reaches a peak altitude of approximately 150 km. The accelerometer commences operation on ejection from the rocket and measures the atmospheric drag on the sphere until the drag reaches the lower limit of sensitivity of the instrument, which is about 10^{-4}g. This generally occurs between an altitude of 105 and 110 km. On the downleg of the flight, measurements begin again at the same altitude and continue through the large decelerations encountered in the reentry region.

The telemetered drag acceleration data is used primarily to calculate atmospheric density. However, to make this data meaningful, the sphere trajectory must be accurately known. By successive integration of the acceleration data, the velocity and trajectory can be determined. As a result of the fact that the acceleration is not measured throughout the flight it is necessary to have accurate position data on the sphere at one instant during its flight (e.g., at the peak of the trajectory). This has

to be supplied by radar or other tracking system.

The original instrumentation developed by the University of Michigan for the Air Force Cambridge Research Laboratories (AFCRL) had several limitations. During the past four years the in-house effort of the Upper Atmosphere Physics Laboratory, AFCRL, with its associated contractors, has been directed toward minimizing these limitations by (1) extending the useful range of the system, (2) increasing accuracy and reliability, and (3) developing a relatively inexpensive system that may be adapted for use in synoptic measurements. Among other benefits, the effort has resulted in the development of more sensitive accelerometers, also based on the time-of-flight principle. These accelerometers operated without failure during the Fish Bowl Series.

During Fish Bowl, nine rockets were fired containing Falling Sphere instrumentation to measure the properties of the upper atmosphere. Eight of these flights used accelerometers of Type I, described in Section 2.2.2 of this report. On the last flight (Rocket 9 on Tight Rope) a new accelerometer (Type II) with promise of a still greater dynamic range was used. This new instrument was designed and developed by the Upper Air Research Laboratory, University of Utah, Salt Lake City, Utah,

(principal support contractor to AFCRL on Project 9.1A). Although the new accelerometer was a pilot model, it performed successfully and is also described in Section 2.2.2.

1.3 THEORY

The forces acting on a free-falling sphere are gravitational attraction and atmospheric drag. By the proper choice of measurement reference system the drag force can be made the significant parameter of interest.

The drag force, $F_D = \frac{1}{2} C_D A V^2 \rho$ (1.1)

where,

C_D = drag coefficient (dimensionless)

A = sphere cross-sectional area (cm^2)

V = sphere velocity (cm/sec)

ρ = air density (gm/cm^3)

But, $F_D = m a_D$

where,

m = mass of sphere (gm)

a_D = drag acceleration of sphere (cm/sec^2)

Therefore,

$$\rho = \frac{2 m a_D}{A V^2 C_D} \qquad (1.2)$$

which is the familiar equation of aerodynamic drag for a free-falling sphere with air density expressed explicitly. The mass-to-area ratio of the sphere is a known constant, and C_D varies slowly as a function of Mach and Reynolds numbers in the measurement environment. Drag acceleration is calculated from $a_D = \frac{2s}{\tau^2}$, where τ is the accelerometer transit time and s is the displacement, in any direction, between accelerometer bobbin and cavity at the beginning of a transit-time measurement.

Using sphere data alone, changes in velocity can be obtained by integrating the total acceleration, which is the vector sum of g, the acceleration due to gravity, and a_D, the sphere drag acceleration. In general, some assumptions have to be made or additional data used in order to obtain the sphere trajectory. For example, the horizontal component of velocity must be determined by radar measurement or estimated from previous flight data. If desired, the error in these values can be made smaller through reiterative processes.

To calculate temperature the hydrostatic equation and the equation of state for a perfect gas are combined. An expression is obtained that may be used to determine temperature in an

altitude range of measured densities based upon an assumed value of temperature at one end of the altitude range. This is shown in the following:

$$dp = -\rho g \, dh \tag{1.3}$$

$$p = \rho \frac{R}{M} T \tag{1.4}$$

$$p_o = \rho_o \frac{R}{M} T_o \tag{1.5}$$

$$p - p_o = -\int_{h_o}^{h} g\rho \, dh \tag{1.6}$$

where,

p = atmospheric pressure at altitude h

p_o = atmospheric pressure at altitude h_o

g = acceleration due to gravity (a function of altitude)

R = universal gas constant

M = mean molecular weight for air

T = temperature at altitude h

T_o = temperature at altitude h_o

The above equations can be combined to obtain

$$T = - \frac{\int_{h_o}^{h} g\rho \, dh}{\rho R/M} + \frac{\rho_o \, T_o}{\rho} \tag{1.7}$$

To determine T, a value must be assumed for T_o. Fortunately,

as the interval $h - h_o$ becomes large, the first term dominates, and any error in T due to inaccuracy in T_o becomes negligible. For example, with an altitude interval of 15 km the first term is about ten times the magnitude of the second term.

The pressure P is then obtained from ρ and T using Equation 1.4 .

CHAPTER 2

PROCEDURE

2.1 SHOT PARTICIPATION

Nine Falling Sphere probe experiments were flown in support of the Fish Bowl Series. All of these flights were successful, and excellent data was obtained. The original plan called for three experimental probes; one each to be launched before Blue Gill and Star Fish, and another to be launched following the Blue Gill nuclear detonation. Due to failures of several of the nuclear tests, the schedule had to be revised to include the use of additional payloads.

During the first part of Fish Bowl, four Falling Sphere rockets were fired. Data was obtained on flights launched on 1 June, 19 June, 8 July (preceding Star Fish), and 23 July 1962, thereby providing a series of desired measurements on the normal atmosphere. Since the measurements were made at different times during the afternoon and night, it is possible to study diurnal variations of atmospheric properties.

Shot participation during the second part of the series was focussed upon obtaining detonation results on the events described in Table 2.1. Five Falling Sphere rockets were launched

during the second part of Fish Bowl. One rocket was fired to measure the properties of the normal atmosphere so that the results could be compared with those of the previous firings. Although the statistical basis is limited, this one measurement may give an indication of the seasonal variation of atmospheric properties. In addition, four rockets were fired at times ranging from 4 to 15 minutes following each successful nuclear detonation to determine if significant changes occurred in the physical properties of the atmosphere near the region traversed by the nuclear fireball. These launch times, referred to H = 0, are listed below:

EVENT	LAUNCH TIME
CHECK MATE	H + 10 minutes
BLUE GILL Triple Prime	H + 15 minutes
KING FISH	H + 10 minutes
TIGHT ROPE	H + 4 minutes

2.2 INSTRUMENTATION (AIRBORNE)

The major components of the Falling Sphere airborne instrumentation consisted of, (1) a 7-inch rigid sphere containing a transit-time accelerometer with associated electronics for telemetry, (2) timing and ejection mechanism for deploying the

sphere at the appropriate altitude during flight, and (3) a C-band beacon for obtaining radar tracking data.

Each of the first four payloads flown was equipped with a radar beacon. During the planning stages of the latter portion of the series, it was not possible to determine in advance whether radar support would be in the form of passive tracking or beacon interrogation. This was due to tracking problems which occurred during the first part of the series. Therefore, the last five payloads were designed so that they could be flown with or without radar beacons. Further discussion of beacon equipment and radar tracking support will be presented in Sections 2.2.6 and 2.4.2 of this report.

The accelerometers used in the first eight firings (Type I) were fabricated from a basic design developed jointly by AFCRL, Raymond Engineering Laboratory, Inc., Middletown, Conn., (Reference 7), and the University of Utah, Salt Lake City, Utah (Reference 6). The flight instruments were supplied by Raymond Engineering Laboratory. On the last event of the series (Tight Rope), a new accelerometer (Type II) with improved performance characteristics was flown with successful results. This prototype instrument was developed and fabricated

by the University of Utah for the purpose of extending the measurement capability of the accelerometer in the high drag acceleration region.

2.2.1 Sphere. The 7-inch diameter of the sphere was not an arbitrary choice, but was mutually determined by the dimensions of the Cajun rocket and the accelerometer. The sphere was machined in three sections from solid bar aluminum alloy (Alcoa 7075 - T4). It contained all instrumentation necessary to telemeter sphere drag data to ground-based telemetry stations. The center section served as a mounting base for all components. Two end caps were used as covers to complete the spherical geometry.

The sphere instrumentation may be divided into three categories: (1) a time-of-flight accelerometer with omni-directional sensitivity; (2) electronic timing, circuitry, and power supply; and (3) telemetry transmitter and antenna. The photograph in Figure 2.1 shows three views of the sphere. In the left position the top cover is removed to show the placement of parts. The semi-circular insulating barrier in the foreground is placed over the battery terminals to prevent short-circuiting when the sphere cover is assembled. One end of the accelerometer can

be seen projecting through the center of the mounting plate. The remaining components consist of power transistors, timing module, and inter-connecting cables.

The center view shows the sphere completely assembled with both covers in place. The white strip along the center section is a Teflon fairing that is used to cover the slot antenna and to minimize surface discontinuities. This material is transparent to radio-frequency radiation at 730 Mc. The bottom cover is removed from the sphere shown on the right side of the photograph. The opposite end of the accelerometer can be seen projecting axially through the center of the mounting base. The transmitter is housed in two shielded sections located in the upper half of the base plate. It is coupled to the antenna by means of a coaxial cable which has a characteristic impedance of 50 ohms. Modular construction was employed throughout to facilitate assembly, wiring, testing,and servicing. Formerly, the sphere covers had been secured to the center section by means of machine screws threaded into each end of the accelerometer. This method produced mechanical stresses on both the accelerometer and the sphere. A study of the problem revealed that these forces were great enough to alter the accelerometer calibration and also

cause distortion of the sphere. A new method was developed for assembly of the covers that eliminated both undesirable features of the earlier design. This resulted in the covers being attached to the center section by means of interrupted threads around their edges. The accelerometer was mounted on the base plate of the center section and was, therefore, independent of the sphere covers.

The absence of mechanical stresses on the sphere covers provided improved sphericity which made it possible to obtain more accurate final balance of the sphere. This was a significant contribution, since accelerometer sensitivity and accuracy would be limited at high altitudes by centrifugal acceleration if the bobbin was mounted off-center and the sphere was spinning. In order to make centrifugal acceleration negligible, it was necessary to locate the center of gravity of the sphere within two or three thousandths of an inch of the common geometrical centers of the sphere and the centered bobbin. This was accomplished by floating the sphere in a liquid having nearly twice its density (tetrabromoethane) and observing the period of rotation due to unbalanced masses. By proper placement of lead masses within the sphere, a coarse balance was obtained after all of the com-

ponents were assembled. The final balance was obtained after the flight batteries were installed and all other tests had been completed. The use of Yardney PM-1 Silvercells also made possible a refinement in sphere-balancing technique. These cells were similar to the Yardney HR-1 in both physical size and electrical characteristics, but in addition they contained a felt insert that absorbed residual electrolyte. This reduced the number of multiple balance points which had been due to shifting of the excess electrolyte within the cells as the sphere was rotated.

A jig was used to maintain sphere orientation during the final assembly while the covers were firmly screwed into position by means of strap wrenches. In order to prevent voltage breakdown of electronic components at high altitudes, atmospheric pressure was maintained in the sphere through the use of O-ring seals. During pre-flight tests, the sphere was pressurized to 15 pounds through a removable pneumatic valve equipped with a pressure guage. The leak rate was then observed to determine whether atmospheric pressure could be maintained in the sphere for the duration of the flight.

Another result of instrumentation redesign worthy of

mention was a 24% reduction in weight of the assembled sphere. This made possible a 24% increase in the sensitivity of the drag acceleration measurement, provided the values of other parameters in the drag equation remained unchanged. The average value of sphere flight times observed during Fish Bowl was approximately 20% longer than the average of those previously reported for the earlier sphere. This was due mainly to the difference in cross-sectional area to mass ratio.

2.2.2 Omni-directional Accelerometer. In order to measure the drag force imposed upon the sphere during its trajectory irrespective of its orientation, it was necessary to use an omni-directional accelerometer. In the so-called transit-time accelerometer, simple spherical geometry was employed in the sensing element to achieve this objective. A precision-ground spherical ball (the bobbin or reference mass) was placed in a spherical cavity located at the center of the accelerometer. The walls of the cavity were covered with a switching matrix which will be described in more detail later in the text. The bobbin could be positioned in the exact center of the cavity by means of four hydraulically actuated locating or centering pins. The hydraulic forces were generated by the action of two solenoid

armatures, one at each end of the accelerometer. The motion of the armatures toward the center of the accelerometer produced compression of a pair of bellows located at opposite ends of the hydraulic line. A cutaway drawing of the accelerometer is shown in Figure 2.2. Some of the components are shown in greater detail in the schematic view of the accelerometer shown in Figure 2.3.

Initial velocity imparted to the bobbin upon release is a source of error in the measurement,and its contribution becomes serious at high altitudes where the drag acceleration is low. Therefore, considerable effort was spent in developing an accelerometer design that would reduce this problem to a minimum. In order to accomplish this each solenoid and its associated armature was connected to all four centering pins through a suitable hydraulic circuit,which is shown in the schematic drawing of Figure 2.4. A centering pin and bellows were located at each point designated "P" in the drawing. The contact surfaces of the centering pins lay on a sphere having a diameter slightly larger than that of the bobbin,in order to provide unobstructed release. Initial velocity could not be imparted to the bobbin except in the case of a sticking pin. As a result of this arrangement all

centering pins experienced hydraulic forces simultaneously and, therefore, moved at the same time. This design was an improvement over the original transit-time accelerometer in which two centering fingers were actuated by different solenoids which could react at different times.

The matrix switch lining the cavity walls of the accelerometer was the key element in the instrument design. It was formed in two halves to match the surfaces of the two hemispherical metal cavities. The first step in the fabrication consisted of forming a screen woven with No. 40 guage insulated magnet wire, 100 wires/inch, both in weft and warp. In the so-called two-over-two basket-weave design employed, each wire in the screen, shown in the top view of Figure 2.5, really consisted of two parallel wires. The objective of this method was to maintain reliability in the event that one wire was damaged during the required sizing operations which will be discussed below. If one of the parallel wires was broken at a joint, there would have been another wire along side it to maintain electrical conductivity.

The construction of the two halves of the accelerometer cavity is identical; therefore, the following description applies to

both. A bead of solder was run around the periphery of the blank screen. This bonded the loose ends together and provided the rigid support necessary for subsequent operations. The solder bead also made all wires of the screen electrically common. The next step was to form the screen into a hemisphere by means of drawing dies. It was then bonded to the surface of a metal hemishperical cavity. The high point of each joint of the screen was stripped of insulation and potting compound. The Stripese insulation used was easily vaporized by the heat of a soldering iron, while excess potting compound was removed by lapping the screen with a precision-ground sizing tool. This operation also produced the desired sphericity.

The remaining task was to connect all of the weft wires together, and likewise, all of the warp wires in order to form the two switch terminals. To separate the weft from the warp wires, small notches were cut in the four corners of the formed screen as illustrated in the lower left (before cutting) and lower right (after cutting) of Figure 2.5. With the weft of the screen connected to one side of the circuit and the warp to the other, switch closure resulted when the bobbin fell on any two adjacent bared high spots. The operation of the matrix switch may

be further clarified by referring to the top illustration of Figure 2.5.

Partial assembly of an accelerometer cavity section is shown in Figure 2.6. Final operations to be performed on this piece included bonding, lapping, gold plating, and connecting leads. As previously noted, two such hemispherical sections formed a complete cavity assembly.

Initially, both the matrix switch and bobbin were gold plated to insure high electrical conductivity when the bobbin made contact with the cavity wall. However, some difficulty was experienced with short-circuiting of the screen due to flaking of plating material. Originally, it was believed that the bobbin was the source of this problem. Consequently, rhodium-plated bobbins were substituted for the gold-plated one, but this failed to provide a complete solution. It was concluded that some of the flaking originated within the matrix switch itself. Steps have been taken to correct this situation in the future. As a result of rigorous pre-flight testing and remedial action, this problem caused no degradation of the flight results.

In operation, an electrical pulse of approximately 200-millisecond duration was delivered to both solenoids, thus actuating

the four centering pins. These pins centered the bobbin so that the displacement between bobbin and cavity was approximately 0.062 inch. The average deviation from this value, measured in any direction, was ± 0.001 inch. At the end of the centering pulse, the solenoids relaxed to their rest positions. Small springs located under the head of each centering pin caused them to be simultaneously retracted with great force. This action released the bobbin, allowing it to free-fall to the wall of the cavity. Coincident with bobbin release, a 20-microsecond pulse was generated and transmitted to the ground stations. Its characteristic width identified it as the start-pulse of an interval that provided a measure of time required for the bobbin to traverse the fixed fall distance of 0.062 inch. At bobbin impact the matrix switch was closed, thus signaling the end of the transit-time. Coincident with impact time, a 10-microsecond pulse was generated and transmitted to the ground stations to complete an accelerometer transit-time measurement. At a finite time following bobbin impact, the accelerometer cycle was repeated.

Measurements made by the Type I accelerometer were in the range from 4×10^{-5} to 4 g with an error of approximately 1.0%.

Although this operating range was suitable for the flights made during the Fish Bowl Series, it was considered desirable to extend the measurement capability of the instrument to 10 g in the high drag acceleration region. The Type II accelerometer was developed to achieve this objective.

The principal modification consisted of eliminating the low efficiency hydraulic actuator and substituting in its place an electromagnetic drive system similar to the voice coil arrangement of a conventional loudspeaker. The magnetic drive force was applied directly to the centering pins by means of a pair of cylindrical fingers, each terminated with two diverging prongs. When the associated solenoids were energized by an electrical pulse, the direction of current flow in each coil was such that the fingers were driven rapidly toward the center of the accelerometer. At the end of their travel, each pair of diverging prongs forcefully engaged the centering pins (similar to those of Type I accelerometer), thereby causing the bobbin to be centered.

When tested on a centrifuge this new instrument measured accelerations up to 10 g with the desired accuracy. However, because of second-stage failure on Rocket 9 (Tight Rope), performance data obtained on the Type II accelerometer was limited.

The sphere did not attain sufficient altitude to enter the region of low drag acceleration; also, the maximum drag acceleration it experienced during the flight was only 1.5 g. The experimental results obtained were nevertheless very interesting and will be discussed in Chapter 3.

The recycling programs of the accelerometers of Types I and II were such that in the high drag region of the atmosphere, which was near 30 km on the downleg portion of the sphere trajectory, it was possible to obtain approximately three transit-time measurements per second. However, in the region of low drag, near zenith altitude, a single transit-time measurement sometimes exceeded two seconds. This feature of variable recycle time removed one of the experimental restrictions imposed by earlier instrumentation. Previously, the accelerometer had been periodically cycled by a motor-driven eccentric cam which permitted only one measurement per second, even when the transit-times were as short as 15 milliseconds. At altitudes where the transit-time exceeded 800 milliseconds, no data was obtained, because the bobbin was recentered before it completed its fall.

The transit-time measurements obtained from the accelerometer and associated circuitry consituted the raw experimental data. This data was obtained as a function of elapsed time from

rocket launch. Sphere drag acceleration, which is proportional to the inverse square of transit-time, was obtained from a simple calculation.

2.2.3 Sphere Electronics and Operation. A physical description of the sphere and accelerometer has been presented in Sections 2.2.1 and 2.2.2. The operational principles of the sphere electronics are illustrated by the functional block diagram and schematic drawing of Figure 2.7. In the simplified drawing of the accelerometer, the two centering pins shown actually represent two pairs of pins, one at the top and one at the bottom of the 1-inch bobbin. The pins forming the top pair are electrically connected to each other, but they are insulated from the bottom pair except when both sets touch the bobbin. This connection through the bobbin was used to determine release time as explained below. Also shown in the block diagram is a circular segment on each side of the bobbin. Each segment represents a portion of the two-terminal matrix switch previously described. The bobbin, on making contact with two screen wires at the end of its fall, short-circuited a low dc voltage that was applied between the two sets of wires which formed the matrix switch. In this manner an impact signal was produced. The timing multi-

vibrator provided a signal that was amplified and fed to the magnetic drive transistor (designated as driver in the block diagram). This energized the coils and caused the bobbin to be centered in its spherical cavity. The cycle was repeated with the bobbin being alternately centered and released.

The cycle of operation can readily be understood when the experimental requirements that determined it are presented. In order to obtain the maximum amount of experimental data on a given flight the following conditions were imposed on the electronic control circuitry; (1) the bobbin should not be re-centered until sufficient time had been allowed for it to complete its fall and make contact with the cavity switch, (2) the bobbin should be re-centered immediately after making contact, except when the fall time was equal to or less than 0.3 sec., (3) a short delay should occur before re-centering if the bobbin transit-time was less than 0.3 sec., and (4) re-centering should be accomplished after a reasonable time (2.5 sec., in this case) in the event the bobbin failed to make good contact with the matrix switch. The first of these conditions was met by a hold-off diode in the flip-flop circuit, the second by sending the impact signal to the flip-flop which in turn initiated the timing multivibrator. The third condition was

provided for by a choice of time constant in the timing multivibrator, and the fourth by an over-ride circuit.

For the sake of simplicity some details of circuit description have been omitted in previous discussions. Thus far, we have mentioned only one pulse that was propagated at the time of bobbin release. Actually, two release signals were used to determine the bobbin time-of-fall. One was taken from the control signal to the magnetic drive transistor and preceded the actual time of release by approximately 0.4 millisecond. However, this time did not remain constant throughout the sphere flight. The other signal was obtained by breaking a circuit as the centering pins separated from the bobbin. The former was used for timing the fall when it was large compared to 1 millisecond. The initial release and bobbin impact signals were fed, via the flip-flop circuit, to the modulator where, by means of delay lines, they produced a 20-microsecond pulse corresponding to bobbin release and a 10-microsecond pulse corresponding to bobbin impact, respectively. A second release signal was produced when contact between pins and bobbin was broken. This signal was fed to the modulator where it produced a 30-microsecond pulse which was also propagated to ground-based stations. This pulse

made it possible to correct the time-of-fall for every measurement obtained during a flight, thereby increasing the accuracy of the experiment. Although the pulse waveform was not rectangular, it had a steep leading edge that made it useful for triggering timing equipment used to obtain time-of-fall corrections when the data was being reduced.

A fourth signal was produced in the modulator and will be referred to as the sub-modulator pulse. This pulse had a width of about 5 microseconds and a repetition frequency of approximately 65 to 125 pulses/second. The repetition rate was made to vary as a function of temperature by including a thermistor as part of the resistance-capacitance circuit in the free-running blocking oscillator that produced the 5-microsecond pulses. This provided a measure of the internal temperature of the sphere during flight. The sub-modulator pulse was also transmitted to the ground stations and, when demodulated, produced an audible signal that assisted in tracking the sphere. The data obtained on the internal temperature of the sphere will be used by the Univ. of Utah to advance the development of sphere electronics.

2.2.4 Circuit Description. The timing of the bobbin release and pickup was accomplished by the timer module which consisted

primarily of two multivibrators. The circuit diagram is shown in Figure 2.8. The multivibrator, made up of transistors Q_1 and Q_2, was basically a monostable or one-shot configuration; however, it was made free-running by a gate signal from the bi-stable multivibrator, Q_4 and Q_5. The signal from the collector of Q_1 was amplified by Q_3 and sent to the base of the magnetic drive transistor, Q_7, as shown in Figure 2.9. The collector current of Q_7 passed through the accelerometer coils, L_3 and L_4 (Figure 2.9) and caused the bobbin to be centered whenever Q_7 was in the conducting stage. The release of the bobbin by the centering pins occurred when the cut-off transistor Q_1 started to conduct. The amplified release signal from the collector of Q_3 was applied not only to the magnetic drive circuit but also back through connector PL-1, pin 3, to the base of Q_4 causing it to conduct. The effect of this action was to reduce Q_1 and Q_2 to a one-shot multivibrator as long as Q_4 was conducting.

The discussion immediately following assumes the fall time of the bobbin to be in excess of 0.3 sec. The second case, for fall times equal to or less than 0.3 sec., will be treated later. As shown by the schematic diagram of Figure 2.8, the released bobbin on making contact with the matrix switch raised the

potential of the base Q_5, thereby turning off Q_4. This raised the potential of the base of Q_2 causing it to conduct. After the switching time of the multivibrator, the cycle was repeated. The release command was fed from the collector of Q_4 to the modulator which is shown in Figure 2.10. Here a 20-microsecond pulse was formed by the pulse forming network (PFN), L_1. The contact signal was fed from the collector of Q_5 to the modulator where a 10-microsecond pulse was produced by PFN, L_2. These two pulses were diode mixed and fed to the base of Q_9. After amplification they controlled the modulator transistors Q_{10} and Q_{11}. The output of the modulator transistor was stepped up through transformer T_1 to plate modulate the transmitter.

For the case of fall times equal to or less than 0.3 sec., the time constant in the base of Q_2 held off the transistor for the minimum time of 0.3 sec.

If the fall time was greater than 2.5 sec., or if proper contact was not made in this time interval, the override circuit started a new cycle. The time constant in the base of Q_6 caused it to conduct, sending a signal to the base of Q_5 to initiate a new cycle.

The transmitter, Figure 2.11, is a 730-Mc, 15-watt peak pulse power transmitter that was modulated by the appropriate pulses described above. The oscillator, V_1, operated at 365 Mc with V_2 serving as a buffer and frequency doubler stage. Tube V_3 operated as a grounded grid power amplifier.

The antenna was a slot cut into the sphere and filled with a Rexolite dielectric. A Teflon cover was used as a fairing to smooth out surface discontinuities on the sphere. Impedence match was obtained by selection of the feed point of the slot.

The power supply, Figure 2.12, for the sphere circuits described above consisted of a transistor converter for producing dc potentials of +80, -9, and +1.3 volts from an input of 6-volt dc. Transistors Q_{13} and Q_{14} were operated as switches utilizing the saturation characteristics of the ferrite core of transformer T_2.

The sub-modulator was a free-running blocking oscillator, Q_{12}. Its frequency was determined by the resistance-capacitance time constant in its base. This time constant was determined by the 0.05-microfarad capacitor, the 100 k-ohm resistor, and the resistance of a thermistor located on the sphere center section. The resistance of the thermistor, and therefore the frequency of

the blocking oscillator, was a function of the temperature of the sphere. The circuit was switched on by applying a negative pulse to the emitter of the oscillator so that it would free-run until the bobbin was released. It was then switched off until contact was made.

2.2.5 Ejection Mechanism. The ejection of the sphere was accomplished by means of a mechanical timer, blasting caps, and an appropriate mechanical design. Ejection times were pre-determined, taking into account the rocket trajectory and the altitude and position of the nuclear detonation.

The sphere was mounted between two threaded sections of the payload called the upper and lower sphere holders. Springs located in the base of each sphere holder were employed to constrain the sphere when it was in the assembled position. A frangible magnesium ring with inside threads was used to obtain a secure butt joint between the two sections that enclosed the sphere. Four blasting caps were embedded in cavities which were spaced 90 degrees apart along the outside threaded section of the lower sphere holder. Two of these cavities can be seen in the photograph shown in Figure 2.13. Mounted inside of the assembly was an acceleration-sensitive timer that was initiated

at rocket lift-off. At a pre-set time the closure of a switch on the timer caused detonation of the explosives. The magnesium ring was shattered, permitting the springs to push the sphere holders apart, thereby deploying the sphere. In the photograph shown in Figure 2.14, the timer (Raymond Engineering Laboratory Model 1060-18G), Ledex switch used for monitoring purposes, umbilical connector, and battery box can be seen located in the lower sphere holder (left). The magnesium ring is seen at the bottom of this inverted view of the lower sphere holder. The interior of the upper sphere holder is shown on the right side of this photograph. Components associated with the sphere battery-charging circuit are seen at the top of the photograph. The addition of this circuitry permitted long stand-by periods before actual rocket launch. One of the ejection springs can be seen at the center of the upper sphere holder, and a fairing ring is shown at its base. In Figure 2.15 the upper sphere holder is in the same position as it appeared in the previous photograph. However, the lower sphere holder (left) is shown in its upright position to show the location of ejection spring, batteries, and terminal boards for electrical circuits associated with the ejection mechanism.

Ejection timers were carefully set and checked before each flight. Operational variations from the pre-set values were observed to be less than 0.1 sec. on all flights, based upon recorded data. During the first part of the series, the nominal value for ejection time on the four flights was 55 sec. However, during the second part of Fish Bowl, ejection times were set as low as 51.6 sec. on Tight Rope and as high as 57.3 sec. on King Fish. Other ejection times were: Check Mate, 53.6 sec.; Blue Gill Triple Prime, 54.92 sec.; background shot, 55.04 sec. Based upon radar data, these ejection times corresponded to altitudes between 190,000 and 220,000 feet, except for the sphere that failed to achieve a normal trajectory following Tight Rope. The effective launch elevation angles varied between 83 and 86 degrees, depending upon trajectory requirements.

The altitude at which the sphere was deployed was chosen so that trajectories of the rocket and the sphere would be essentially the same up to peak altitude due to the low drag acceleration encountered. This facilitated the determination of sphere peak altitude from radar observations.

2.2.6 Radar Beacon. Photographs of a typical C-band radar beacon assembly used with the Falling Sphere payloads are shown

in Figures 2.16 and 2.17. Figure 2.16 shows the complete beacon installation with only the access skin-plate removed. In Figure 2.17 the base-plate of the beacon section is removed to show a more detailed view of the component arrangement. The beacon assembly consisted of a 14.5-inch section mounted posteriorly to the lower sphere holder. The C-band beacons (radar transponder, Model C/T-CV, 551) were supplied by Aero Geo Astro Corporation, Alexandria, Virginia. The antennas, which can be seen (Figures 2.16 and 2.17) mounted 180 degrees apart on the skin of the beacon section, were supplied by the Physical Sciences Laboratory, New Mexico State University at Las Cruces, N.M.

The four flights completed during the first part of the series were equipped with beacons. The equipment worked satisfactorily in all cases. However, some difficulties were experienced by the DAMP Ship on Rockets 1 and 2,and no usable radar tracking data was recovered. The results obtained on Rockets 3 and 4 were more satisfactory. The problems in obtaining good radar tracking by DAMP Ship were due partly to its varying distance and location with respect to the launch site. Consequently, during the second part of the Fish Bowl Series, tracking support was requested and obtained from the Pacific Missile Range (PMR) Range Tracker which had the

advantages of fixed location and no motion due to the sea. Since PMR expressed a preference for passive tracking (skin tracking of a target by means of reflected signals only), no radar beacons were employed with these payloads, although the beacon assemblies were fabricated and available for immediate use.

2.2.7 Assembled Payload. A photograph of the individual payload components is shown in Figure 2.18. The critical dimensions and weights are listed below each item. When all of these components were assembled, the complete payload configuration appeared as in the photograph shown in Figure 2.19. It was approximately 57 inches long, and it weighed approximately 62 lb., including 9 lb. of lead ballast at the tip of the nose cone to increase the stability of the rocket during flight. The nose cone carried no instrumentation.

The beacon section was eliminated on the payloads flown during the second part of the series. This reduced the payload length to approximately 42.5 inches and the weight to approximately 40 lb. These changes in the payload configuration were compensated for by adding enough lead ballast inside the tip of the nose cone to raise the total weight to about 55 lb. This provided the necessary flight stability.

2.2.8 Rocket Operation. The fin alignment data and performance of the Nike-Cajun rockets used to carry Falling Sphere payloads aloft are discussed in this section. For all Project 9.1a flights the spin of the Nike was adjusted for 2 rps (ARC SVG Atlantic Research Corporation, Space Vehicles Group or Aerolab fins) while the Cajun fin assembly was adjusted for zero spin (5 flights with ARC SVG, no wedges; 4 flights with Aerolab fins, no wedges). The use of lead ballast in the nose cone has been discussed. Figure 2.20 shows a photograph of the Nike-Cajun, with sphere payload attached, on the launcher. Except for the failure to obtain second-stage ignition on the last rocket (Tight Rope), all flights were normal.

A summary of Project 9.1a rocket launchings is presented in Table 2.2.

2.3 INSTRUMENTATION (GROUND-BASED)

Two ground stations were employed in the Falling Sphere experiment for the purpose of, (1) establishing a time reference signal initiated by a first-motion switch on the rocket launcher, (2) receiving signals telemetered from the sphere, (3) providing electronic discrimination (in pulse width and amplitude) as a means of minimizing spurious pulses, and (4) accepting and storing the data in a suitable form for processing. The two manned stations operated independently of each other, but they

obtained identical information. The reliability of the experiment was thereby increased through the use of redundancy.

A simplified functional block diagram of the main ground station is presented in Figure 2.21. The description that follows applies to both stations, since the back-up station differed only in minor details.

Frequency divider circuits in the time base generator permitted the use of reference signals that were compatible with the frequency response of each type of recorder used for data storage. A digital clock was also driven from the time-base generator. This allowed ground station operators to observe the progress of the sphere flight in real time, from ejection to impact. At a specified time preceding rocket lift-off, a first-motion switch on the launcher was appropriately connected to the time-base generator so that the output signals were cut off. The signal level could be restored for testing purposes by means of a first-motion defeat switch installed at the ground station. At rocket lift-off, the first-motion switch operated, the digital clock commenced counting time, and the pulse decoder unit presented the time reference signals to the recorders and display equipment.

After ejection of the sphere, signals were picked up by two oppositely polarized helical antennae. These were remotely directed to obtain maximum signal strength from the sphere. Both visual and aural electronic aids were used to obtain good sphere tracking. Separate pre-amplifiers were located at the base of each antenna. These boosted the level of received signals before transferring them to separate receivers. The effects of fading due to spinning of the sphere were minimized by electronically mixing the outputs of the two receivers in the pulse decoder unit. The resultant signal was one of nearly constant amplitude, although the receivers were not equipped with automatic gain control (AGC) circuits.

Noise rejection circuits, such as limiters and pulse width discriminators, were employed in the pulse decoder unit in order to improve the quality of signals in the presence of high-level interference.

Separate pulse width discriminators provided unambiguous start and stop pulses to the recorders that were employed to store the data. These start and stop pulses corresponded to accelerometer bobbin release and impact times, respectively. The arrival of the first start pulse from the sphere initiated

a time interval measurement in the digital read-out equipment that was completed with a stop pulse. The time of occurrence (to a hundredth of a second) referred to rocket lift-off, and the numerical value of the transit-time measurement (to the nearest hundredth of a millisecond) were immediately printed out on paper tape. The sequence was repeated for each transit-time measurement.

The time base (reference signals) and accelerometer transit-time measurements were also stored in a 7-channel magnetic tape recorder. Two channels were used for recording elapsed time, while the remaining five channels were employed to store transit-time measurements with and without noise rejection.

A four-channel Brush strip chart recorder was used to store the same basic data but with somewhat reduced accuracy due to lower frequency response inherent in the instrument. This recorder served as a coarse back-up for data storage and was also used for pre-flight testing. A photograph of part of the main ground station during laboratory checkout is shown in Figure 2.22. The direct read-out equipment may be seen in the foreground.

In principle, the operation of the second ground station was the same as that of the main station. The circuitry employed

was somewhat less sophisticated but completely adequate. It was operated from a separate location within line of sight of the rocket launcher.

2.4 DATA REQUIREMENTS

2.4.1 Data Obtained by Project. Measurements obtained from sphere telemetry information were the raw experimental data obtained by the project from a successful flight. The data was used to compute sphere drag acceleration as a function of elapsed time from rocket lift-off. This constituted the first step in the data reduction process required to obtain atmospheric density, temperature, and pressure profiles.

2.4.2 Radar Tracking. An accurate analysis of the experimental results obtained required good radar tracking data on the Cajun rocket or the sphere. The trajectory of the sphere was determined by performing double numerical integrations using as initial values the peak altitude and peak time of the sphere. Peak altitude can best be provided by an accurate radar track. The correct altitude assignment of density, temperature, and pressure profiles depended upon the accuracy of this radar data. On the other hand, sphere peak time can be more accurately derived from analysis of the drag acceleration data obtained during

the flight of the sphere.

2.4.3 Meteorological Support. Density, pressure, and temperature data up to 30 km was a prime experimental requirement. Rawinsonde data was obtained on all Project 9.1a flights of the series with the exception of Rockets 2 and 3. Unfortunately, the data available was limited to 25 km. Therefore, it was necessary to match the density data obtained from sphere telemetry with extrapolated values of Rawinsonde density. From the theory (Section 1.3) it can be seen that to calculate the temperature at one altitude the temperature at some other altitude must be known. Since a good value of temperature obtained from a balloon measurement was not available at the required altitude, a temperature had to be assumed. However, the resulting inaccuracy was not large.

TABLE 2.1 EVENT DESCRIPTION

Event	Time (Z)	Yield (kt) (nominal)	Altitude (km)
	1962		
Star Fish (Prime)	09 0900 July	1400	400.15
Check Mate	20 0830 Oct		
Blue Gill (Triple Prime)	26 1000 Oct		
King Fish	01 1210 Nov		
Tight Rope	04 0730 Nov		

TABLE 2.2 SUMMARY OF ROCKET LAUNCHINGS (Nike-Cajuns)

Rocket No.	Date	Launch Time		
		Hours (local time)	Referred to H=0	
	1962			
1	1 June	1800	(H - 4 hours)*	Blue Gill
2	19 June	2230	(H - 1 hour)*	Star Fish
3	8 July	2230	H - 30 minutes	Star Fish Prime**
4	23 July	1920	(H - 2 hr. 40 min)*	Blue Gill Prime
5	19 Oct	2240	H + 10 minutes	Check Mate **
6	26 Oct	0015	H + 15 minutes	Blue Gill ** - Triple Prime
7	29 Oct	2300	N/A	Background measurement
8	1 Nov	0220	H + 10 minutes	King Fish **
9	3 Nov	2134	H + 4 minutes	Tight Rope **

* With reference to start of the detonation window.
** Nuclear detonation.

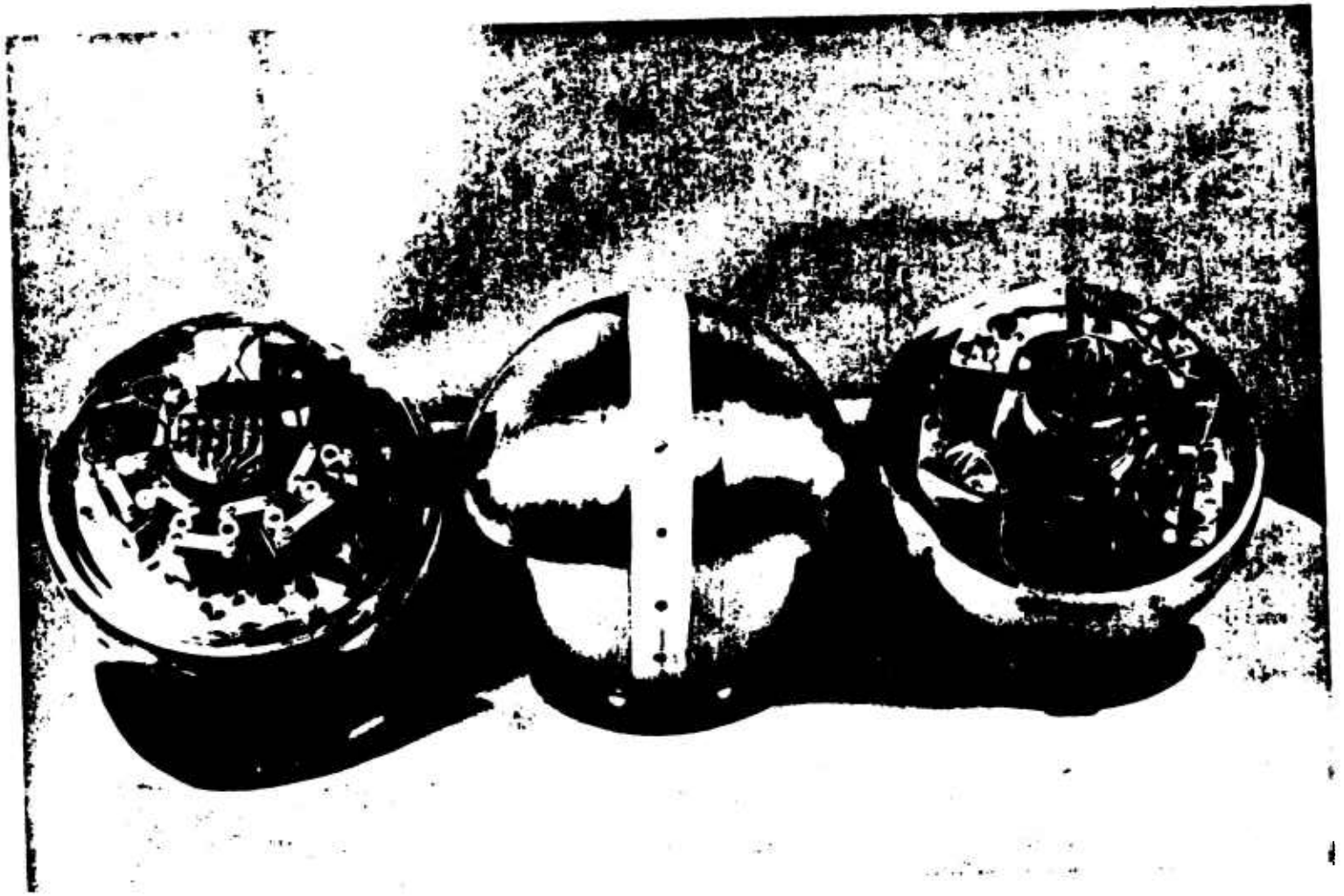

Figure 2.1 Photograph of sphere instrumentation. (AFCRL 153-391)

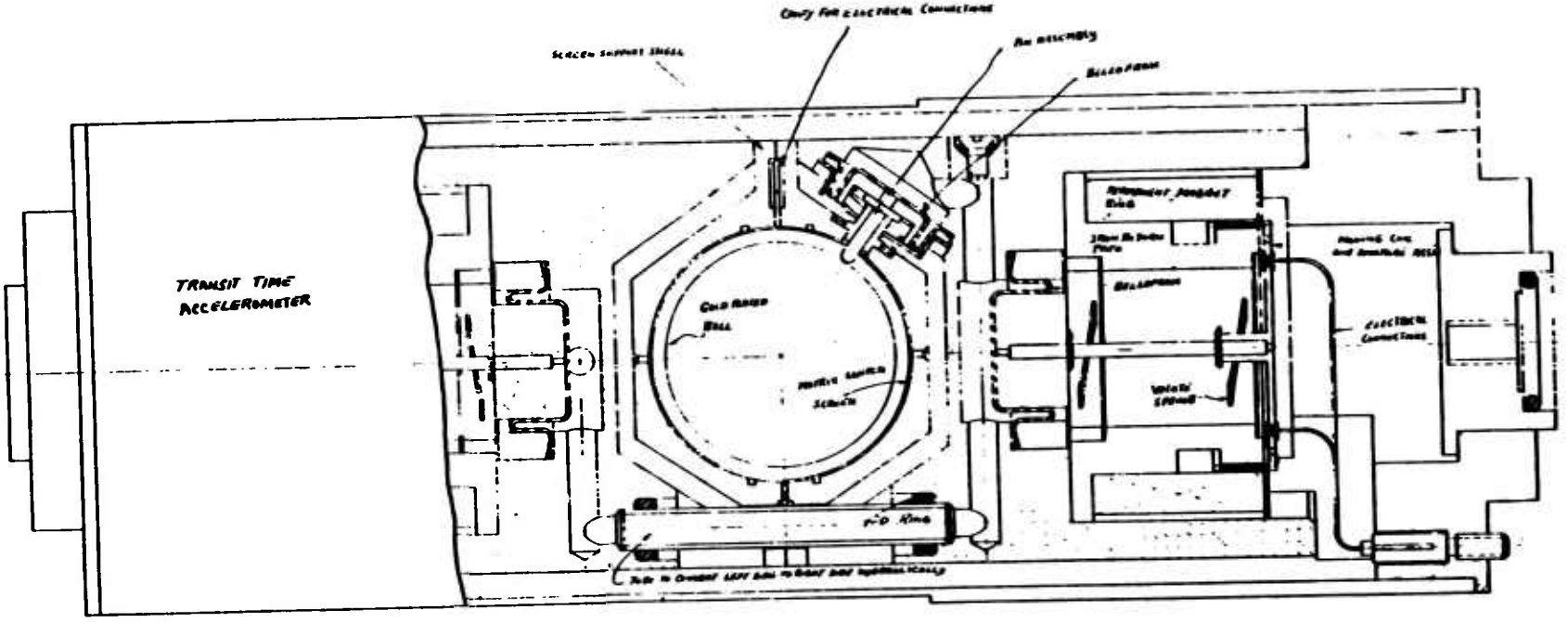

Figure 2.2 Cutaway drawing of omni-directional accelerometer.

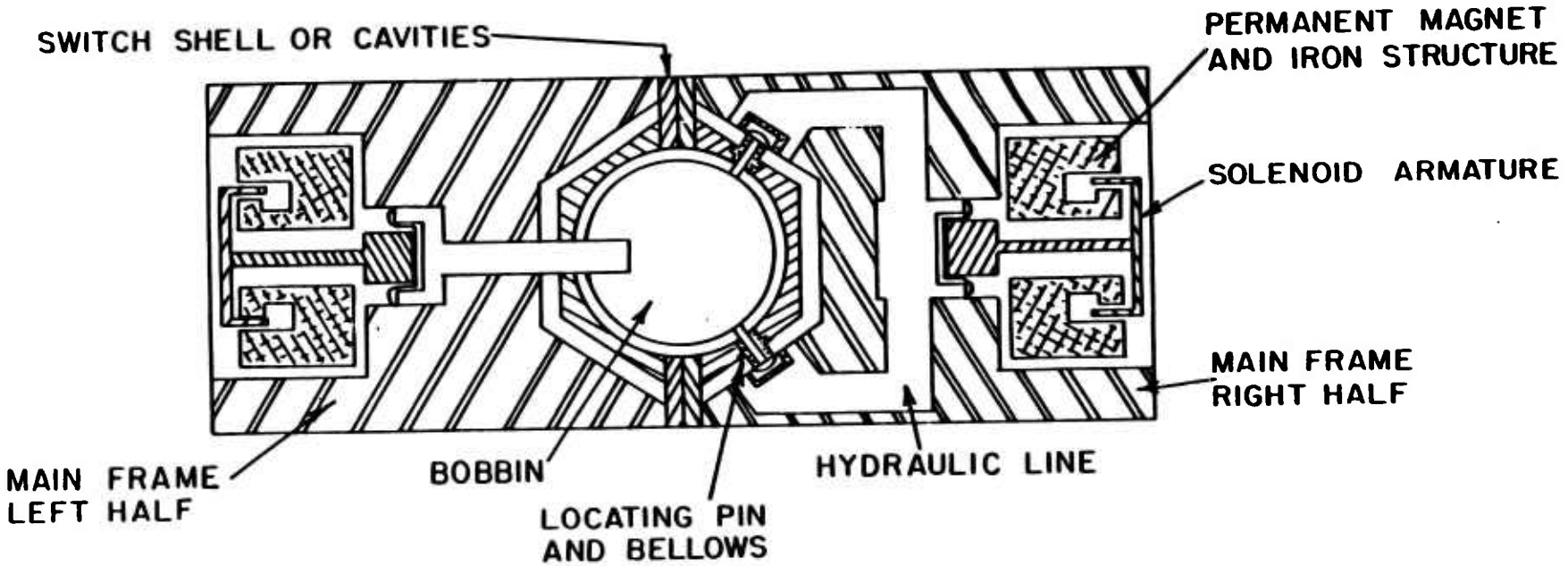

Figure 2.3 Schematic drawing of omni-directional accelerometer.

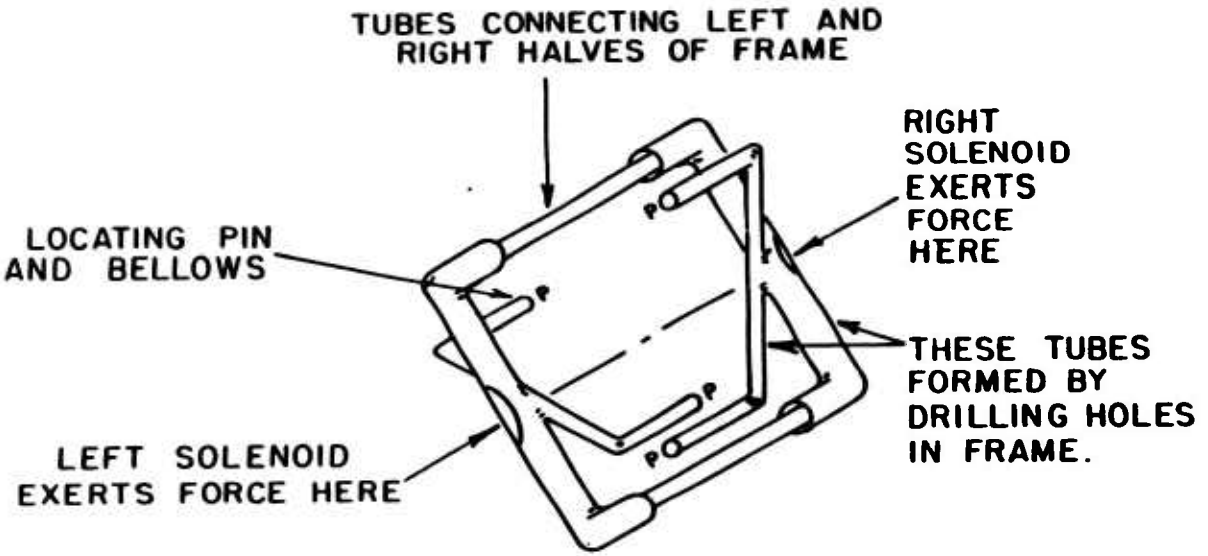

Figure 2.4 Schematic drawing of accelerometer hydraulic circuit.

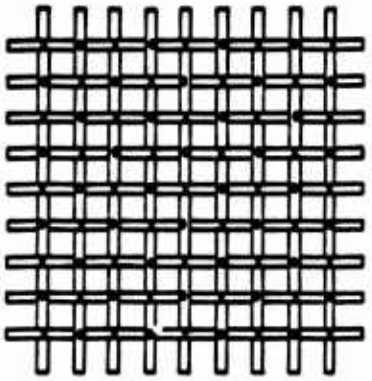

THE ELECTRICAL INSULATION IS REMOVED FROM THE WIRE AT EACH INTERSECTION. TO COMPLETE THE CIRCUIT (CLOSE THE SWITCH), THE BOBBIN SHORTS ANY SPOT MARKED "X" TO ANY ADJACENT SPOT MARKED "O". EACH "WIRE" ACTUALLY CONSISTS OF TWO WIRES LAID SIDE BY SIDE.

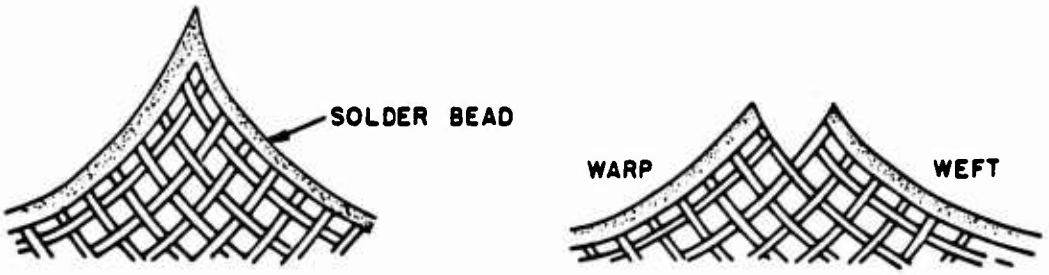

WEFT IS SEPARATED FROM WARP BY CUTTING AWAY A SMALL SECTION OF EACH CORNER OF THE SCREEN AS SHOWN.

Figure 2.5 Schematic drawings of matrix switch details.

Figure 2.6 Photograph of partially assembled accelerometer cavity (half section). (AFCRL 153-421)

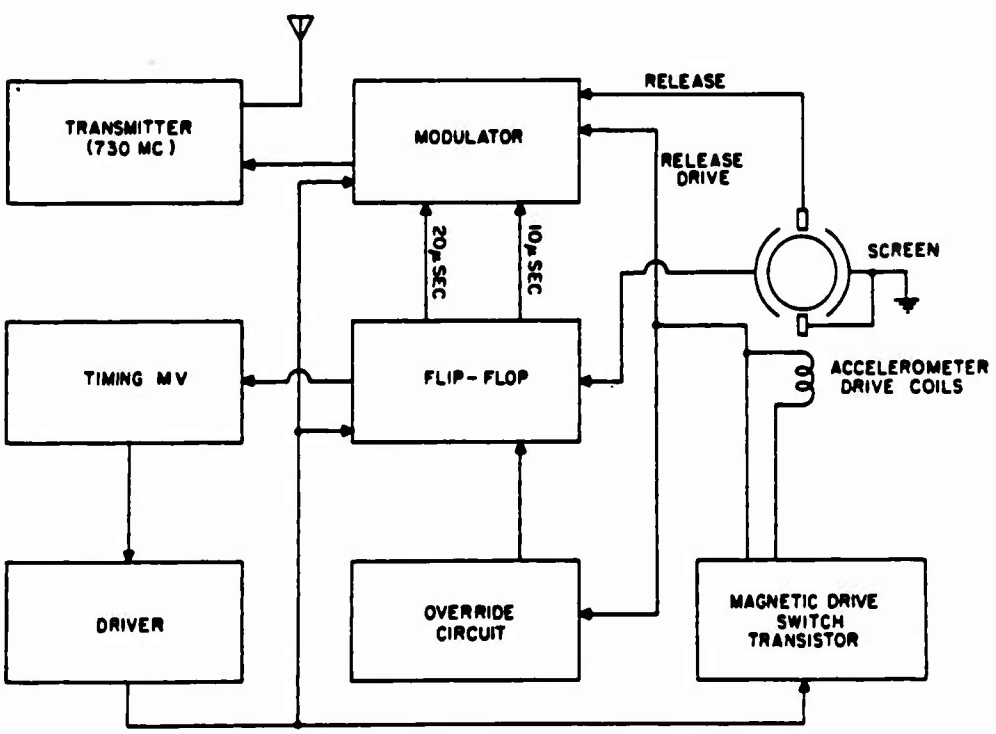

Figure 2.7 Functional block diagram of sphere instrumentation.

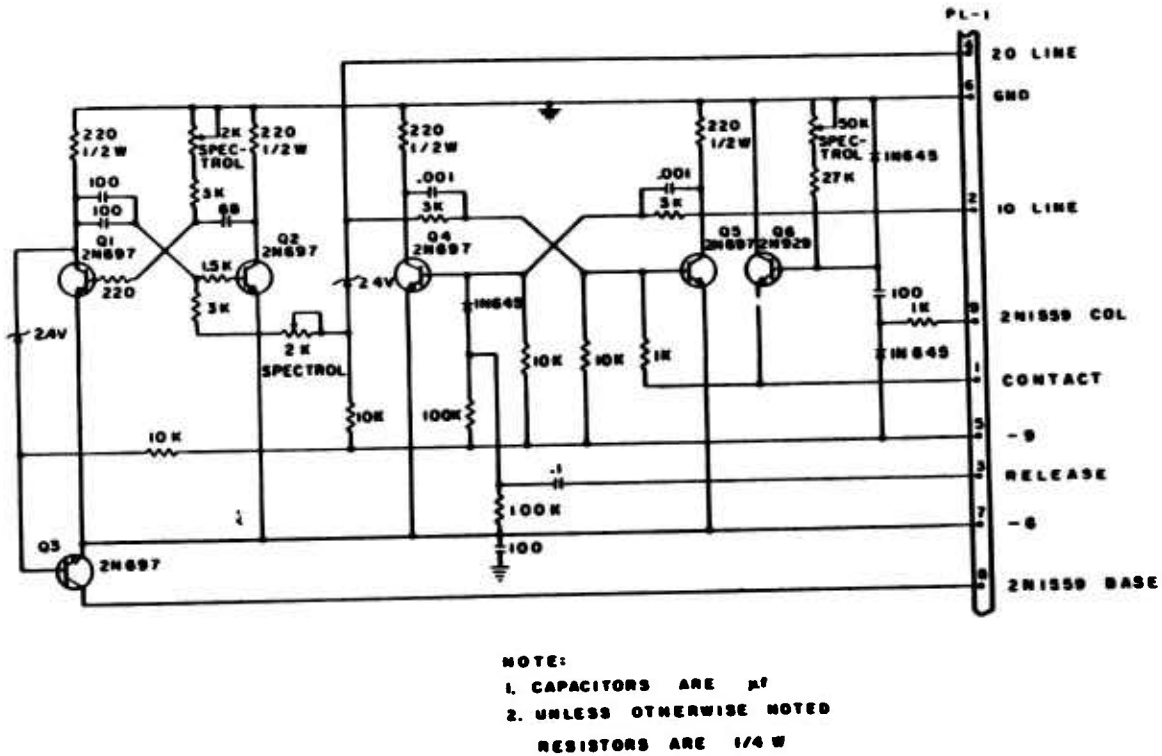

Figure 2.8 Sphere timer module, circuit diagram.

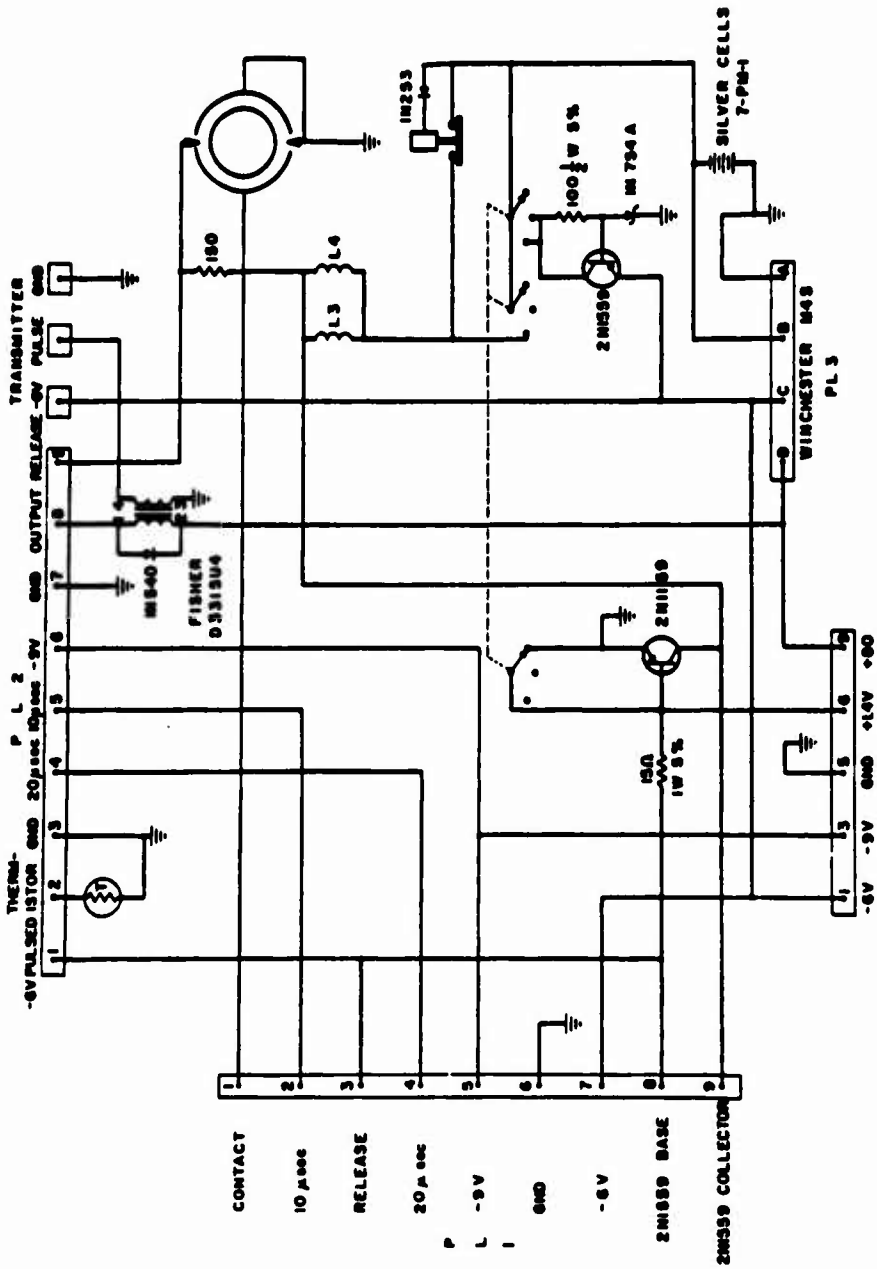

Figure 2.9 Sphere center section components, circuit diagram.

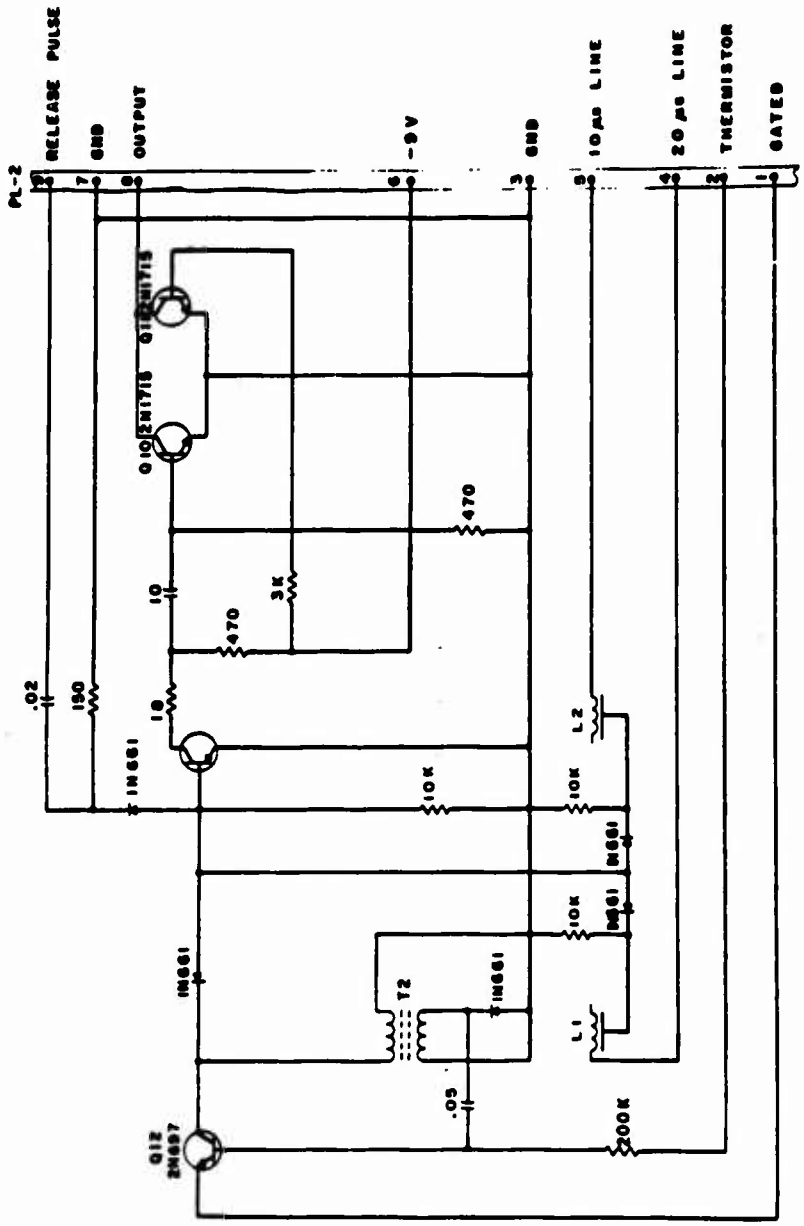

Figure 2.10 Sphere modulator, circuit diagram.

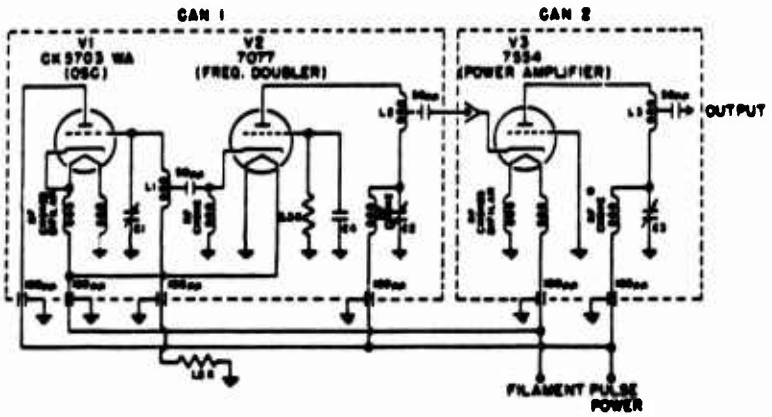

C1, C2, C3 - JFD VC216 .8-4.8 μμf.
C4 - 1⅝" x ⅝" PLATE MOUNTED TO CAN WITH APPROX .007 MICA SEPARATION.
L1, L2 - 1½ TURNS #16 SOLID COPPER WIRE - INSIDE DIA. ⅝".
L3 - 1¼ TURNS 12 SOLID COPPER WIRE - INSIDE DIA. ⅝".
RF CHOKES - 10-14 TURNS #30 WOUND ON ¼" TEFLON.
RF CHOKE - WOUND ON ¼" DIA. FORM.

Figure 2.11 730-Mc sphere transmitter, circuit diagram.

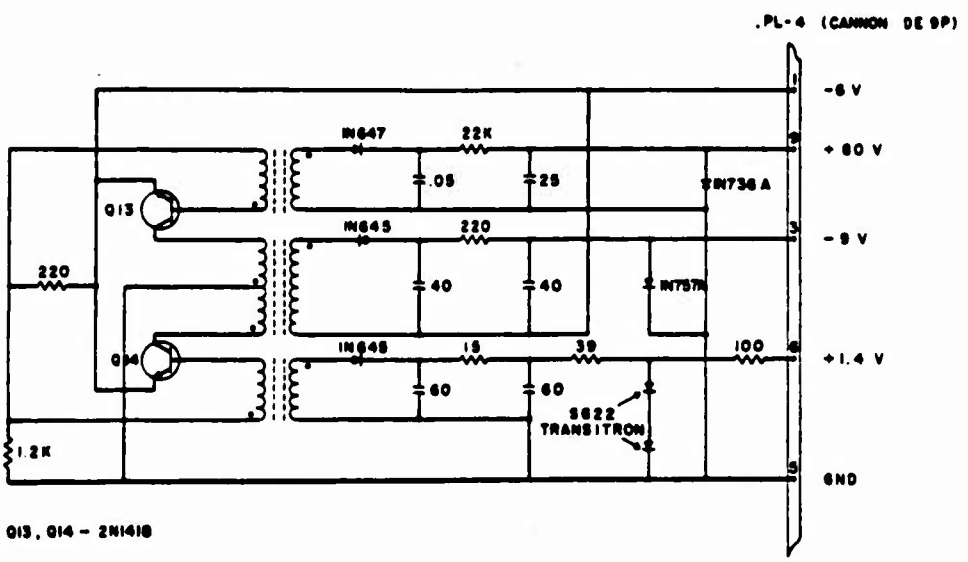

Q13, Q14 - 2N1418

PRIMARY	40	TURNS	NO. 30
SECONDARY	10	"	NO. 38
100 V	350	"	NO. 40
-6 V	20	"	NO. 36
3 V	11	"	NO. 34

Figure 2.12 Sphere power supply, circuit diagram.

Figure 2.13 Photograph of sphere ejection assembly. (AFCRL 153-40)

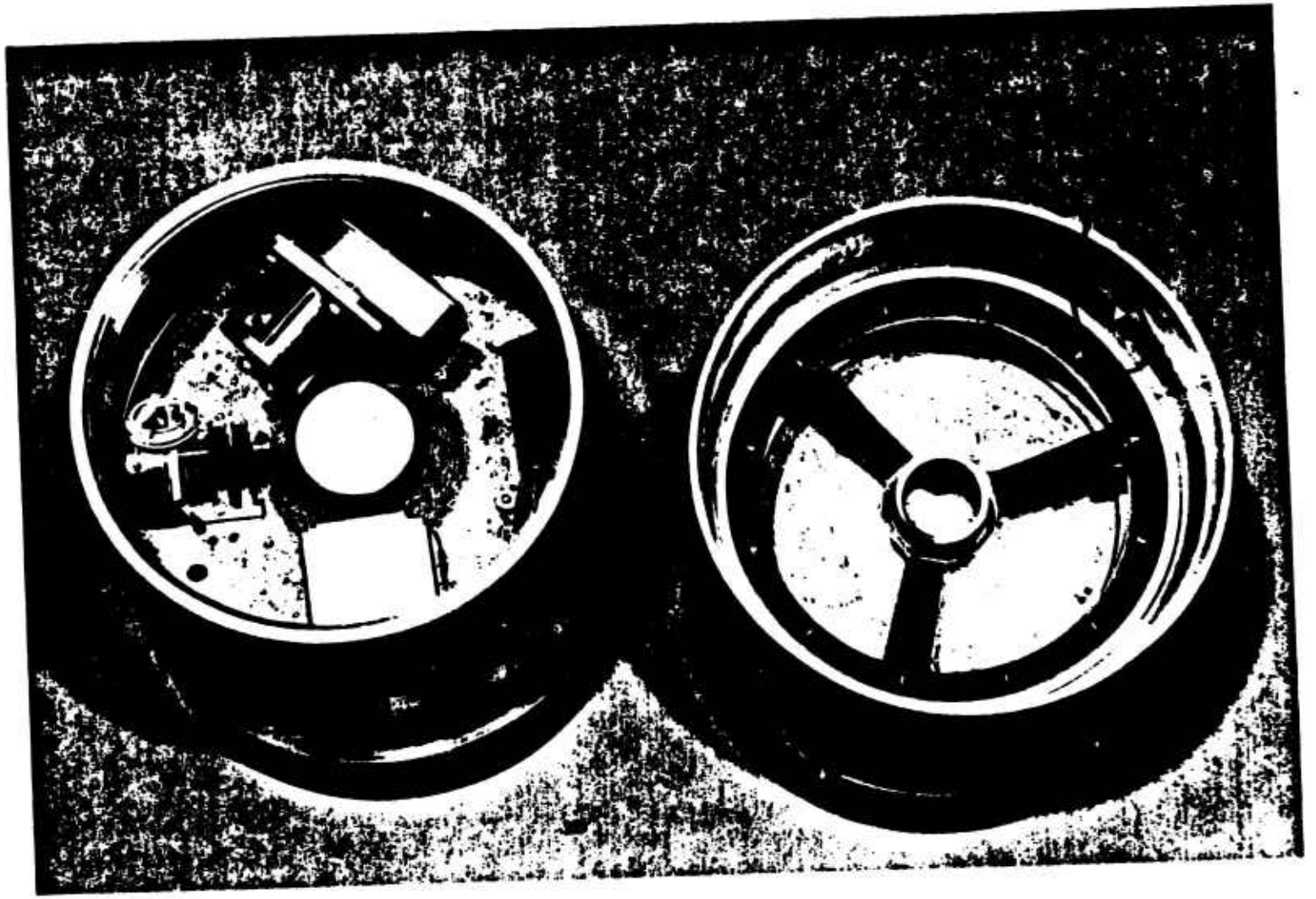

Figure 2.14 Photograph of sphere ejection and monitoring components. (AFCRL 153-298)

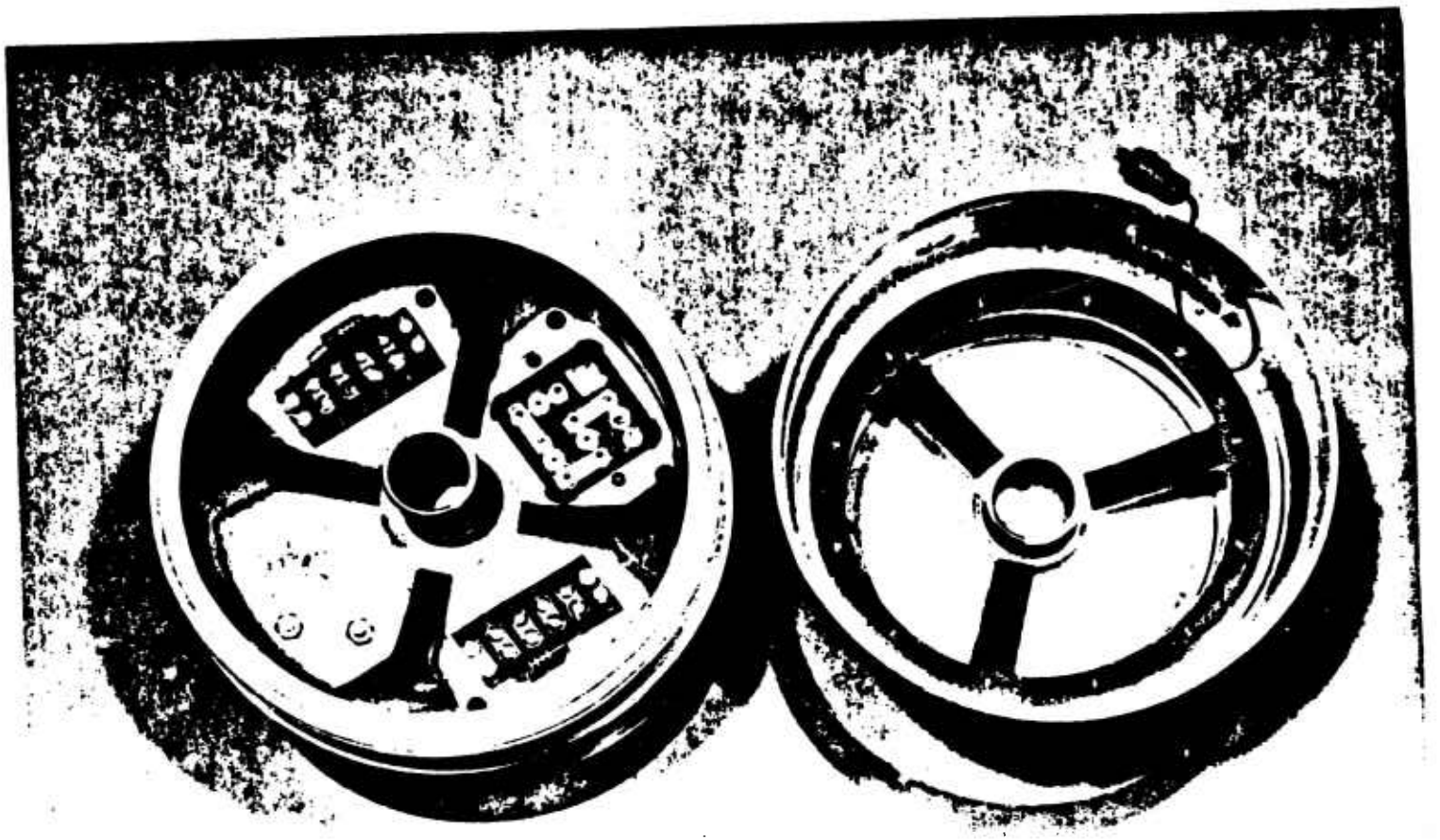

Figure 2.15 Photograph of upper and lower sphere holders (interior view). (AFCRL 153-299)

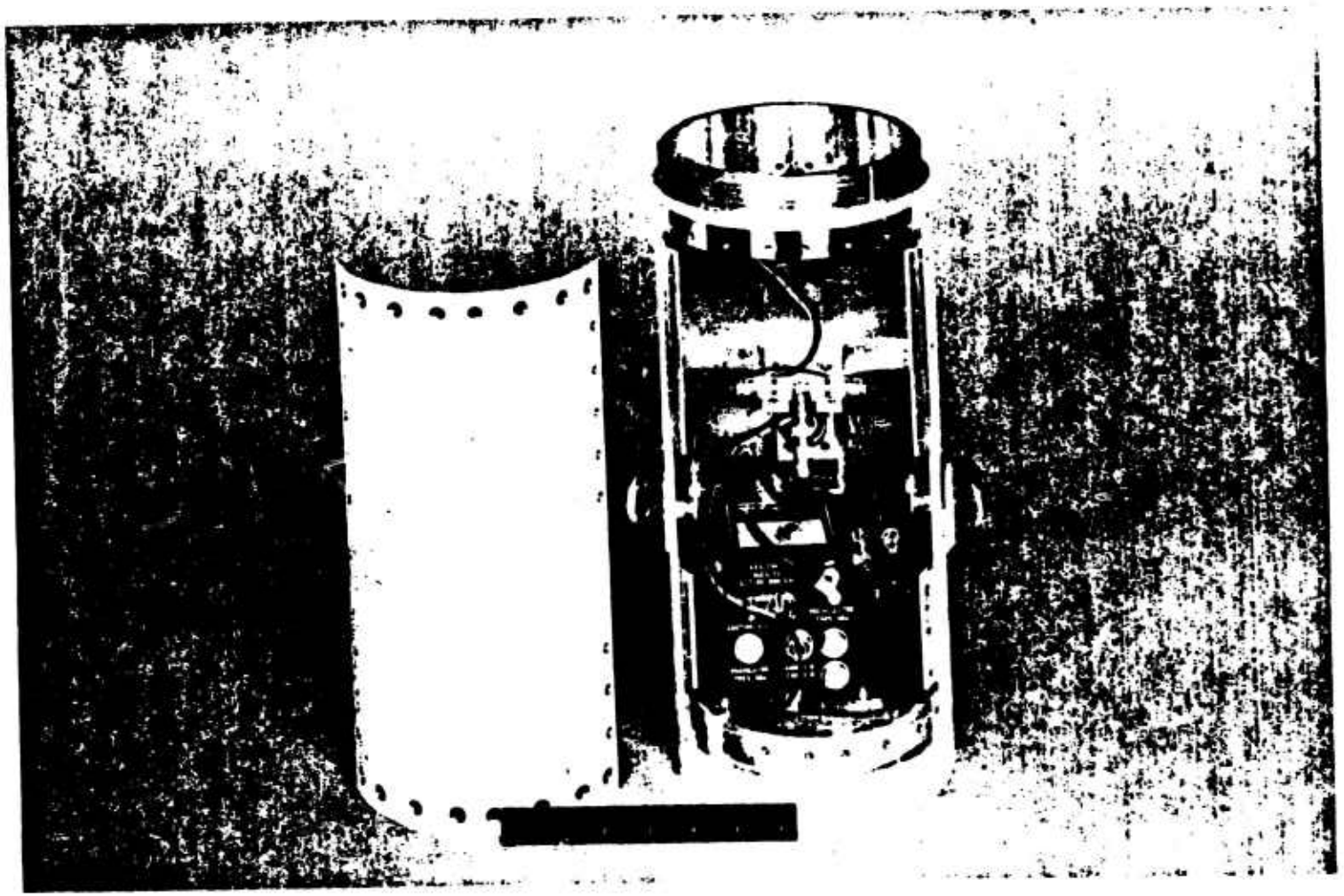

Figure 2.16 Photograph of C-band beacon assembly. (AFCRL 153-294)

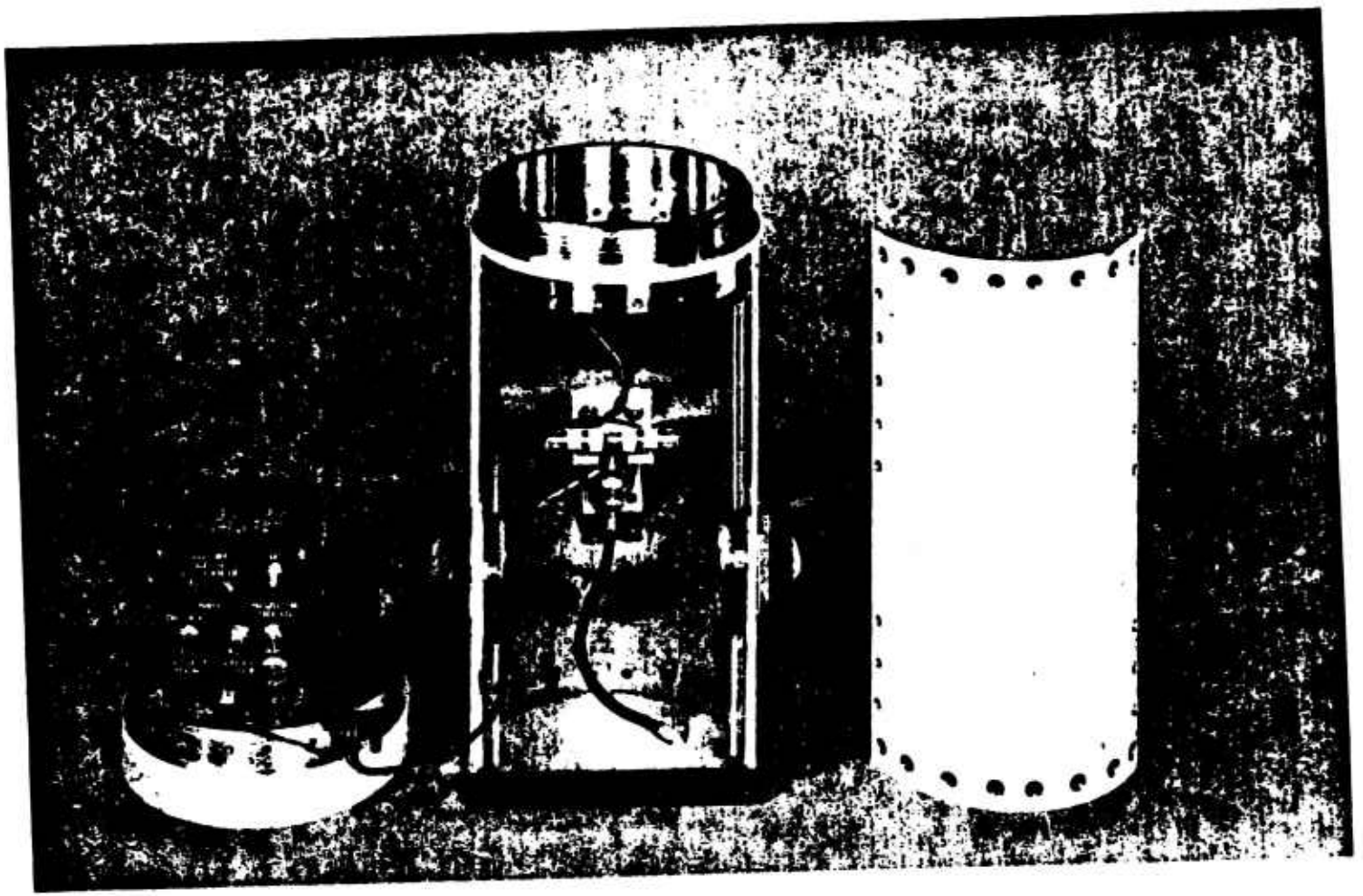

Figure 2.17 Photograph of C-band beacon assembly (detailed view of components). (AFCRL 153-292)

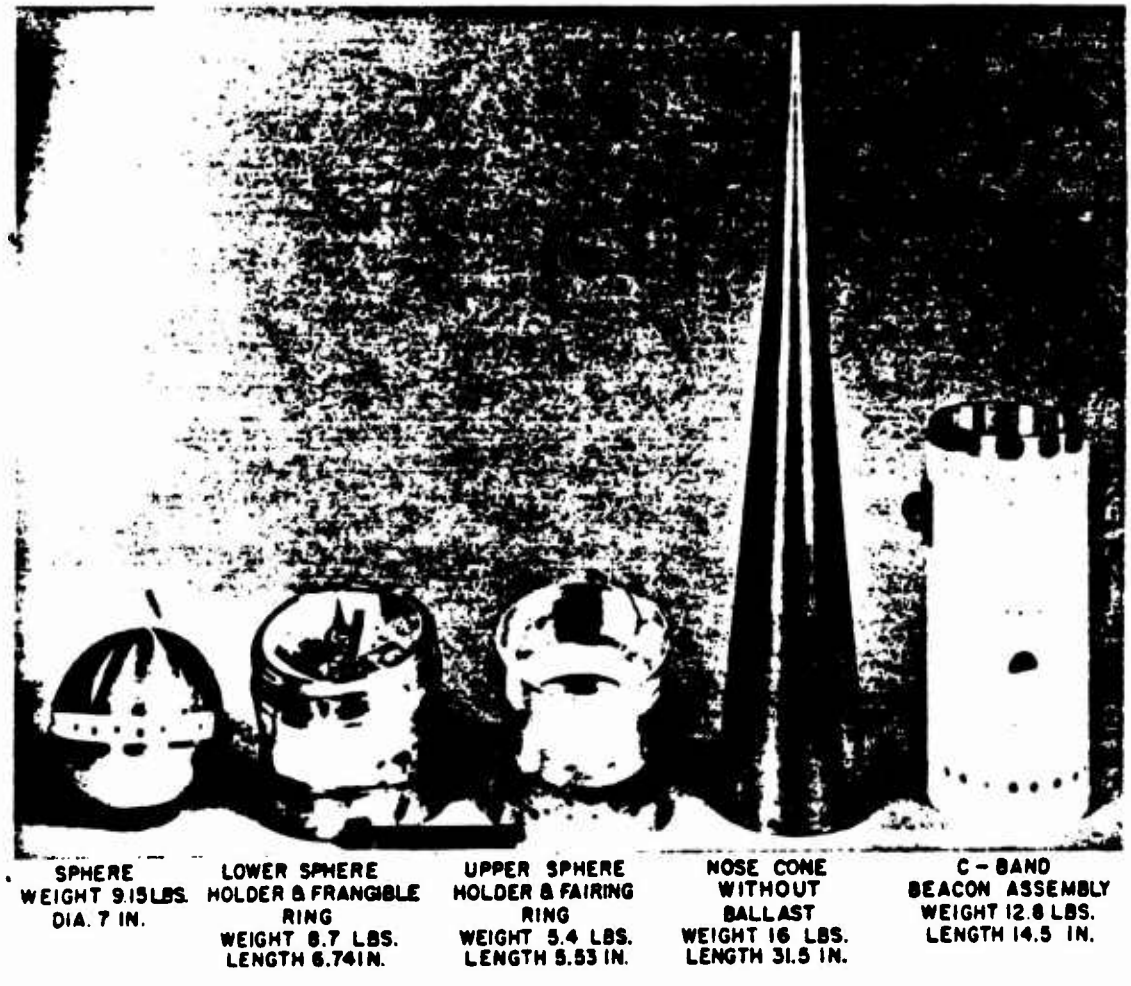

Figure 2.18 Photograph of payload components. (AFCRL 153-417).

Figure 2.19 Photograph of assembled payload. (AFCRL 153-431)

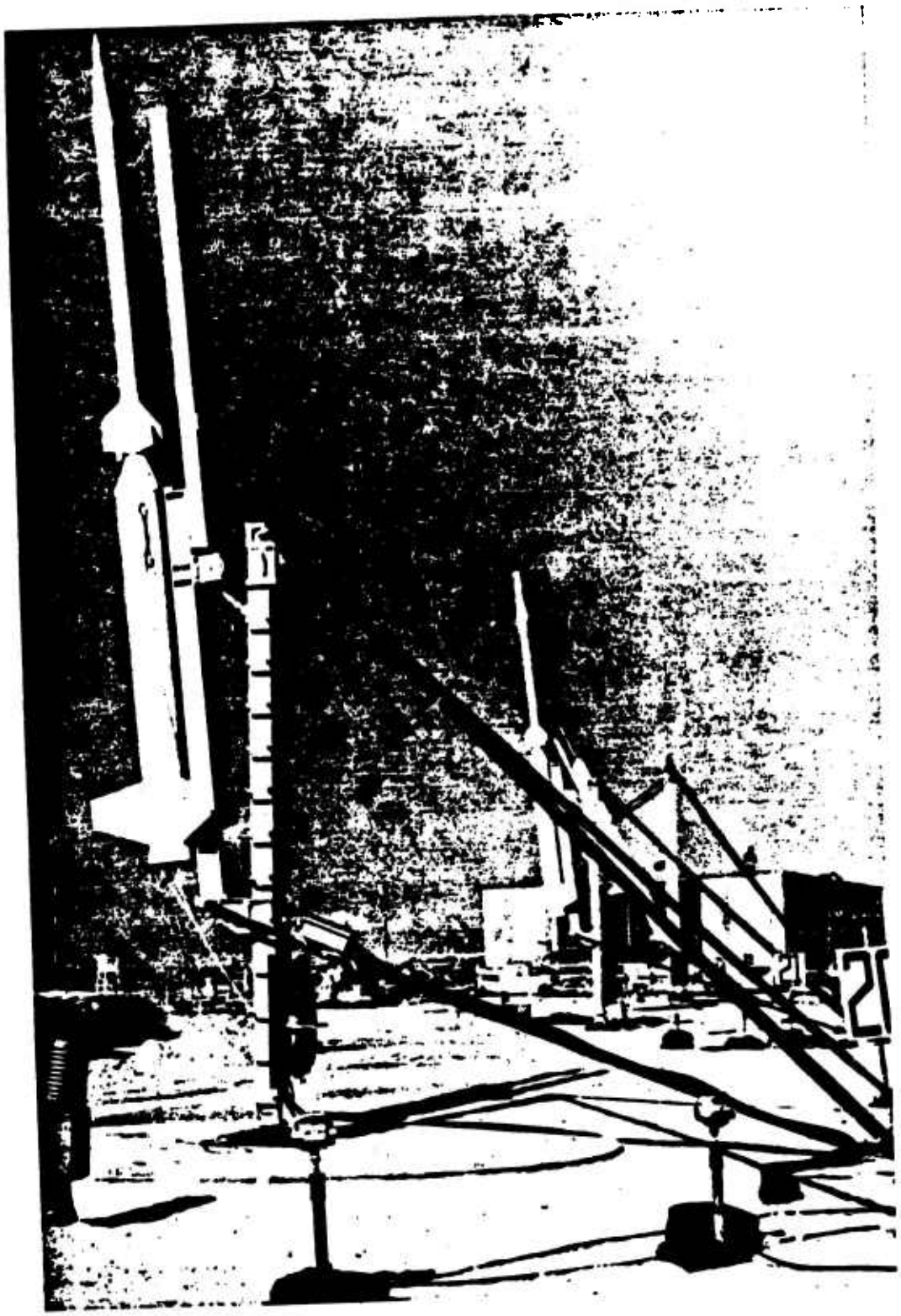

Figure 2.20 Photograph of Nike-Cajun, with sphere payload, on launcher. (AFCRL photo)

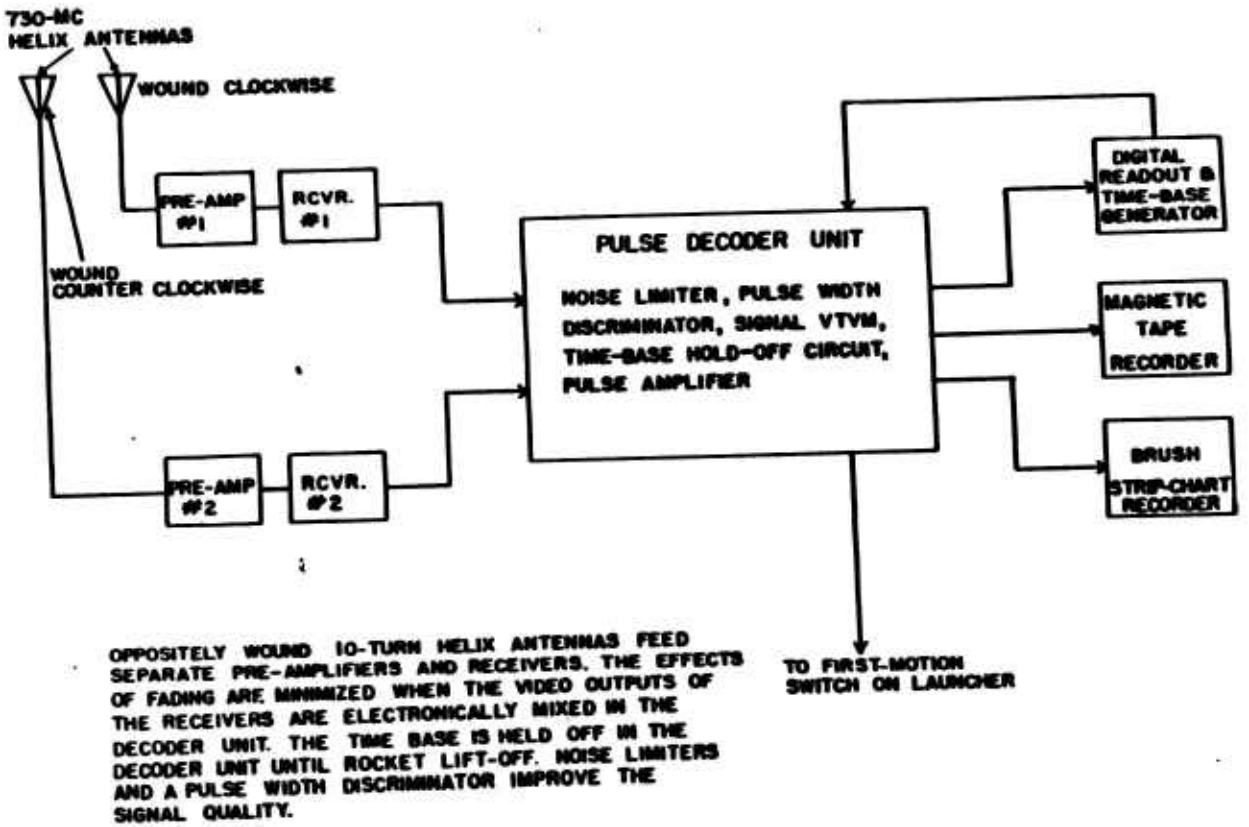

Figure 2.21 Functional block diagram of main ground station.

Figure 2.22 Photograph of telemetry equipment during laboratory checkout. (AFCRL 6101)

CHAPTER 3

RESULTS

3.1 SUMMARY

A Falling Sphere rocket was successfully fired preceding each attempted nuclear detonation during the first part of Fish Bowl (Rockets 1 through 4). Excellent data was obtained from each flight. In addition, another measurement was made on the normal atmosphere (Rocket 7) during the second part of the series for comparison with other pre-test data. These flights were made at different times of the day and night during the interval between June 1 and October 29, 1962 (see Table 2.2). The data obtained will permit a study of diurnal and seasonal variations of atmospheric properties in the vicinity of the test site.

Successful measurements were also obtained from flights made shortly after the nuclear detonations on Check Mate, Blue Gill Triple Prime, King Fish,and Tight Rope. Changes in the physical properties of the atmosphere did occur. However, the magnitude of the changes was not as great as expected in some cases.

3.2 DRAG ACCELERATION DATA

The raw data obtained from the sphere during its flight

consisted of measurements of accelerometer transit-times (τ) as a function of elapsed time referred to rocket lift-off. Drag acceleration, corresponding to each measurement, was computed from the equation

$$a_D = 2\, s/\tau^2 , \qquad (3.1)$$

where a_D is the mean drag acceleration during the time interval τ, s is the fixed displacement between the centered bobbin of the accelerometer and its cavity, and τ is the time required for the accelerometer bobbin to complete a fall after release. Curves of drag acceleration versus elapsed time were then plotted for use in subsequent data processing and analysis. Drag acceleration curves for each of the nine Project 9.1a flights are presented in Figures 3.1 through 3.9.

The following general comments apply to all the drag acceleration data except that shown in Figure 3.9 which will be treated separately. The sphere was ejected from the rocket at a predetermined time after launch. Coincident with ejection, an automatic switch initiated operation of the accelerometer. Signals telemetered from the sphere were received in real time and recorded at the ground-based stations. Ejection times for each flight are presented in Table 3.7. This gives a summary of

sphere trajectory data referred to rocket launch time (also see Section 2.2.5). As the sphere ascended in a path approximating that of the rocket, the observed drag acceleration diminished until an altitude was attained where the accelerometer could no longer respond to the minute drag accelerations encountered by the sphere. This is evidenced by increased scatter in the data as the drag curve approached a plateau-like region at the bottom of the curve. The data obtained just preceding or immediately following this region in each curve corresponded to the highest altitude for which drag acceleration measurements were made by the sphere (in the range 103-112 km). The plateau region consists of experimental points of nearly constant value. In general, they are parallel to the time axis and nearly symmetrical with respect to sphere peak time. These experimental points resulted from the pre-set over-ride circuit in the sphere electronics (Sections 2.2.3 and 2.2.4) and do not constitute actual measurements of drag acceleration. The plateau region of the curve was used to determine the low-g sensitivity of each flight accelerometer and to prevent spurious drag acceleration results. The threshold sensitivity of the flight accelerometers varied from approximately 6×10^{-3} ft/sec^2 (1.87×10^{-4} g) to 9.54×10^{-4} ft/sec^2

(2.97×10^{-5}g). Although this latter value represents more than 1.5 orders of magnitude improvement in sensitivity over previous models, it is believed that accelerometers now under development will exhibit even greater measurement capability at high altitudes. It is now known that the threshold sensitivity of the accelerometers was limited in part by inadequate electrical contact between bobbin and cavity switch when the pressure exerted at bobbin impact was very small (of the order of milligrams).

On the descending portion of the sphere trajectory, approximately 90-95 seconds after peak time, the drag forces encountered by the sphere again became large enough for accurate measurement by the accelerometer. Good measurements were then obtained until the sphere approached re-entry conditions. Here the drag accelerations rapidly increased to nearly 6g. However, at this value of acceleration, the accelerometer no longer functioned satisfactorily, because the force required to center the bobbin was larger than that available. Thus, in this region of high drag, spurious accelerations larger than the actual accelerations were indicated. When the retarding acceleration decreased, the accelerometer once again functioned normally.

Figure 3.1 is a curve of the drag acceleration data obtained on Rocket 1. This rocket was launched four hours before the scheduled Blue Gill detonation. The sphere was ejected from the Nike-Cajun rocket approximately 56 seconds after launch. The time of ejection corresponded very closely with the time of the first data point on the curve. The upleg portion of the mean drag data is represented in the figure by a straight line with a negative slope. Approximately 80% of the upleg data fell on this line, although some scatter in the data was observed as the sphere approached the altitude where the drag acceleration became less than $6 \times 10^{-3} ft/sec^2$.

During the elapsed time interval between 100 and 275 seconds, approximately, the experimental points describe a line nearly parallel to the time axis (zero slope). This represents an electronically determined value of accelerometer threshold sensitivity, but does not constitute a measurement of drag acceleration. It is the plateau region previously described. At a time corresponding to the mid-point of the plateau (187.7 seconds referred to rocket launch) the sphere reached peak altitude and then began its descent. After 275 seconds of elapsed time drag acceleration measurements were again obtained from the sphere.

The mean drag data of the downleg portion of the curve is represented by the straight line with a positive slope. The slope remained constant until the sphere approached re-entry conditions. Here the slope began to decrease. The peak drag acceleration deduced from calculations corresponded to the inflection point of the curve which occurred at approximately 350 seconds. At later times the slope of the curve became increasingly negative until it reached another plateau-like region where the scatter in the data was most probably due to atmospheric turbulence. This conclusion is justified on the basis that the accelerometer performs with great reliability and accuracy in this range of drag accelerations.

Due to the additional air resistance offered by the sphere, its impact time was about 483 seconds compared to approximately 375 seconds for the Cajun rocket. The sphere reached ground level with a speed of about 150 ft/sec (approximately 100 miles/hour) although its peak velocity was over 4000 ft/sec, emphasizing the sharp retardation due to atmospheric drag.

It is also interesting to note that in the time interval, 56 to 90 seconds, the rate of data acquisition was slightly more than one point per second, while in the 20-second interval between

310 and 330 seconds, the rate of acquisition was just over two points per second. This illustrates the capability of the instrumentation to handle data at a rate compatible with the changing drag force imposed upon the sphere during its flight.

The data obtained from Rocket 2, fired at 2230W on 19 June 1962, was generally similar to that obtained from Rocket 1. However, as observed in Figure 3.2, the quality of the data was vastly improved. It can be seen that the experimental points provided a much better approximation to straight lines than the data of Figure 3.1. This was probably due to better performance characteristics of the accelerometer used during this flight, or it could be attributed in part to more accurate balancing of the sphere, thus minimizing inaccuracies due to spin effects. On this flight, sphere ejection also occurred at approximately 56 seconds after rocket launch, but the sphere reached zenith altitude almost 2 seconds later than the previous one, probably due to a slightly higher launch elevation angle. The effective angle of elevation was estimated to be 85° for Rocket 2 compared to 83° for Rocket 1. Impact time was 486.28 seconds.

Except for small differences in related values of ejection

time, peak time, peak altitude, and impact time (see Table 3.7) the general comments on the first two curves of drag acceleration versus elapsed time apply to Rockets 3, 4, and 7 (see Figures 3.3, 3.4 and 3.7). Rocket 3 was fired on 8 July 1962 Rocket 4 was fired on 23 July 1962. In each case, acceleration data of good quality was obtained, and the points were spaced sufficiently close over the region of measurement to obtain a linear function without resorting to excessive smoothing.

It should be mentioned again that Rocket 7, Figure 3.7, was fired for the purpose of obtaining background data on the normal atmosphere, and hence, was not associated directly with a nuclear test. On this flight the sphere was ejected at approximately 55 seconds after launch and impact was recorded at 492 seconds. This was the longest flight recorded for rockets used to make measurements on the normal atmosphere. This can be accounted for in part by the difference in payload weights. Since no beacon equipment was required on Rockets 5, 6, 7, 8, and 9, the average payload weight was reduced to 55 lb compared to about 62 lb for Rockets 1 through 4. The spread in impact times for Rockets 1, 2, 3, 4, and 7 was only 9 seconds (a minimum value of 483 seconds for Rocket 1 and a maximum value of 492 seconds for Rocket 7).

The average impact time for these flights was 486.67 seconds.

The drag acceleration data obtained during the Check Mate event (Rocket 5) is presented in the curve Figure 3.5. The Falling Sphere probe was launched at H + 10 minutes. The first sphere signal was recorded at 53.74 seconds after rocket launch, indicating normal ejection. The first three or four measurements of drag acceleration obtained immdiately following ejection gave spurious values that were smaller than the actual ambient values. This was probably due to the short-duration disturbances set up in the surrounding atmosphere by the explosion that was associated with ejection. Excellent data was obtained over the useful range of the accelerometer. However, this curve exhibits some features that are significantly different from those obtained from measurements made on an atmosphere undisturbed by a nuclear detonation. With reasonable assumptions, both theory and experiment predict that the drag function in a normal atmosphere should vary nearly exponentially with altitude. Hence, a semi-log plot of the upleg and downleg drag acceleration data should give approximately straight lines of equal, but opposite slopes. However, this curve shows a change in slope occurring in both the upleg and downleg portions of the flight. The available data suggests that the ob-

served deviations in slopes were produced by nuclear test effects. Furthermore, the data indicates that the sphere was in flight for 505 seconds after rocket launch. This flight duration is about 18 seconds longer than the average of those flown in an undisturbed atmosphere. The unusually long flight time observed after Check Mate was probably due to atmospheric disturbances induced by the nuclear test.

A Falling Sphere probe (Rocket 6) was launched 15 minutes after the Blue Gill Triple Prime burst. The drag acceleration data obtained from this flight is shown in Figure 3.6. Although one can detect a very small change of slope in the drag acceleration data, the abrupt changes observed in Figure 3.5 are not present in this curve. Sphere ejection was accomplished at the predetermined time of 55 seconds after launch. The flight duration was 495 seconds; 3 seconds longer than that of the background shot (Rocket 7) in an undisturbed atmosphere, and 10 seconds shorter than the Check Mate flight (Rocket 5).

The drag acceleration data obtained from a sphere probe launched at H + 10 minutes on the King Fish event is shown in Figure 3.8. The sphere was ejected at 57 seconds after launch. This later ejection time, a lower angle of elevation (83° effective), and an appropriate azimuth were chosen so the sphere would

more closely enter the region disturbed by the test. The sphere impact time of 492 seconds was 9 seconds later than that of the background shot, Rocket 1, which was fired at the same effective angle of elevation (83°). The change in slope of the downleg acceleration curve indicated that the density (or its percentage deviation from normal) changed sharply at this time, which corresponded to an altitude of about 55 km. This indication is confirmed by the density data which is plotted in Figure 3.27 and discussed in Section 4.1 .

The data obtained after the Tight Rope event (Rocket 9) requires special consideration due to second-stage ignition failure on the Nike-Cajun rocket. The rocket was launched at H + 4 min. The drag acceleration curve presented in Figure 3.9 shows that normal ejection occurred at 51.57 seconds after launch. The curve looks quite different from those previously presented. This is because drag acceleration data was obtained through the peak of the sphere trajectory due to the low altitude (and low velocity) at which sphere ejection occurred. The observed drag acceleration was 4 ft/sec^2 at ejection and decreased to approximately 0.26 ft/sec^2 at peak altitude. The highest acceleration was 48 ft/sec^2 (about 1.5 g) except in the region of turbulence where there existed a wide spread in drag acceleration values.

The sphere impacted at 211 seconds. The new accelerometer developed by the University of Utah was flown in this sphere. The data indicated that the instrument worked very well throughout the limited flight, but conditions were not favorable enough to compare performance with the other type accelerometer used during the series.

It should be noted that no noticeable attenuation of the telemetry signal at 730 Mc was observed in the flights following nuclear detonations. However, this probably would not have been the case if the flights had been at earlier times following the detonation and had been positioned so that the signal had to traverse the fireball to be received.

3.3 PEAK TIME DERIVATION

The peak time of a sphere flight refers to that time at which the sphere attains maximum altitude. Its accurate determination is quite essential to the data reduction process. An error in peak time produces a less accurate sphere trajectory, and this inaccuracy is reflected in the final results. The peak times can be deduced, in principle, from the drag acceleration curves in Figures 3.1 through 3.9, but greater accuracy can be obtained from the use of the special plots shown in Figures 3.10 through 3.18 (Rockets 1 through 9).

It was assumed that the drag acceleration was symmetrical with regard to peak time. Therefore, peak time for each sphere trajectory was determined by carefully comparing the time intercepts of the drag acceleration data obtained on the upleg and dowleg portions of the flight.

In these special curves, drag acceleration was plotted at appropriate intervals of time referred to rocket lift-off, so that the upleg and downleg portions described straight lines that intersected at peak time as determined by the equation

$$t_p = (t_1 + t_2)/2 \qquad (3.2)$$

where t_p is the peak time, t_1 is in the range 50 sec $< t_1 <$ 125 sec, and t_2 is in the range 265 sec $< t_2 <$ 340 sec. An exception to the above values of t_1 and t_2 occurs in the peak time derived from the curve of Figure 3.18 (Rocket 9), because this was not a normal flight. However, it should be noted that if the accelerometer were capable of making measurements throughout a normal sphere trajectory, Figure 3.18 would be a typical drag acceleration curve rather than the exception, and the determination of peak time would be further simplified.

Peak times, derived in this manner for each flight, are summarized in Table 3.7. This table also gives a summary of

sphere ejection times, peak altitudes, and impact times for Rockets 1 through 9.

The success of any graphical method used for deriving peak time depends upon the quality of the data obtained on the upleg and downleg portions of the flight. Excellent data was obtained on all flights, thus making it possible for peak time to be determined with high accuracy in each case.

3.4 RADAR TRAJECTORY DATA

Radar data on the sphere altitude as a function of time during its flight is required for the determination of ambient atmospheric properties. The experimental accuracy of the density and pressure profiles is limited by the precision with which the sphere altitude can be determined as a function of time. This requires that peak altitude (Z_o) be determined by radar with a maximum error of 100 meters.

The DAMP Ship was responsible for radar support of Project 9.1a rockets during the first part of Fish Bowl. The DAMP Ship failed to track Rockets 1 and 2, but some useful radar data were obtained on Rocket 1 from a partial track made by the PMR Range Tracker during a practice mission. Radar coverage by the DAMP Ship was reasonably complete on Rockets

3 and 4, but the accuracy did not meet the experimental requirements stated above. This was probably due in part to uncertainties in the position of the ship.

The radar data for Rockets 3 and 4 are presented in Tables 3.1 and 3.2, respectively, and were furnished to the project through the courtesy of Archie Gold from RCA. The tracking radar used was an AN/FPQ-4. Included in the tables are radar data on the flight azimuth and horizontal range as a function of time. However, this was not a requirement for obtaining measurements on the ambient atmospheric parameters. Except for some scatter in the data, there seem to be no inconsistencies in the tabulated values.

For the Falling Sphere measurements following high-altitude nuclear detonations, it was necessary to have the flight azimuth and horizontal range as a function of time, in addition to the requirements of altitude versus time stated above. This is because the atmospheric properties following a nuclear detonation are a function of position relative to the nuclear fireball.

During the second part of the Fish Bowl Series, radar tracking support was provided by the Range Tracker. Due to its close proximity to the launch site, skin track of the rocket was

considered to be satisfactory. It was therefore possible to dispense with the radar beacons used during the first part of the series when the rockets were tracked by the DAMP Ship. In the absence of a beacon, radar acquisition was achieved by using an optical viewfinder during the rocket burn phase.

Rocket 5, launched at H + 10 minutes on Check Mate was not tracked due to an oversight. However, the remaining four rockets were tracked with reasonably good success: Rocket 6, launched at H + 15 minutes on Blue Gill Triple Prime; Rocket 7, launched at 2300 hours (local time) on 29 October 1962 to obtain background data; Rocket 8, launched at H + 10 minutes on King Fish; and Rocket 9, launched at H + 4 minutes on Tight Rope.

The tracking data is summarized in Tables 3.3, 3.4, 3.5, and 3.6. Reduction of the radar data was performed by Umberto Ysnago at the PMR Computer Facility on Johnston Island

It was desired to have a radar track at least through the peak of the rocket trajectory and this was accomplished on three rockets. Rocket 8 (Table 3.5) was not tracked through peak altitude, but the data obtained was still of considerable value.

It should be noted that the time given in each table corresponded to the length of time the radar had been operating and not

the time of flight of the rocket. To obtain the latter time, a zero correction has to be made. This correction is different in each table and is provided in a footnote. The horizontal range and azimuth are from the particular radar in use. All data is from the shipboard FPS 16 unless otherwise specified. The altitude was measured relative to a plane tangent to the earth at the site of the radar. These values have been corrected for the curvature of the earth to give actual height above the earth before being entered in the tables. Where data is not shown in the tables, there was no radar track of the rocket.

Table 3.4 (Rocket 7) required some clarification, since it was tracked at various times by one or more of the three radar systems. System II was the first to acquire, followed by System I. Both systems tracked for 80 seconds, after which time System II lost track. Twenty-seven seconds later, System III acquired, and System I and System III tracked for 68 seconds, when System I lost track. This probably occurred at the peak of the trajectory. System III continued to track almost to impact. The question can be raised as to how many objects were tracked. When System I first acquired, it must have been tracking the same object as System II, since there was only one object

(the Cajun) at that time, other than the Nike Booster which has a quite different trajectory. However, at flight time of 55 seconds the rocket breaks into three pieces: the motor case, falling sphere, and nose cone. At later times the radars may be tracking one object or any two objects. The estimated impact time of the object tracked by System III was 465 seconds, radar time, or 433.5 seconds, flight time. The impact time of the sphere was measured from telemetry to be 493.1 seconds, flight time. From the relative impact times, the object tracked was probably the rocket motor.

3.5 SPHERE TRAJECTORY DETERMINATION

When adequate radar tracking data is available, the ideal method of determining the sphere trajectory is that given below. This was the method used to determine the trajectory for six of the nine sets of data reduced for this report (Rockets 3, 4, 6, 7, 8, and 9). When the required radar data was not available (as in the case of Rockets 1, 2, and 5), more laborious and less accurate methods of determining the sphere trajectory were employed.

3.5.1 Calculation of Sphere Velocity. The first task is to calculate the sphere velocity V and its horizontal and vertical components as a function of time during its flight.

The basic equation is

$$\overline{V} = \overline{V}_o + \int_{t_o}^{t} (\overline{g} - \overline{a}_D)\, dt \qquad (3.3)$$

where $\overline{V}$ is the sphere velocity at time t

$\overline{V}_o$ is the sphere velocity at time t_o

$\overline{g}$ is the acceleration due to gravity

$\overline{a}_D$ is the drag acceleration, which equals

$$\frac{1}{2} C_D \frac{A}{m} \rho V \overline{V} \qquad (3.4)$$

Where: ρ = atmosphere density

C_D = drag coefficient

A = sphere cross sectional area

m = mass of sphere

The actual calculations are made using the vertical or horizontal components, and with small intervals of time during which changes in the magnitude or direction of the drag acceleration can be neglected.

The equations used are

$$V_v = V_{vo} + (\pm g - a_D \frac{V_v}{V}) (t - t_o) \qquad (3.5)$$

$$V_H = V_{H_o} - a_D \frac{V_H}{V} (t - t_o) \qquad (3.6)$$

$$V^2 = V_v^2 + V_H^2 \qquad (3.7)$$

The calculations are started taking t_o as the sphere peak time (most accurately obtained from the sphere telemetry data). At that time, $V_{vo} = 0$, and a value for V_{H_o} is obtained from the radar data. Because of considerable fluctuations in the values of V_H given by the radar, a mean value over an appreciable time interval is used. A value is taken for g appropriate to the mean altitude over which data was obtained and the latitude of Johnston Island.

$$g_{alt} = 31.20 \text{ ft/sec}^2$$
$$= 950.976 \text{ cm/sec}^2 \qquad (3.8)$$

A vacuum trajectory is calculated from the peak until such time as the drag acceleration is appreciable, working back toward the time of sphere ejection and also forward toward the time of sphere re-entry. Once the drag acceleration has to be included, the calculations are continued using an iterative process with the above equations, with one-second time intervals.

3.5.2 Calculation of Sphere Altitude. The basic equation is

$$\int_{to}^{t} dz = \int_{to}^{t} V_v \, dt \qquad (3.9)$$

For the vacuum region, where the drag acceleration is negligible

this becomes

$$Z = Z_o - \frac{1}{2} g (t - t_o)^2 \qquad (3.10)$$

where Z_o is taken to be the peak altitude, obtained from radar data. The calculation is continued in the drag region, by iteration using

$$Z_2 - Z_1 = \frac{1}{2} (V_{v2} + V_{v1}) (t_2 - t_1) \qquad (3.11)$$

where $t_2 - t_1$ is taken to be one second.

A summary of sphere trajectory data is given in Table 3.7. Sphere ejection and impact times were obtained from telemetry. Peak times (t_o) were determined by methods discussed in Section 3.3. Peak altitude (Z_o) and the horizontal velocity (V_{H_o}) of the sphere at peak altitude were determined by radar when adequate tracking data were available. Note that the peak altitudes in Table 3.7 are corrected values. The nine sets of density data that have been reduced for this report used the values of t_o, Z_o, and V_{H_o} that are given in Table 3.7.

Small errors in the determination of sphere peak time and peak altitude can produce large errors in the density and pressure curves. The altitude deviation in the density and pressure curves due to an incorrect value of t_o is the result of a cumulative error that results from the iterative method employed in the calculations.

A small error can produce a large effect, because the neutral density and pressure vary approximately exponentially as a function of altitude. An error in Z_o simply causes the altitude to be displaced in both the density and pressure curves by the amount of the error and in the same direction, but because of their exponential variation, the change in the pressure and density at a specified altitude may be of considerable magnitude. It is for these reasons that corrected values of Z_o appear in Table 3.7. A detailed discussion of these corrections will be given in the next section (3.6) on atmospheric density.

In the absence of radar tracking data it was possible to make satisfactory estimates of V_{H_o} based upon knowledge of the effective elevation angle of the rocket and other related data. Since the value of V_H was always small compared to the total sphere velocity in the region of measurement, minor inaccuracies in the initial value (V_{H_o}) produced negligible errors in the calculated densities. The values of V_{H_o} for Rockets 1, 2, and 5, were estimated, while the remaining values were obtained from radar data.

3.6 ATMOSPHERIC DENSITY

Atmospheric density was calculated from data obtained from the nine Project 9.1A flights using the relation

$$\rho = \frac{2 m a_D}{A V^2 C_D} \qquad (3.12)$$

This equation was presented and discussed in Chapter 1 as Equation 1.2. The mass to area ratio (m/A) of each sphere was measured before flight; the drag acceleration (a_D) was obtained as a function of time, from telemetry, as discussed in Section 3.2; the sphere velocity (V) was determined from sphere trajectory data by methods described in Section 3.5; and the appropriate values of drag coefficient (C_D) as a function of Mach and Reynolds numbers, were taken from the plot shown in Figure 3.19. Although the plot is similar to the one contained in Reference 4, changes in the values of C_D have been made consistent with new data presented in References 8 and 9. In addition, the curves have been extended from a minimum Reynolds number of 10^1 to 5×10^{-1}. This extension into a region where little experimental data is available was necessary, because, with the improved accelerometer, measurements were made at higher altitudes than formerly. Also plotted in Figure 3.19 are values of the Mach and Reynolds numbers of Sphere 1 as a func-

tion of time during its flight.

The density profiles calculated from Equation 3.12 are shown in Figures 3.20 through 3.28. On each figure is plotted upleg and downleg data. The former begins at the time of sphere ejection, and the latter ends just above re-entry, where the accelerometer high-g limit is reached. At low altitudes the density curves were joined to that of the Rawinsonde data obtained at the same time (when available). Also, the measured densities in each figure are compared with the values of two models. These are a Tropical Atmosphere for 15°N, up to 90 km (Reference 10) and the U.S. Standard Atmosphere (Reference 11).

The density curve shown in Figure 3.20 was deduced from data obtained by Rocket 1. This rocket was fired at 1800 hours (local time) on 1 June 1962, which corresponded to a scheduled launch time of H - 4 hours on Blue Gill (see Table 2.2 for summary of all rocket launchings). The dashed curve, beginning at zero altitude and continuing to 90 km, is that of the Tropical Atmosphere model. Overlapping this is a dotted curve containing the portion of the U.S. Standard Atmosphere between 85 and 110 km. Both these models are included in all the density curves presented in this section, with the exception of Figure 3.28, which will be

discussed separately. Values of the densities in these two models are given in Tables 3.8 (Density, 0-115 km; U.S. Standard Atmosphere, 1962) and 3.9 (Density, 0-90 km; Tropical Atmosphere, 15°N). The mean value of the density data determined experimentally from the upleg and downleg of the sphere flight is represented in the figure by the solid curve. The upleg data begins at 61.6 km and ends at 105 km, while the downleg data begins at 107.9 and ends at 39.1 km. The maximum altitude for which related Rawinsonde data were obtained was 24.0 km. The computed values of sphere and Rawinsonde densities are given in Table 3.10.

The results obtained from Rocket 2 are plotted in Figure 3.21. This rocket was fired at 2230 hours (local time) on 19 June 1962. Since no radar track of this rocket was obtained, altitudes were determined as accurately as possible from sphere telemetry and other related data. The final altitude correction was made by comparing the measured density curve with the two models. No Rawinsonde data was available on this flight. Computed values of sphere densities are given in Table 3.11.

Figure 3.22 shows the results obtained on Rocket 3 which was fired at 2230 hours (local time) on 8 July 1962. The rocket was tracked by radars on the DAMP Ship which was in position

for Star Fish. However, there were errors in the radar-determined altitudes. Two solid curves are used to present mean density values, one corresponding to radar altitudes and the other to corrected altitudes. The data used in each curve is identified by appropriate symbols in the figure legend. No Rawinsonde data was available for this flight. Computed values of sphere densities are given in Table 3.12.

Densities obtained from measurements on Rocket 4 are shown in Figure 3.23. This rocket was fired at 1920 hours (local time) on 23 July 1962. Mean densities corresponding to radar altitudes determined by the DAMP Ship are represented by one solid curve, while the mean densities corresponding to the corrected altitudes are represented by another solid curve. The data used are identified by appropriate symbols in the figure legend. Rawinsonde densities are plotted up to 24 km. Computed values of sphere and Rawinsonde densities are given in Table 3.13.

Densities measured shortly after Check Mate are plotted in Figure 3.24. Unfortunately, due to an oversight, the rocket was not tracked. The lowest altitude at which a density measurement was obtained was matched to the altitude of the same density on the Tropical Atmosphere. By double integration of the drag

acceleration it was then possible to determine all other altitudes. The rocket was launched at H + 10 minutes, and measurements were made between approximately H + 11 and H + 12 minutes (upleg) and H + 15 and H + 16 minutes (downleg). The mean values of the upleg and downleg density data are represented in the figure by two solid curves. Rawinsonde densities are plotted to 24 km. Computed values of sphere and Rawinsonde densities are given in Table 3.14.

The measured densities plotted in Figure 3.25 were obtained from Rocket 6, launched at H + 15 minutes on Blue Gill Triple Prime. A successful radar skin-track of the rocket was made by the PMR Range Tracker, although a small correction had to be made in the altitude data obtained. One solid curve represents the mean densities obtained from the upleg data, while the other solid curve represents the mean densities obtained from the downleg data. Both have been corrected for radar errors in altitude. On this flight, the upleg data, commencing with sphere ejection, extended up to approximately 112 km, while downleg data was obtained as low as 36 km. Rawinsonde densities are plotted up to 24 km. Computed values of measured sphere and Rawinsonde densities corresponding to the plotted values are

given in Table 3.15.

Rocket 7 was flown to obtain background measurements on a normal atmosphere. It was launched at 2300 hours (local time) on 29 October 1962. The density results obtained are plotted in Figure 3.26. Presentation of the data is similar to that of Figures 3.22 and 3.23 (Rockets 3 and 4). Two solid curves are used; one representing the mean densities corresponding to radar determined altitudes, and the other corresponding to corrected altitudes. This provides an opportunity to qualitatively assess the relatively large change in density produced by a small error in altitude. The range over which the measurements were made is comparable to that of Rocket 6 which was previously discussed. Rawinsonde densities are plotted up to 24 km. Table 3.16 gives computed values of sphere and Rawinsonde densities corresponding to the plotted data.

The density profile measured by Rocket 8, launched at H+10 minutes on King Fish, is plotted in Figure 3.27. The mean densities obtained from the upleg and downleg data are again represented by two distinct curves. These curves, when compared with the models and density profiles obtained on a normal atmosphere, will provide information on density perturbations through-

out the sphere trajectory. This comment applies to all post-detonation flights conducted by Project 9.1a. Rawinsonde densities are plotted to 24 km. Computed values of Rawinsonde and sphere densities, corresponding to the plotted data, are given in Table 3.17.

The density data obtained from Rocket 9, launched at H + 4 minutes on Tight Rope, is plotted in Figure 3.28. Due to lack of second-stage ignition the rocket failed to achieve a normal trajectory. This resulted in measurements being made in the altitude range 10 to 21.7 km. This was a very fortunate coincidence, since this region was highly disturbed following the nuclear detonation. The low peak altitude of the sphere flight also accounts for the small amount of data obtained on the upleg portion of the trajectory, since sphere ejection occurred at the normal time of 51.6 sec. In this figure the Tropical Atmosphere is plotted between 0 - 24 km (dashed curve) and also Rawinsonde measurements made shortly before the detonation. Table 3.18 gives the computed values of sphere and Rawinsonde densities corresponding to the plotted data.

It should be emphasized that the set of density values presented in this section were calculated from actual experimental values of drag acceleration measured by the sphere accelerometer.

The experimental curves represent mean densities. The scatter of the experimental points is due, at least in part, to the inability of the accelerometer to accurately measure, with consistency, the small drag accelerations encountered at high altitudes. No attempt was made to smooth these points. In the experimental curves, in regions where the interval between successive measurements was small, every second data point was omitted in order to facilitate reading the results off the curve. The corresponding set of density tables (Tables 3.10 through 3.18), in general, give computed values for only the data plotted.

The determination of the sphere peak altitude (Z_0) may be summarized as follows. For Rocket 9, which had a peak altitude of only 21.7 km, the radar data was used. For all other rockets the peak altitude was determined by matching the lowest altitude at which a density was measured (about 35 km) to the altitude of the same density on the Tropical Atmosphere. By double integration of the drag acceleration it was then possible to determine the peak altitude with precision. The principle on which this method is based is that the atmospheric density is known precisely at altitudes near 35 km, but is not accurately known near 100 km.

The following table summarizes the corrections to the radar-

measured peak altitudes that were derived by this method.

Rocket	Corrected Peak Altitude km	Radar Peak Altitude km	Correction km
3	145.8	147.8	-2.0
4	148.2	146.9	1.3
6	153.7	152.7	1.0
7	153.7	151.7	2.0
8	149.5	149.0	0.5

3.7 CALCULATION OF ATMOSPHERIC TEMPERATURE

It is possible to deduce temperature profiles from values of density as a function of altitude. To obtain accurate temperatures, precise values of density and a good method of analysis are required. The theory and techniques required have been discussed in a number of publications, including the "Revision of U. S. Standard Atmosphere, 90 to 700 km" (Reference 12). The method of starting from a low altitude and extrapolating the temperature upward in straight-line segments was attempted and abandoned for two reasons. One was that it is a trial and error method and thus relatively slow and unsuitable for the reduction of a large quantity of data. Secondly, this technique does not yield a unique solution, and a temperature profile could be obtained which differed

considerably from the actual one.

Thus, the method of integrating down was tried and found to be rapid and, with one known reservation, accurate and unique. In this method the formula

$$T_M = T_{M_r} \frac{\rho_r}{\rho} + \frac{Q}{\rho} \int_h^{h_r} \rho \, dh \qquad (3.13)$$

is used. T_{M_r} and ρ_r are temperature and density, respectively, at the reference altitude h_r, which is the highest altitude at which measurements were made. T_M and ρ are the corresponding quantities at any lower altitude h, and Q is a constant. The molecular-scale temperature used in Equation 3.13 is defined by

$$T_M = \frac{M_o}{M} T \qquad (3.14)$$

where M_o is the mean molecular weight at sea level, M is the mean molecular weight at a given altitude, and T is the kinetic temperature. Up to a geometric altitude of 90 km, the molecular weight ratio $M_o/M = 1$, and therefore $T_M = T$. Above 90 km, M_o/M is greater than unity, and hence, T_M is greater than T. Since the density data obtained by Project 9.1a during Fish Bowl included altitudes above 90 km, a simplification in the calculations resulted from the use of Equation 3.13. This gave molecular temperatures as a function of altitude. Equation 1.7 (see

Section 1.3, Theory) could have been used to determine kinetic temperatures. However, it would have involved assumptions as to the composition, and hence, values of M above 90 km.

In order to use the downward integration technique it is necessary to assume a value of T_{M_r} and apply numerical integration to the density profile. The only source of inaccuracy when using this method is in the value of T_{M_r}, and any error due to this is negligible at altitudes more than 10 km below the reference level. One big advantage is that the values of the calculated temperatures are independent of any error in the altitude assignment of the densities, since only ratios of densities and altitude increments are involved in Equation 3.13.

Molecular temperature curves calculated from measurements obtained from Rockets 1 through 9 are shown in Figures 3.29 through 3.37. Except for Figure 3.37, these data are compared with two models: the Tropical Atmosphere model, 0-90 km (Reference 10) and the portion of the U.S. Standard Atmosphere, 1962 (Reference 11) between 85-115 km. The Tropical and U.S. Standard Atmospheres are represented in the figures by dashed and dotted curves, respectively. Values of the Tropical Atmosphere temperatures are given in Table 3.20 and values of the

U. S. Standard Atmosphere temperatures are given in Table 3.19. Rawinsonde temperatures obtained before each flight are plotted in the curves, when this data was available. Rocket 9 (Figure 3.37) did not achieve a normal trajectory. It is for this reason that just the portion of the Tropical Atmosphere between 0-24 km was used to compare sphere and Rawinsonde temperature measurements.

Figure 3.29 shows the temperature data obtained from Rocket 1. Molecular temperature (degrees, K) is plotted as a function of geometric altitude (km). Both the upleg and downleg temperature data (appropriately identified in the figure legend) were individually calculated from values taken from the density curves in altitude increments of 4 km. The value used for T_{M_r} in Equation 3.13 was 250.65°K, the molecular temperature at 108 km in the U.S. Standard Atmosphere. Rocket launch dates and times are summarized in Table 2.2. Rawinsonde temperature data obtained shortly before the flight is plotted from ground level to 24 km. Table 3.21 gives the values of temperature used to plot the sphere and Rawinsonde curves of Figure 3.29.

Temperature data obtained from Rockets 2 and 3 are shown in Figures 3.30 and 3.31, respectively. Because of similarities

in the temperature curves plotted from data obtained on these two flights, they are discussed jointly. In both figures the calculated temperature data are derived from a single curve which is the mean value of measured upleg and downleg densities. Rawinsonde data was not available for either flight. The value used for T_{M_r} for Rocket 2 was 230.65°K, the molecular temperature at 104 km in the U.S. Standard Atmosphere. As a result of a subsequent lowering of the altitude by 0.6 km this temperature should have been lowered by 3°K. However, the correction was not important, since the value used for T_{M_r} is only an estimate whose effect is small at lower altitudes. For example, a change of 3°K at 104 km corresponds to a change of only 0.15°K at 94 km. The value used for T_{M_r} for Rocket 3 was 210.65°K, the molecular temperature at 100 km in the U.S. Standard Atmosphere. Again, as a result of a subsequent lowering of the altitude by 2 km this temperature should have been lowered by 6°K. The values of the plotted data appear in Tables 3.22 and 3.23.

The temperature profiles calculated from data obtained on Rockets 4 and 7 are shown in Figures 3.32 and 3.35. The general description of the results obtained apply equally to both flights. The temperature curves were computed from mean density data

associated with each flight. Equal altitude increments of 4 km were used to calculate the temperature data. The value used for T_{M_r} for both rockets 4 and 7 was 250.65°K, the molecular temperature at 108 km in the U.S. Standard Atmosphere. Rawinsonde temperature results are plotted from ground level to 24 km. The values of sphere and Rawinsonde temperature data used in the figures are given in Tables 3.24 and 3.27.

All the temperature results thus far presented (Rockets 1, 2, 3, 4, and 7) were obtained from flights that were used to make measurements on the normal atmosphere. The results to be discussed in the remainder of this section were obtained from rockets that were launched shortly after a nuclear detonation. For launch details, see Table 2.2, Summary of Rocket Launchings.

The results obtained from Rockets 5, 6, and 8 are shown in Figures 3.33, 3.34, and 3.36. Each curve consists of two distinct temperature profiles computed from separate density data obtained on the ascending and descending portions of the sphere trajectory. In most cases, measurements obtained on a normal atmosphere show negligible differences between the upleg and downleg density and temperature data. This fact provides the justification for the type of mean data plot shown in Figures 3.30,

3.31, 3.32, and 3.35. However, on the flights following a nuclear detonation, temperature perturbations, with a time and position dependence, were anticipated. It was, therefore, reasonable to expect that significant differences in atmospheric parameters could occur during the time required for the sphere to make measurements on the upleg and downleg portions of its trajectory.

For Rocket 5 (Figure 3.33) the value used for T_{M_r} for the downleg data was 260.65°K, the molecular temperature at 110 km in the U.S. Standard Atmosphere. For the upleg data it was necessary to use a value for T_{M_r} that was 25 degrees higher. For Rocket 6 it was satisfactory to use a value of 270.0°K for T_{M_r} for both the upleg and downleg data. This is virtually the molecular temperature in the U.S. Standard Atmosphere (270.65°K) at 111 km. Again, it was satisfactory to use the same value of T_{M_r} (220.65°K) for both the upleg and downleg data of Rocket 8. This is the molecular temperature in the U.S. Standard Atmosphere at 102 km. Subsequently, the altitudes were raised by 0.5 km. However, the change in the temperatures was negligible, as in previous cases where small corrections in altitude were made.

Temperature data obtained by Rawinsondes before the nuclear detonations are plotted from ground level to 24 km. Tables 3.25, 3.26, and 3.28 give the values of temperature that were plotted for Rockets 5, 6, and 8.

In Figure 3.37 is plotted the temperature of the Tropical Atmosphere model between 0 and 24 km and Rawinsonde temperature data obtained just before the Tight Rope event. Two solutions of Equation 3.13 for the temperature measured shortly after the detonation are plotted. For such highly disturbed conditions it is difficult to know what value to take for T_{M_r}. The solutions given may only be regarded as typical and correspond to values of T_{M_r} at 21.6 km of 450°K and 350°K, respectively. The significance and interpretation of these results will be discussed in Chapter 4. The temperatures plotted in Figure 3.37 are given in Table 3.29.

3.8 ATMOSPHERIC PRESSURE

The pressure data given in Tables 3.32 through 3.40 and plotted in Figures 3.38 through 3.46 were computed from the density and temperature data obtained from Rockets 1 through 9, respectively. The relationship between density, temperature, and pressure is given by the perfect gas law which is expressed

by the equation,

$$P = \rho \frac{R T_M}{M_o} \tag{3.15}$$

where P is the pressure, ρ is the density, T_M is the molecular temperature, R is the universal gas constant, and M_o is the mean molecular weight at sea level. This is the equation that was used to compute the pressure curves. All the curves were plotted in altitude increments of 4 km, except for Figure 3.46 which was plotted in altitude increments of 2 km.

In Figures 3.38 through 3.45 the Tropical Atmosphere model (Reference 10) is plotted between 0-90 km. Also plotted is the portion of the U.S. Standard Atmosphere, 1962 (Reference 11) between 85-110 km approximately, depending upon the altitude range of the data. In Figure 3.46, the portions of both models between 0-24 km are plotted. Table 3.30 gives values of the U.S. Standard Atmosphere pressure between 0-115 km. The values given in the table overlap the experimental data at both the highest and lowest altitudes. Table 3.31 gives values of the Tropical Atmosphere pressure between 0-90 km. Rawinsonde data obtained shortly before each flight (with the exception of Rockets 2 and 3) were plotted to 24 km.

In Figure 3.38 the pressure results obtained on Rocket 1 are

shown. Consistent with the density and temperature curves, the upleg and downleg data required separate plots. Upleg data was obtained over the altitude range 60-108 km, approximately, while downleg data was obtained between 108-36 km.

The pressure curve computed from data obtained on Rocket 2 is shown in Figure 3.39. The single experimental curve in the figure represents the mean value of the upleg and downleg data. Pressure results were obtained in the altitude range 35-103 km, approximately.

The pressure results obtained from Rocket 3 are shown in Figure 3.40. The experimental data are plotted in two separate curves, both of which represent mean values of upleg and downleg data. The curve shown about 2 km higher than the models was obtained from radar altitude data. An altitude correction was made to obtain the second curve, but it should be noted that this is not a new correction. It merely reflects the original altitude correction that was made in the corresponding density plot.

Figures 3.41 and 3.44 show the pressure results obtained on Rockets 4 and 7. Each of these plots is similar to that of Rocket 3, except that the second curve obtained by using radar determined altitudes is omitted. The corrected curve shown in each figure

represents the mean data obtained on the upleg and downleg portions of the sphere flight, with the same altitudes used in the preceding density and temperature plots for these rockets.

The pressure results obtained on Rockets 5, 6, 8, and 9 are shown in Figures 3.42, 3.43, 3.45, and 3.46. These rockets were launched shortly after nuclear detonations, and the results show small pressure perturbations that were probably produced by the nuclear tests. In Figures 3.42, 3.43, and 3.45, the curves obtained from the upleg and downleg data are, in general, different at a given altitude. These differences are similar to those observed in the corresponding curves of density and temperature. The data shown in Figures 3.42 and 3.43 (Rockets 5 and 6) cover an altitude range of approximately 34 to 110 km, while that of Figure 3.45 (Rocket 8) is in the altitude range 39-103 km.

In Figure 3.46 (Rocket 9) three experimental pressure profiles are shown. These curves are based upon three temperature profiles, each corresponding to a different value of T_{M_r} (initial temperature) assumed at 21.6 km. The respective values of T_{M_r} are 350, 450, and 650°K. Note that the temperature curve corresponding to $T_{M_r} = 650°K$ was not plotted in Figure 3.37.

TABLE 3.1 RADAR TRAJECTORY DATA, ROCKET 3, BACKGROUND MEASUREMENT, STAR FISH PRIME

* Radar Time	Azimuth from DAMP Ship	Altitude	Horizontal Range	* Radar Time	Azimuth from DAMP Ship	Altitude	Horizontal Range
seconds	degrees T	km	km	seconds	degrees T	km	km
-1781.32	192.03	33.22	12.08	-1729.26	190.14	94.37	13.78
-1779.32	191.08	36.50	14.89	-1727.26	190.13	96.50	14.03
-1773.32	188.13	37.20	14.79	-1725.26	190.09	98.18	14.45
-1765.31	188.09	43.05	16.03	-1723.26	190.11	100.26	14.66
-1761.31	190.12	56.46	12.20	-1721.26	190.13	102.22	14.89
-1759.31	190.22	60.12	9.48	-1719.26	190.09	103.64	15.29
-1757.31	189.86	62.00	10.34	-1717.26	190.08	105.62	15.55
-1755.31	188.76	65.86	13.78	-1715.26	190.19	107.37	15.81
-1753.31	190.28	68.20	10.24	-1713.26	190.06	109.82	16.18
-1751.31	190.27	70.51	10.53	-1711.26	190.04	110.45	16.52
-1749.31	190.29	73.24	10.72	-1709.26	190.04	112.14	16.79
-1747.31	190.24	74.95	11.22	-1707.26	190.05	113.72	17.05
-1745.31	190.23	77.81	11.40	-1705.26	190.10	115.18	17.34
-1743.31	190.28	79.90	11.70	-1703.26	189.98	116.85	17.66
-1741.26	190.27	81.97	12.04	-1701.26	189.97	118.28	17.97
-1739.26	190.20	84.08	12.36	-1699.26	189.99	119.83	18.19
-1737.26	190.13	86.36	12.60	-1697.26	189.98	121.09	18.54
-1735.26	190.18	88.35	12.92	-1695.26	189.97	122.64	18.81
-1733.26	190.20	90.63	13.15	-1693.26	189.96	124.08	19.00
-1731.26	190.18	92.47	13.49	-1691.26	190.07	125.80	19.13

* Referred to actual H = 0

TABLE 3.1 (cont'd)

* Radar Time	Azimuth from DAMP Ship	Altitude	Horizontal Range	* Radar Time	Azimuth from DAMP Ship	Altitude	Horizontal Range
seconds	degrees T	km	km	seconds	degrees T	km	km
-1689.26	189.93	126.15	19.82	-1649.26	189.82	143.82	25.53
-1687.26	189.93	127.77	19.92	-1647.26	189.75	143.91	26.01
-1685.26	189.95	129.31	20.09	-1645.26	189.75	145.13	26.00
-1683.26	189.94	129.80	20.61	-1643.26	189.71	144.82	26.55
-1681.26	189.90	130.94	20.95	-1641.26	189.76	144.98	26.90
-1679.26	189.86	132.17	21.16	-1639.36	189.77	145.04	27.44
-1677.26	189.88	133.18	21.47	-1637.26	189.68	145.77	27.53
-1675.26	189.90	134.16	21.77	-1635.26	189.73	145.91	27.78
-1673.26	189.86	135.00	22.09	-1633.26	189.87	146.19	27.94
-1671.26	189.85	135.94	22.40	-1631.26	189.69	146.40	28.37
-1669.26	189.85	137.10	22.56	-1629.26	189.71	146.64	28.61
-1667.26	189.84	137.61	23.00	-1627.26	189.67	146.27	29.10
-1665.26	189.80	138.29	23.36	-1625.26	189.67	146.46	29.35
-1663.26	189.79	139.30	23.55	-1623.26	189.69	146.83	29.49
-1661.26	189.81	139.83	23.97	-1621.26	189.65	146.46	29.94
-1659.26	189.80	140.64	24.16	-1619.26	189.64	146.43	30.26
-1657.26	189.77	141.29	24.47	-1617.26	189.64	146.40	30.51
-1655.26	189.76	142.42	24.61	-1615.26	189.60	146.24	30.82
-1653.26	189.98	142.40	25.00	-1613.26	189.62	146.14	31.08
-1651.26	189.80	143.41	25.19	-1611.26	189.64	145.91	31.38

*Referred to actual H = 0

TABLE 3.1 (cont'd)

*Radar Time	Azimuth from DAMP Ship	Altitude	Horizontal Range	*Radar Time	Azimuth from DAMP Ship	Altitude	Horizontal Range
seconds	degrees T	km	km	seconds	degrees T	km	km
-1609.26	189.61	145.66	31.71	-1569.26	189.45	132.92	37.74
-1607.26	189.60	145.26	32.07	-1567.26	189.45	131.87	38.05
-1605.26	189.56	144.94	32.40	-1565.26	189.44	130.57	38.43
-1603.26	189.56	144.94	32.52	-1563.26	189.44	129.73	38.65
-1601.26	189.56	144.36	32.89	-1561.26	189.40	128.44	39.02
-1599.26	189.54	143.72	33.31	-1559.26	189.40	127.26	39.33
-1597.26	189.57	143.75	33.39	-1557.26	189.39	126.36	39.50
-1595.26	189.53	143.16	33.73	-1555.26	189.39	125.16	39.78
-1593.26	189.53	142.66	34.05	-1553.26	189.41	123.63	40.14
-1591.26	189.55	141.93	34.36	-1551.26	189.40	122.37	40.43
-1589.26	189.54	141.07	34.75	-1549.26	189.40	121.05	40.70
-1587.26	189.51	140.43	35.08	-1547.26	189.36	119.46	41.14
-1585.26	189.50	139.55	35.45	-1545.26	189.36	118.33	41.30
-1583.26	189.52	139.19	35.60	-1543.26	189.38	116.81	41.59
-1581.26	189.49	138.57	35.84	-1541.26	189.32	114.91	42.05
-1579.26	189.51	137.52	36.23	-1539.26	189.35	113.79	42.20
-1577.26	189.48	136.64	36.57	-1537.21	189.34	111.72	42.64
-1575.26	189.47	135.92	36.79	-1535.21	189.30	109.82	43.05
-1573.26	189.46	134.70	37.22	-1533.21	189.30	108.78	43.16
-1571.26	189.49	133.84	37.45	-1531.21	189.30	107.06	43.47

*Referred to actual H = 0

TABLE 3.1 (cont'd)

* Radar Time	Azimuth from DAMP Ship	Altitude	Horizontal Range	*Radar Time	Azimuth from DAMP Ship	Altitude	Horizontal Range
seconds	degrees T	km	km	seconds	degrees T	km	km
-1529.21	189.96	104.61	43.54	-1489.21	189.10	62.57	49.86
-1527.21	189.54	103.01	44.00	-1487.21	189.12	60.34	50.10
-1525.21	189.25	101.27	44.51	-1485.21	189.09	57.51	50.47
-1523.21	189.28	99.44	44.79	-1483.21	189.06	55.00	50.78
-1521.21	189.25	97.82	45.03	-1481.21	189.09	52.45	51.04
-1519.21	189.24	95.88	45.35	-1479.21	189.08	49.69	51.37
-1517.21	189.24	93.81	45.68	-1477.21	189.05	47.20	51.65
-1515.21	189.20	91.60	46.04	-1475.21	189.05	44.63	51.93
-1513.21	189.20	90.08	46.20	-1473.20	189.02	41.72	52.26
-1511.21	189.34	87.76	46.45	-1471.20	189.04	39.57	52.47
-1509.21	189.22	85.75	46.80	-1469.20	189.01	36.56	52.85
-1507.21	189.22	83.53	47.14	-1467.20	188.98	34.07	53.11
-1505.21	189.24	81.91	47.29	-1465.15	189.06	32.15	53.24
-1503.21	189.18	79.05	47.74	-1463.15	189.09	30.21	53.40
-1501.21	189.18	76.85	48.04	-1461.15	188.97	26.65	53.90
-1499.21	189.20	74.51	48.32	-1459.15	188.97	24.81	54.11
-1497.21	189.14	72.04	48.71	-1457.15	188.99	22.39	54.43
-1495.21	189.11	70.13	48.91	-1455.15	188.97	20.37	54.58
-1493.21	189.13	67.43	49.25	-1453.15	188.99	19.73	54.62
-1491.21	189.10	64.95	49.58	-1451.15	188.94	18.05	54.83

*Referred to actual H = 0

TABLE 3.2 RADAR TRAJECTORY DATA, ROCKET 4, BACKGROUND MEASUREMENT, BLUE GILL TRIPLE PRIME

Radar Time	Azimuth	Altitude	Horizontal Range	Radar Time	Azimuth	Altitude	Horizontal Range
seconds	degrees T	km	km	seconds	degrees T	km	km
13.30	188.54	9.74	3.16	73.30	185.71	84.21	10.00
16.30	188.32	11.18	3.60	76.30	185.68	87.45	10.39
19.30	188.20	12.66	3.74	79.30	185.56	90.50	10.86
22.30	188.07	16.03	3.87	82.30	185.44	93.53	11.44
25.30	187.92	21.05	4.00	85.30	185.32	96.55	11.87
28.30	187.78	25.73	4.12	88.30	185.20	99.41	12.28
31.30	187.54	30.31	4.47	91.30	185.08	102.09	12.84
34.60	187.50	34.75	4.58	94.30	184.97	104.87	13.26
37.30	187.36	39.06	4.89	97.30	184.85	107.41	13.78
40.30	187.13	43.37	5.29	100.30	184.74	109.94	14.24
43.30	186.99	47.42	5.65	103.30	184.72	112.44	14.66
46.30	186.86	51.54	6.08	106.30	184.52	114.78	15.19
49.30	186.72	55.54	6.48	109.30	184.50	117.05	15.68
52.30	186.69	59.37	6.78	112.30	184.39	119.22	16.12
55.30	186.46	63.19	7.34	115.30	184.28	121.30	16.61
58.30	186.33	66.90	7.74	118.30	184.57	123.30	17.11
61.30	186.30	70.60	8.12	121.30	184.06	125.23	17.63
64.30	186.08	74.06	8.66	124.30	184.04	127.09	18.02
67.30	186.05	77.60	9.05	127.30	183.94	128.85	18.57
70.30	185.93	80.92	9.53	130.30	183.83	130.58	19.02

TABLE 3.2 (cont'd)

Radar Time	Azimuth	Altitude	Horizontal Range	Radar Time	Azimuth	Altitude	Horizontal Range
seconds	degrees T	km	km	seconds	degrees T	km	km
133.30	183.73	132.10	19.57	196.30	181.61	145.64	25.80
136.30	183.71	133.64	19.94	199.30	187.48	145.91	25.96
139.30	183.52	135.04	20.51	202.30	182.50	145.00	30.56
142.30	183.50	136.38	20.97	205.30	182.87	147.06	28.24
145.30	183.40	137.70	21.37	208.30	182.74	145.03	30.36
148.30	183.30	138.85	21.93	211.30	192.80	143.45	31.36
151.30	183.20	139.93	22.40	214.30	182.29	142.22	33.04
154.30	183.19	140.98	22.82	217.30	182.16	143.94	31.22
157.30	183.09	141.82	23.40	220.30	182.24	143.55	31.27
160.30	182.99	142.70	23.85	223.35	182.10	142.79	30.04
163.30	182.89	143.41	24.37	226.30	182.38	140.90	32.51
166.30	182.88	144.20	24.75	229.30	181.72	139.88	33.57
169.30	182.78	144.64	25.35	232.30	181.49	140.78	32.68
172.30	182.60	145.31	25.78	235.30	181.48	140.86	32.84
175.30	182.67	145.49	26.36	238.30	182.64	141.32	31.32
178.30	182.49	145.91	26.87	241.30	181.87	128.89	40.08
181.30	184.69	144.21	27.18	244.30	176.25	133.92	43.98
187.30	181.65	143.67	26.94	247.30	180.80	132.54	36.45
190.30	181.64	142.98	22.40	250.30	181.03	128.93	38.14
193.35	181.52	140.02	22.04	253.30	180.87	126.84	39.01

TABLE 3.2 (cont'd)

Radar Time	Azimuth	Altitude	Horizontal Range	Radar Time	Azimuth	Altitude	Horizontal Range
seconds	degrees T	km	km	seconds	degrees T	km	km
256.30	180.79	125.03	39.54	316.30	179.55	70.06	49.49
259.30	180.63	123.04	40.09	319.30	179.47	66.49	49.96
262.30	180.62	121.08	40.49	322.30	179.40	62.63	50.58
265.30	180.54	118.89	41.09	325.30	179.33	59.08	50.95
268.30	180.46	116.81	41.48	328.30	179.33	55.05	51.48
271.30	180.38	114.40	42.09	331.30	179.26	51.19	51.95
274.30	180.31	112.10	42.55	334.30	179.11	47.11	52.51
277.30	180.30	109.70	42.97	337.30	179.12	43.05	52.95
280.30	180.23	107.10	43.52	340.30	179.05	38.90	53.48
283.30	180.15	104.46	44.04	343.30	178.98	34.75	53.94
286.30	180.07	101.77	44.55	346.30	178.91	30.59	54.44
289.30	180.00	98.95	45.06	349.30	178.84	26.49	54.91
292.30	180.00	96.14	45.54	352.30	178.77	22.77	55.31
295.30	180.00	93.20	45.98	355.30	178.77	19.32	55.65
298.30	179.92	90.07	46.52	358.30	178.77	16.35	55.96
301.30	179.84	86.94	47.06	361.35	178.70	14.17	56.22
304.30	179.77	83.85	47.46	364.30	178.70	12.54	56.36
307.30	179.69	80.45	48.01	367.30	178.63	11.03	56.50
310.30	179.62	77.15	48.50	370.30	178.63	9.06	56.58
313.30	179.62	73.68	49.00	373.30	178.56	8.68	56.70

TABLE 3.3 RADAR TRAJECTORY DATA, ROCKET 6, BLUE GILL TRIPLE PRIME

Radar Time	Altitude	Horizontal Range	Azimuth	Radar Time	Altitude	Horizontal Range	Azimuth
seconds	feet	feet	degrees	seconds	feet	feet	degrees
4	--	--	[a]191.6784	24	106245	10924	168.1979
5	--	--	[a]191.2884	25	111218	11457	167.8247
6	--	--	[a]188.4045	26	116157	11992	167.5391
7	--	--	[a]189.4317	27	121058	12521	167.3890
8	--	--	[a]189.9371	28	125923	13041	167.1974
9	--	--	[a]187.7783	29	130754	13548	166.9194
10	38644	4285	179.1204	30	135548	14075	166.6540
11	40855	4237	178.9985	31	140310	14612	166.4535
12	43725	4528	177.3718	32	145040	15147	166.3154
13	48079	5010	175.4372	33	149738	15665	166.2396
14	53546	5507	174.1535	34	154402	16188	166.0583
15	59255	6092	173.2341	35	159031	16715	165.8039
16	64759	6659	172.3548	36	163629	17248	165.8472
17	70160	7198	171.6960	37	168196	17745	165.7040
18	75481	7727	170.9846	38	172728	18263	165.5179
19	80736	8267	170.3213	39	177230	18798	165.3813
20	85932	8803	169.7202	40	181696	19335	165.2117
21	91076	9345	169.3896	41	186131	19841	165.1660
22	96175	9877	169.0311	42	190535	20360	165.0458
23	101233	10401	168.6827	43	194907	20887	165.0112

TABLE 3.3 (Cont'd.)

Radar Time	Altitude	Horizontal Range	Azimuth	Radar Time	Altitude	Horizontal Range	Azimuth
seconds	feet	feet	degrees	seconds	feet	feet	degrees
44	199242	21434	164.9356	64	279379	31743	164.1697
45	203548	21950	164.8412	65	283046	32288	164.1093
46	207827	22453	164.7643	66	286699	32808	164.0059
47	212072	22953	164.6438	67	290328	33315	163.9857
48	216279	23483	164.6304	68	293926	33821	163.9197
49	220458	24002	164.6507	69	297477	34308	163.9039
50	224608	24521	164.5896	70	301003	34812	163.8700
51	228725	25023	164.4677	71	304516	35360	163.7371
52	232814	25535	164.4687	72	307982	35934	163.7282
53	236870	26058	164.4588	73	311404	36507	163.7539
54	240894	26580	164.3664	74	314806	36958	164.0138
55	244895	27104	164.2380	75	318189	37420	164.0643
56	248867	27614	164.1477	76	321535	37971	164.0258
57	252798	28122	164.1796	77	324834	38582	163.9170
58	256679	28687	164.2559	78	328119	39134	163.9362
59	260547	29214	164.1738	79	331361	39574	163.8662
60	264395	29703	164.0801	80	334578	39982	163.7810
61	268199	30192	164.0135	81	337719	40514	163.7244
62	271956	30704	164.0711	82	340855	41198	163.7742
63	275679	31311	164.1505	83	343990	41683	163.9146

TABLE 3.3 (Cont'd.)

Radar Time	Altitude	Horizontal Range	Azimuth	Radar Time	Altitude	Horizontal Range	Azimuth
Seconds	feet	feet	degrees	seconds	feet	feet	degrees
84	347091	42162	164.0615	112	421058	56474	163.9781
85	350148	42599	164.1505	113	423023	56849	163.5843
86	353183	43036	164.1134	114	425059	57118	163.3021
87	356132	43535	163.9379	115	427210	57548	163.1679
88	359050	44281	163.7237	116	429312	58098	163.1998
89	362004	44953	163.6341	117	431328	58762	163.3735
90	364920	45291	163.7124	118	433346	59652	163.5802
91	367764	45674	163.7265	119	435317	60430	163.8363
92	370624	46359	163.7265	120	437340	60533	164.2366
93	373510	46867	163.7536	121	439305	60644	164.6301
102	397418	51209	163.6798	122	441172	61295	164.9226
103	399942	51609	163.4875	123	443069	61674	165.0016
104	402417	52218	163.5047	124	445003	61672	164.7932
105	404763	52827	163.6767	125	446807	62138	164.5738
106	407005	53379	163.8422	126	448513	63279	164.3740
107	409449	53759	164.0382	127	450249	63976	164.1491
108	412001	54131	164.2253	128	452024	64242	163.9661
109	414352	54597	164.3173	129	453713	64805	163.7632
110	416592	55188	164.3877	130	455370	65588	163.6485
111	418861	55893	164.2703	131	457170	65946	163.6705

TABLE 3.3 (Cont'd.)

Radar Time	Altitude	Horizontal Range	Azimuth	Radar Time	Altitude	Horizontal Range	Azimuth
seconds	feet	feet	degrees	seconds	feet	feet	degrees
132	459174	65927	163.7292	152	484981	76226	164.1669
133	460919	66361	164.0478	153	485869	77009	164.2655
134	462347	67221	164.2792	154	486836	77543	164.3722
135	463765	68078	164.4653	155	487724	78017	164.5017
136	465285	68655	164.6301	156	488580	78535	164.5401
137	466749	69023	164.7901	157	489498	79111	164.6352
138	468198	69254	164.9765	158	490472	79651	164.8622
139	469634	69391	165.0462	159	491347	80079	165.0448
140	471072	69599	164.8697	160	492100	79930	165.1090
141	472386	70300	164.8007	161	492744	79641	165.1080
142	473619	71113	164.6153	162	493421	79867	164.9909
143	474876	71657	164.4031	163	494065	80798	164.9109
144	476131	72182	164.1903	164	494628	81720	164.8834
145	477272	73280	164.0341	165	495164	82641	164.8134
146	478363	74376	163.9290	166	495713	83492	164.6644
147	479460	75259	163.9867	167	496189	84336	164.4107
148	480617	75515	164.0320	168	496605	85123	164.2871
149	481766	75413	164.1175	169	497044	85794	164.2734
150	482941	75219	164.0691	170	497485	86296	164.2418
151	484032	75531	164.0873	171	497919	86694	164.2583

TABLE 3.3 (Cont'd.)

Radar Time	Altitude	Horizontal Range	Azimuth	Radar Time	Altitude	Horizontal Range	Azimuth
Seconds	feet	feet	degrees	seconds	feet	feet	degrees
172	498312	87184	164.2256	187	500467	94162	165.0819
173	498643	87709	164.2703	188	500393	94592	165.0403
174	499029	88121	164.3791	189	500305	95120	165.0469
175	499427	88461	164.4601	190	500103	95801	165.0280
176	499688	88726	164.5439	191	499806	96538	165.0558
177	499891	88882	164.5532	192	499584	97116	165.0167
178	500172	89005	164.6084	193	499478	97444	164.9755
179	500400	89389	164.6915	194	499253	97649	164.9051
180	500544	89807	164.8519	195	498894	97704	164.9246
181	500633	90340	164.8859	196	498564	97986	165.0750
182	500737	90924	164.8354	197	498175	98801	165.2000
183	500824	91335	164.8663	198	497626	99927	165.2007
184	500810	91727	164.9188	199	497099	10078	165.1763
185	500692	92598	165.0239	200	496548	101558	165.2175
186	500579	93541	165.0802				

[a] Data from MPS 26.

[b] To obtain the actual flight time, add 8.5 seconds to the radar time throughout the table.

TABLE 3.4 RADAR TRAJECTORY DATA, ROCKET 7, BACKGROUND MEASUREMENT

System I(FPS 16)				System II (MPS 26)			
Radar Time	Altitude	Horizontal Range	Azimuth	Radar Time	Altitude	Horizontal Range	Azimuth
seconds	feet	feet	degrees	seconds	feet	feet	degrees
42	--	--	--	42	27814	4498	177.5613
43	--	--	--	43	29950	4701	175.9790
44	--	--	--	44	31874	4962	173.4885
45	--	--	--	45	33748	5164	171.0066
46	--	--	--	46	35541	5338	174.2071
47	--	--	--	47	37261	5536	172.8245
48	--	--	--	48	38920	5757	171.9607
49	--	--	--	49	40475	5945	165.4527
50	--	--	--	50	42008	6136	162.7902
51	42720	5582	161.3898	51	44050	6413	161.3898
52	47650	6471	160.3928	52	47305	6844	160.3928
53	52008	7149	159.7367	53	52036	7476	159.7367
54	57371	7818	159.1510	54	57609	8251	159.1510
55	62980	8576	158.5948	55	63230	9051	158.5948
56	68402	9307	158.1636	56	68668	9817	158.1636
57	73738	10030	157.7938	57	74204	10526	157.7938
58	79003	10754	157.5360	58	79298	11300	157.5360
59	84204	11472	157.2500	59	84521	12123	157.2500
60	89350	12193	156.5592	60	89589	12869	156.9592
61	94446	12909	156.6873	61	94580	13555	156.6873

TABLE 3.4 (Cont'd.)

System I (FPS 16)				System II (MPS 26)			
Radar Time	Altitude	Horizontal Range	Azimuth	Radar Time	Altitude	Horizontal Range	Azimuth
seconds	feet	feet	degrees	seconds	feet	feet	degrees
62	99499	13631	156.4916	62	99584	14248	156.4916
63	104510	14340	156.3745	63	104627	14985	156.3745
64	109488	15036	156.1754	64	109603	15769	156.1754
65	114426	15739	156.0364	65	114540	16590	156.0364
66	119326	16455	155.9049	66	119473	17228	155.9049
67	124189	17169	155.8702	67	124365	17887	155.8702
68	129017	17877	155.7837	68	129204	18644	155.7837
69	133811	18580	155.5835	69	133995	19462	155.5835
70	138570	19289	155.4551	70	138768	20210	155.4551
71	143295	20006	155.3861	71	143517	20947	155.3861
72	147990	20710	155.4421	72	148141	21602	155.4421
73	152652	21414	155.2965	73	152711	22234	155.2965
74	157280	22095	155.1980	74	157317	22975	155.1980
75	161872	22805	155.1437	75	161930	23846	155.1457
76	166434	23524	155.1066	76	166486	24642	155.1066
77	170965	24224	155.0527	77	171026	25311	155.0527
78	175461	24922	155.0146	78	175552	25906	155.0146
79	179925	25646	154.8454	79	180051	26535	154.8454
80	184358	26343	154.8859	80	184488	27378	154.8859
81	188763	27039	154.9618	81	188865	28242	154.9618

TABLE 3.4 (Cont'd.)

System I (FPS 16)				System II (MPS 26)			
Radar Time	Altitude	Horizontal Range	Azimuth	Radar Time	Altitude	Horizontal Range	Azimuth
seconds	feet	feet	degrees	seconds	feet	feet	degrees
82	193132	27722	154.8382	82	193216	29003	154.8382
83	197464	28421	154.6569	83	197597	29698	154.6569
84	201766	29143	154.6456	84	201730	30202	154.6456
85	206038	29857	154.7832	85	205798	30761	154.7832
86	210276	30544	154.8457	86	210066	31599	154.8457
87	214493	31204	154.6943	87	214470	32585	154.6943
88	218674	31907	154.6013	88	218626	33412	154.6013
89	222819	32592	154.6291	89	222742	34228	154.6291
90	226929	33296	154.6394	90	226935	34774	154.6394
91	231006	34020	154.7214	91	230886	35086	154.7214
92	235052	34743	154.6455	92	234866	35566	154.6535
93	239084	35432	154.6257	93	238961	36513	154.6257
94	243085	36084	154.6332	94	243069	37523	154.6332
95	247043	36759	154.7324	95	246967	38225	154.7324
96	250952	37511	154.5512	96	250916	38802	154.5512
97	254842	38268	154.5752	97	254790	39639	154.5752
98	258705	38940	154.5590	98	25802	40488	154.5590
99	262528	39621	154.5436	99	262353	40990	154.5436
100	266308	40362	154.6717	100	266070	41536	154.6717
101	270087	41068	154.5766	101	269894	42494	154.5766

TABLE 3.4 (Cont'd.)

System I (FPS 16)				System II (MPS 26)			
Radar Time *	Altitude	Horizontal Range	Azimuth	Radar Time	Altitude	Horizontal Range	Azimuth
seconds	feet	feet	degrees	seconds	feet	feet	degrees
102	273843	41733	154.5450	102	273745	43548	154.5450
103	277546	42418	154.5388	103	277506	44165	154.5388
104	281220	43107	154.6346	104	281260	44561	154.6346
105	284856	43805	154.6291	105	284775	45251	154.6291
106	288454	44501	154.6222	106	288278	46157	154.6222
107	292035	45224	154.5268	107	291888	46916	154.5268
108	295606	45908	154.5968	108	295482	47500	154.5968
109	299117	46571	154.6720	109	298766	48156	154.6720
110	302574	47258	154.5639	110	302096	48821	154.5639
111	306047	47951	154.6171	111	305618	49456	154.6171
112	309515	48709	154.6432	112	309228	50212	154.6432
113	312919	49460	154.4990	113	312676	51155	154.4990
114	316282	50131	154.3596	114	315922	52000	154.3596
115	319595	50819	154.4203	115	319372	52499	154.4203
116	322828	51515	154.4653	116	322736	527113	154.4653
117	326047	52191	154.5724	117	325811	53080	154.5724
118	329288	52819	154.6497	118	328860	53684	154.6497
119	332496	53574	154.6789	119	331885	54190	154.6789
120	335654	54261	154.6428	120	334620	54615	154.6428
121	338783	54917	154.4478	121	337214	55166	154.4478

TABLE 3.4 (Cont'd.)

System I (FPS 16)				System II (MPS 26)			
Radar Time	Altitude	Horizontal Range	Azimuth	Radar Time	Altitude	Horizontal Range	Azimuth
seconds	feet	feet	degrees	seconds	feet	feet	degrees
122	341887	55507	154.5154	122	340157	55909	154.5154
123	344991	56201	154.6263	123	343701	56587	154.6263
124	348055	56891	154.7142	124	347572	57302	154.7142
125	351051	57670	154.5663	125	351089	58082	154.5663
126	354040	58301	154.5796	126	354090	59165	154.5796
127	356996	58948	154.7142	127	356863	60414	154.7142
128	359939	59629	154.6655	128	359415	61585	154.6655
129	363881	60417	154.5783	129	361646	62212	154.5783
130	365805	61231	154.5203	130	363944	62424	154.5203
131	368678	61989	154.5934	131	--	--	--
132	371511	62595	154.6215	132	--	--	--
133	374282	63209	154.6960	133	--	--	--
134	377007	63965	154.7129	134	--	--	--
135	379704	64702	154.8121	135	--	--	--
136	382387	65380	154.7523	136	--	--	--
137	385069	65970	154.7249	137	--	--	--
138	387678	66630	154.6360	138	--	--	--
139	390273	67273	154.7410	139	--	--	--
140	392799	68022	154.7760	140	--	--	--
141	395264	68855	154.8217	141	--	--	--

TABLE 3.4 (Cont'd.)

System I (FPS 16)				System III(MPS 25)			
Radar Time	Altitude	Horizontal Range	Azimuth	Radar Time	Altitude	Horizontal Range	Azimuth
seconds	feet	feet	degrees	seconds	feet	feet	degrees
142	397677	69488	154.7911	142	--	--	--
143	400129	69937	154.8591	143	--	--	--
144	402664	70501	154.7980	144	--	--	--
145	405055	71398	154.6977	145	--	--	--
146	407339	72405	154.7190	146	--	--	--
147	409620	73298	154.4873	147	--	--	--
148	411897	73874	154.4732	148	--	--	--
149	414188	74252	154.5862	149	--	--	--
150	416556	74535	155.0308	150	--	--	--
151	418832	75041	155.3120	151	--	--	--
152	420962	75824	155.3391	152	--	--	--
153	423075	76651	155.3010	153	--	--	--
154	425142	77420	154.9738	154	--	--	--
155	427188	78177	154.8038	155	--	--	--
156	429248	78861	154.7328	156	--	--	--
157	431271	79567	155.0098	157	431461	79935	155.0098
158	433258	80345	155.0376	158	433355	80691	155.0376
159	435242	80944	155.0074	159	435299	81393	155.0074
160	437168	81620	155.0342	160	437222	82096	155.0342
161	439074	82303	155.0160	161	439134	82776	155.0160

TABLE 3.4 (Cont'd.)

	System I (FPS 16)				System III(MPS 25		
Radar Time	Altitude	Horizontal Range	Azimuth	Radar Time	Altitude	Horizontal Range	Azimuth
seconds	feet	feet	degrees	seconds	feet	feet	degrees
162	440945	83005	154.8965	162	440998	83452	154.8965
163	442801	83620	154.8196	163	442834	84147	154.8196
164	444623	84387	154.8687	164	444693	84784	154.8687
165	446396	85191	155.1049	165	446476	85453	155.1049
166	448149	85859	155.1987	166	448192	86112	155.1987
167	449902	86367	155.2196	167	449977	86719	155.2196
168	451610	87026	155.1173	168	451858	87369	155.1173
169	453269	87614	155.0836	169	453471	88175	155.0836
170	454879	88379	155.0466	170	454917	88878	155.0466
171	456449	89255	155.2158	171	456470	89513	155.2158
172	458061	89801	155.3662	172	458074	90147	155.3662
173	459624	90286	155.3370	173	459603	90843	155.3370
174	461113	90961	155.3899	174	--	--	--
175	462622	91556	155.4105	175	462635	92213	155.4105
176	464116	92035	155.2907	176	464108	92863	155.2907
177	465571	92488	155.1327	177	465545	93401	155.1327
178	466931	93180	155.1156	178	466937	94082	155.1156
179	468258	94056	154.9896	179	468276	94890	154.9896
180	469543	94973	155.0795	180	469561	95658	155.0795
181	470808	95795	154.9079	181	470860	96292	154.9079

TABLE 3.4 (Cont'd.)

System I (FPS 16)				System III (MPS 25)			
Radar Time	Altitude	Horizontal Range	Azimuth	Radar Time	Altitude	Horizontal Range	Azimuth
seconds	feet	feet	degrees	seconds	feet	feet	degrees
182	472073	96505	155.0318	182	472211	96799	155.0318
183	473323	97092	155.2708	183	473441	97451	155.2708
184	474503	97780	155.3157	184	474547	98320	155.3157
185	475628	98621	155.4589	185	475653	99139	155.4589
186	476765	99327	155.4730	186	476838	99716	155.4730
187	477888	99989	155.4455	187	477976	100288	155.4455
188	478958	100736	155.2718	188	479043	101037	155.2718
189	480003	101411	155.0926	189	480051	101824	155.0926
190	481040	101926	155.1870	190	481067	102447	155.1870
191	482058	102417	155.3559	191	482052	103089	155.3559
192	483001	103172	155.3635	192	483013	103822	155.3635
193	483908	103965	155.4740	193	483955	104484	155.4740
194	484798	104685	155.4476	194	484846	105162	155.4476
195	485670	105286	155.3645	195	485686	105853	155.3645
196	486491	105978	155.3404	196	486505	106516	155.3404
197	487281	106689	155.4438	197	487313	107156	155.4438
198	488066	107327	155.5550	198	488082	107912	155.5550
199	488836	107934	155.4356	199	488846	108543	155.4356
200	489571	108537	155.3645	200	489579	109145	155.3645
201	490250	109230	155.3188	201	490238	109879	155.3188

TABLE 3.4 (Cont'd.)

System I (FPS 16)				System III (MPS 25)			
Radar Time	Altitude	Horizontal Range	Azimuth	Radar Time	Altitude	Horizontal Range	Azimuth
seconds	feet	feet	degrees	seconds	feet	feet	degrees
202	490933	109756	155.3157	202	490867	110609	155.3157
203	491568	110395	155.3089	203	491480	111191	155.3089
204	492141	111069	155.2145	204	492093	111699	155.2145
205	492677	111861	155.1094	205	492658	112440	155.1094
206	493080	113123	155.1159	206	493196	113210	155.1159
207	493545	114353	155.2732	207	493712	113856	155.2732
208	494127	114488	155.3631	208	494163	114479	155.3631
209	494713	114195	155.4496	209	494591	115074	155.4496
210	495111	114855	155.4345	210	495026	115605	155.4345
211	495503	115643	155.4589	211	495466	116155	155.4589
212	495819	116316	155.2824	212	495867	116684	155.2824
213	496234	116865	155.0682	213	496135	117208	155.0682
214	496520	117642	154.9954	214	496325	118103	154.9954
215	496604	118626	155.1286	215	496572	118945	155.1286
216	496665	119901	155.2968	216	496814	119669	155.2968
217	496908	120585	155.6937	217	496991	120398	155.6937
218	497145	120860	155.9193	218	497136	121263	155.9193
219	497273	121382	156.1964	219	497217	122087	156.1964
220	497371	122147	156.5146	220	497253	122933	156.5146
221	497424	122829	156.7385	221	497377	123493	156.7385

TABLE 3.4 (Cont'd.)

System I (FPS 16)				System III (MPS 25)			
Radar Time	Altitude	Horizontal Range	Azimuth	Radar Time	Altitude	Horizontal Range	Azimuth
seconds	feet	feet	degrees	seconds	feet	feet	degrees
222	497493	123616	156.8185	222	497521	123807	156.8185
223	497577	124308	156.8737	223	497643	124261	156.8737
224	497769	124781	156.9046	224	497680	124871	156.9046
225	--	--	--	225	497578	125444	156.9836
226	--	--	--	226	497434	125807	157.0481
227	--	--	--	227	497396	126376	157.0255
228	--	--	--	228	497277	127084	156.9585
229	--	--	--	229	497092	127858	156.9585
230	--	--	--	230	496929	128535	156.9702
231	--	--	--	231	496622	129445	156.9784
232	--	--	--	232	496272	130367	156.9499
233	--	--	--	233	495949	131223	156.9057
234	--	--	--	234	495633	131773	156.8957
235	--	--	--	235	495257	132351	156.9675
236	--	--	--	236	494856	133050	157.0145
237	--	--	--	237	494427	133796	156.9355
238	--	--	--	238	494057	134221	156.9575
239	--	--	--	239	493652	134536	157.0293
240	--	--	--	240	493096	135173	157.0166
241	--	--	--	241	492464	136229	157.0159

TABLE 3.4 (Cont'd.)

System III (MPS 25)				System III (MPS 25)			
Radar Time	Altitude	Horizontal Range	Azimuth	Radar Time	Altitude	Horizontal Range	Azimuth
seconds	feet	feet	degrees	seconds	feet	feet	degrees
242	491789	137216	156.9836	262	473994	150382	158.6690
243	491154	138056	156.9269	263	472896	150836	157.5436
244	490540	138689	156.8058	264	471693	151399	156.3989
245	489945	139199	157.5892	265	470359	152161	155.3130
246	489185	140040	157.7070	267	467726	153458	153.0344
247	488356	141004	157.7145	269	464930	154836	154.0575
248	487613	141609	157.7080	270	463579	155470	155.4819
249	487017	141798	157.6191	272	460453	157220	158.0795
250	486319	142221	157.5233	274	457386	158706	160.3458
251	485409	142928	156.5294	276	454374	159326	162.1183
252	484400	143715	155.3477	277	452711	159834	163.1301
253	483454	144511	155.7162	279	449522	160883	163.9046
254	482551	145314	157.2085	280	447758	161632	164.1982
255	481559	146043	158.7143	283	442103	164658	164.2476
256	480591	146577	160.1006	284	440151	165300	164.1147
257	479563	147219	160.6815	285	438234	165970	162.6543
258	478473	147988	161.0327	298	410962	174532	157.7581
259	477349	148738	160.9830	300	406278	176016	157.7018
260	476238	149362	160.1573	359	233348	235037	157.8632
261	475120	149910	159.5541	377	139736	227673	157.9216

TABLE 3.4 (Cont'd.)

System III (MPS 25)				System III (MPS 25)			
Radar Time	Altitude	Horizontal Range	Azimuth	Radar Time	Altitude	Horizontal Range	Azimuth
seconds	feet	feet	degrees	seconds	feet	feet	degrees
378	138148	232095	157.9226	399	61141	233174	159.3968
380	127101	227750	157.9137	400	58546	233411	159.3999
381	122488	226830	157.9219	401	56077	233643	159.3951
382	118616	227109	157.9542	402	53729	233863	159.4188
383	114873	227573	157.9607	403	51557	234061	159.4384
384	111137	227999	157.9796	404	49550	234240	159.4332
385	107441	228455	157.9806	405	47674	234408	159.4384
386	103785	228864	157.9473	406	45923	234557	159.4202
387	100194	229256	157.6849	407	44268	234696	159.4013
388	96614	229630	156.7921	408	42704	234823	159.4078
389	93049	229994	159.0291	409	41222	234942	159.4181
390	89536	230352	157.7046	410	39831	235044	159.4123
391	86079	230717	156.4865	411	38520	235139	159.4126
392	82693	231077	157.4402	412	37313	235221	159.4308
393	79354	231432	157.4471	413	36176	235300	159.4610
394	76087	231763	157.4251	414	35105	235368	159.4631
395	72940	232061	158.0379	415	34059	235433	159.4641
396	69855	232351	158.8471	416	33003	235504	159.4603
397	66833	232636	159.2832	417	32003	235567	159.4603
398	63895	232917	159.3910	418	31071	235619	159.4589

TABLE 3.4 (Cont'd.)

System III (MPS 25)				System III (MPS 25)			
Radar Time	Altitude	Horizontal Range	Azimuth	Radar Time	Altitude	Horizontal Range	Azimuth
seconds	feet	feet	degrees	seconds	feet	feet	degrees
419	30152	235671	159.4562	439	15112	236122	159.4565
420	29209	235720	159.4535	440	14353	236134	159.4576
421	28323	235765	159.4535	441	13798	236132	159.4552
422	27493	235799	159.4514	442	13243	236129	159.4548
423	26676	235831	159.4517	443	12553	236133	159.4548
424	25837	235863	159.4514	444	11897	236134	159.4521
425	25020	235898	159.4511	445	11309	236130	159.4497
426	24259	235925	159.4507	446	10766	236123	159.4462
427	23511	235953	159.4541	447	10291	236115	159.4459
428	22751	235977	159.4511	448	9656	236112	159.4459
429	22024	235994	159.4531	449	8978	236109	159.4438
430	21264	236018	159.4531	450	8469	236105	159.4438
431	20506	236041	159.4535	451	8040	236106	159.4377
432	19803	236056	159.4535	452	7452	236111	159.4380
433	19078	236069	159.4535	453	6855	236116	159.4359
434	18386	236079	159.4538	454	6266	236114	159.4366
435	17750	236087	159.4541	455	5679	236115	159.4363
436	17014	236102	159.4552	456	5069	236115	159.4359
437	16324	236112	159.4559	457	4459	236113	159.4387
438	15780	236112	159.4559	458	4030	236109	159.4394

[a] To obtain the actual flight time, subtract 31.5 sec from the radar time throughout the table.
[b] The sphere peak time was 192.4 seconds, and its impact time was 493.1 seconds.

TABLE 3.5 RADAR TRAJECTORY DATA, ROCKET 8, KING FISH

Radar Time	Altitude	Horizontal Range	Azimuth	Radar Time	Altitude	Horizontal Range	Azimuth
seconds	feet	feet	degrees	seconds	feet	feet	degrees
62	230654	20657	181.9342	82	305156	29300	183.1486
63	234667	21642	182.0980	83	308543	29685	183.1891
64	238654	21488	182.5038	84	311893	30125	183.1595
65	242625	21955	182.9041	85	315195	30561	183.1022
66	246542	22395	182.9628	86	318498	30988	183.1053
67	250445	22824	182.9817	87	321782	31355	183.2917
68	254322	23225	183.0037	88	325041	31829	183.3762
69	258159	23643	182.8468	89	328262	32394	183.5214
70	261958	24087	182.7785	90	331449	32876	183.5849
71	265731	24547	182.7668	91	334605	33244	183.6811
72	269473	24968	182.8547	92	337725	33611	183.8290
73	272177	25397	182.0064	93	340806	34073	183.9715
74	276847	25833	183.0473	94	343865	34485	184.1514
75	280479	26291	183.1074	95	346914	34897	184.3313
76	284075	26761	183.2059	96	349888	35304	184.1222
77	287682	27183	183.1575	97	352817	35812	183.8287
78	291273	27523	183.2807	98	355758	36213	183.4500
79	294804	27943	183.2344	99	358723	36660	183.3556
80	298274	28446	183.1441	100	361631	37122	183.3621
81	301735	28895	183.0850	101	364482	37591	183.6402

TABLE 3.5 (Cont'd.)

Radar Time	Altitude	Horizontal Range	Azimuth	Radar Time	Altitude	Horizontal Range	Azimuth
seconds	feet	feet	degrees	seconds	feet	feet	degrees
102	367286	37977	183.8733	122	416904	46563	184.8363
103	370052	38425	184.1037	123	419040	47196	184.5606
104	372759	38886	184.3478	124	421191	47473	184.3533
105	375382	39272	184.4408	125	423308	47625	184.1796
106	377913	39722	184.4892	126	425381	47978	184.0261
107	380457	40104	184.5885	127	427399	48675	184.1233
108	383086	40462	184.6200	128	429375	49453	184.3474
109	385735	40803	184.5181	129	431342	50062	184.5627
110	388370	41277	184.3413	130	433316	50352	184.6674
111	390890	41707	184.0560	131	435228	50743	184.8556
112	393273	42206	183.9217	132	437120	51135	184.9651
113	395644	42941	183.8805	133	438967	51565	185.0156
114	398106	43419	183.8932	134	440767	52098	185.0183
115	400587	43449	184.0405	135	442578	52358	185.0262
116	403108	43788	184.2008	136	444377	52553	185.0403
117	405533	44528	184.5490	137	446081	53171	184.9898
118	407877	45100	184.7999	138	447740	53961	184.8381
119	410165	45409	184.9060	139	449414	54280	184.7721
120	412474	45762	184.9929	140	451067	54643	184.5473
121	414714	46011	184.9768	141	452661	55179	184.4882

TABLE 3.5 (Cont'd.)

Radar Time	Altitude	Horizontal Range	Azimuth	Radar Time	Altitude	Horizontal Range	Azimuth
seconds	feet	feet	degrees	seconds	feet	feet	degrees
142	454260	55452	184.4216	154	470797	60524	186.3387
143	455858	55458	184.3976	155	472002	61048	186.3603
144	457355	56090	184.4559	156	473117	61634	186.4136
145	458769	56937	184.7660	157	474231	61738	186.3662
146	460215	57521	185.0719	158	475373	61728	186.2773
147	461677	57766	185.3372	159	476431	62288	186.0400
148	463067	58091	185.7132	160	477421	63169	185.5645
149	464399	58612	185.8715	161	478410	63545	185.1278
150	465760	58982	186.0575	162	479436	63511	184.7999
151	467144	59245	186.2330	163	480380	63891	184.7416
152	468426	56910	186.3466	164	481261	64470	184.7546
153	469590	60143	186.4074	165	482114	64757	185.0365

[a] To obtain the approximate flight time, add 5 seconds to the radar time throughout this table.

[b] Peak flight time was 190.7 seconds, and the peak altitude was approximately 490.000 ft.

TABLE 3.6 RADAR TRAJECTORY DATA, ROCKET 9, TIGHT ROPE

Radar Time	Altitude	Horizontal Range	Azimuth	Radar Time	Altitude	Horizontal Range	Azimuth
seconds	feet	feet	degrees	seconds	feet	feet	degrees
48	67509	4809	179.4297	68	71001	6151	178.1594
49	67974	4849	178.9576	69	70835	6213	178.1378
50	68414	4887	178.6641	70	70646	6280	178.1776
51	68837	4948	178.5580	71	70435	6354	178.0646
52	69228	5040	178.5910	72	70187	6431	178.0265
53	69575	5115	178.6802	73	69902	6495	177.9572
54	69886	5179	178.7015	74	69589	6561	177.8755
55	70177	5238	178.5559	75	69257	6649	177.8885
56	70442	5304	178.5449	76	68891	6729	177.9101
57	70665	5376	178.4014	77	68484	6801	178.0107
58	70850	5450	178.3266	78	68040	6870	177.9249
59	71007	5520	178.2528	79	67569	6954	177.8559
60	71133	5595	178.2981	80	67068	7018	177.8253
61	71228	5663	178.3602	81	66535	7090	177.8707
62	71286	5725	178.3431	82	65971	7162	177.8542
63	71317	5792	178.3067	83	65382	7239	177.8635
64	71328	5861	178.1388	84	64769	7310	177.8700
65	71305	5938	178.1258	85	64123	7384	177.7673
66	71235	6010	178.1608	86	63431	7474	177.7193
67	71131	6084	178.1621	87	62712	7563	177.6976

TABLE 3.6 (Cont'd.)

Radar Time	Altitude	Horizontal Range	Azimuth	Radar Time	Altitude	Horizontal Range	Azimuth
seconds	feet	feet	degrees	seconds	feet	feet	degrees
88	61972	7642	177.6856	108	49784	8000	178.4557
89	61172	7704	177.6684	109	49221	8078	178.5031
90	60376	7814	178.1206	110	48582	8092	178.4361
91	60015	7787	178.5704	111	47971	8100	178.3860
92	59875	7633	178.5968	112	47387	8110	178.2284
93	59474	7516	178.4976	113	46852	8162	178.0523
94	58752	7579	178.4296	114	46287	8206	177.9136
95	58089	7623	178.5113	115	45742	8238	177.7443
96	57410	7651	178.5027	116	45191	8251	177.5442
97	56747	7693	178.5250	117	44645	8299	177.3636
98	56100	7746	178.5868	118	44098	8367	177.2266
99	55454	7789	178.6661	119	43558	8398	177.0384
100	54789	7814	178.6558	120	43022	8440	176.7864
101	54132	7834	178.6390	121	42490	8486	176.5736
102	53472	7851	178.6531	122	41958	8535	176.3243
103	52848	7889	178.6006	123	41442	8580	176.0559
104	52243	7936	178.5796	124	40930	8631	175.7383
105	51630	7957	178.6957	125	40423	8689	175.4986
106	50934	7930	178.7145	126	39918	8756	175.2473
107	50317	7931	178.5762	127	39424	8819	174.9308

TABLE 3.6 (Cont'd.)

Radar Time	Altitude	Horizontal Range	Azimuth	Radar Time	Altitude	Horizontal Range	Azimuth
seconds	feet	feet	degrees	seconds	feet	feet	degrees
128	38932	8883	174.6029	148	28882	10285	168.5186
129	38440	8948	174.2136	149	28345	10310	168.5556
130	37951	9016	173.8198	150	27812	10326	168.6672
131	37460	9088	173.4346	151	27280	10333	168.7778
132	36975	9167	173.0775	152	26751	10329	168.9638
133	36490	9243	172.7064	153	26225	10317	169.1571
134	36006	9316	172.3006	154	25699	10300	169.3913
135	35521	9397	171.9092	155	25177	10275	169.5794
136	35036	9477	171.4718	156	24653	10244	169.8215
137	34551	9547	171.0787	157	24129	10212	170.0178
138	34065	9614	170.6818	158	23608	10179	170.2839
139	33528	9688	170.2898	159	23093	10143	170.5071
140	33082	9772	169.9172	160	22580	10108	170.7477
141	32586	9863	169.5873	161	22072	10074	170.9637
142	32077	9949	169.3199	162	21567	10047	171.0670
143	31559	10025	169.0703	163	21066	10024	171.1841
144	31031	10091	168.8368	164	20565	10006	171.2373
145	30496	10155	168.6665	165	20069	9995	171.2219
146	29960	10208	168.5824	166	19576	9986	171.1608
147	29421	10252	168.5158	167	19088	9981	171.0797

TABLE 3.6 (Cont'd.)

Radar Time	Altitude	Horizontal Range	Azimuth	Radar Time	Altitude	Horizontal Range	Azimuth
seconds	feet	feet	degrees	seconds	feet	feet	degrees
168	18601	9983	170.9369	188	9554	10182	168.5584
169	18118	9989	170.8181	189	9130	10211	168.5278
170	17638	9992	170.5957	190	8707	10241	168.5000
171	17161	9996	170.4061	191	8287	10269	168.4719
172	16687	10000	170.1922	192	7869	10294	168.4389
173	16214	10000	169.9461	193	7454	10318	168.4097
174	15745	9998	169.8009	194	7041	10337	168.4056
175	15281	9995	169.5942	195	6631	10353	168.3974
176	14820	9988	169.4308	196	6223	10364	168.4066
177	14365	9982	169.2982	197	5819	10373	168.4248
178	13913	9982	169.1424	198	5415	10378	168.4918
179	13465	9989	169.0466	199	5015	10381	168.5457
180	13021	10000	168.9426	200	4616	10379	168.6075
181	12579	10013	168.8759	201	4219	10377	168.7201
182	12139	10031	168.8286	202	3832	10372	168.8279
183	11703	10052	168.7671	203	3428	10363	168.9601
184	11269	10075	168.7218	204	3035	10355	169.0981
185	10837	10098	168.6737	205	2644	10346	169.2677
186	10409	10124	168.6404	206	2254	10338	169.4579
187	9981	10153	168.6006	207	1866	10328	169.6745
				208	1479	10318	169.9681
				209	1094	10310	170.3038

[a] To obtain flight time, subtract 1.9 seconds from the radar time throughout this table.

TABLE 3.7 SUMMARY OF SPHERE TRAJECTORY DATA

Rocket No.	Ejection Time* (sec)	Peak altitude+ (km)	Peak time* (sec)	Horizontal Velocity at Peak (m/sec)	Impact Time* (sec)
1	55.97	144.1	187.7	251.4	482.98
2	54.66	142.7	189.5	130.0	486.28
3	55.57	145.8+	185.0	150.0	483.64
4	55.80	148.2+	187.9	162.4	488.54
5	53.74	157.4	195.0	149.4	504.96
6	55.09	153.7+	192.0	149.4	495.02
7	55.29	153.7+	192.1	143.0	491.94
8	56.99	149.5+	191.5	121.9	492.08
9	51.58	21.7	62.1	27.9	210.65

*All times are referred to rocket launch.

+Corrected values.

TABLE 3.8 DENSITY, 0 THROUGH 115 km, U.S. STANDARD ATMOSPHERE, 1962

Density, ρ (gm/cm^3)
vs
Geometric Altitude, Z (km)

Z	ρ	Z	ρ
0	1.2250(-3)	60	3.0592(-7)
5	7.3643(-4)	65	1.6665(-7)
10	4.1351	70	8.7535(-8)
15	1.9475(-4)	75	4.335
20	8.8910(-5)	80	1.999 (-8)
25	4.0084	85	7.955 (-9)
30	1.8410(-5)	90	3.170
35	8.4634(-6)	95	1.211 (-9)
40	3.9957	100	4.974 (-10)
45	1.9663	105	2.117 (-10)
50	1.0269(-6)	110	9.829 (-11)
55	5.6075(-7)	115	4.623 (-11)

TABLE 3.9 DENSITY, 0 THROUGH 90 km, Tropical Atmosphere (15° N)

Z	ρ	Z	ρ
0.000	1.1666(-3)	60.673	3.0783(-7)
4.009	7.9509(-4)	64.761	1.8629(-7)
10.032	4.1965	70.898	8.2710(-8)
14.054	2.5682(-4)	75.000	4.6006
20.096	9.3903(-5)	80.131	2.0811(-8)
26.150	3.3797	85.272	8.2487(-9)
30.192	1.7898(-5)	90.000	3.5224
34.242	9.7049(-6)		
40.320	4.0355		
46.416	1.7542		
50.480	1.0497(-6)		
54.556	6.4536(-7)		

Note: The bracketed number gives the power of ten by which the initial number is to be multiplied.

TABLE 3.10 DENSITY DATA, ROCKET 1

Density, ρ (gm/cm^3)
vs
Geometric Altitude, Z(km)

Upleg Data

Z	ρ	Z	ρ
61.6	3.19(-7)	84.8	1.11(-8)
64.1	2.23	86.9	7.28(-9)
66.6	1.68	90.0	4.39
69.0	1.24(-7)	92.0	3.08
71.4	8.77(-8)	95.0	1.89
73.7	6.26	96.9	1.34(-9)
76.0	4.42	99.7	7.86(-10)
78.3	3.29	101.5	5.19
80.5	2.30	103.3	3.67
82.7	1.54	105.0	2.59

Downleg Data

Z	ρ	Z	ρ
107.9	1.48(-10)	76.5	3.88(-8)
105.4	2.52	74.2	5.37
102.8	4.33	71.9	7.18(-8)
101.0	6.43	69.5	1.02(-7)
99.1	9.02(-10)	67.1	1.40
97.3	1.22(-9)	64.9	1.94
95.4	1.73	62.2	2.70
93.4	2.49	59.7	3.61
91.4	3.42	57.2	4.99
89.4	4.80	54.6	6.70
87.3	6.68	52.1	9.28(-7)
85.3	9.83(-9)	49.5	1.36(-6)
83.1	1.35(-8)	46.9	1.86
80.9	2.03	44.3	2.44
78.7	2.77	41.7	3.52
		39.1	4.92

Rawinsonde Data

Z	ρ	Z	ρ
0.09	1.17(-3)	10.91	3.80(-4)
1.50	1.03(-3)	12.37	3.19
3.13	8.67(-4)	14.15	2.56
4.39	7.62	16.50	1.75
5.84	6.54	18.61	1.17(-4)
7.55	5.44	20.70	8.13(-5)
9.65	4.35	23.96	4.66

TABLE 3.11 DENSITY DATA, ROCKET 2.

Density, ρ (gm/cm^3)

vs

Geometric Altitude, Z(km)

Upleg Data

Z	ρ	Z	ρ
62.65	2.37 (-7)	75.71	3.63 (-8)
65.17	1.75	77.73	2.62
67.82	1.24 (-7)	80.90	1.48 (-8)
71.01	7.47 (-8)	83.15	9.97 (-9)
72.98	5.68	90.19	2.90

Downleg Data

Z	ρ	Z	ρ
100.84	3.99 (-10)	62.53	2.42 (-7)
92.08	1.77 (- 9)	59.30	3.56
88.95	3.41	57.40	4.65
85.07	6.73 (-9)	54.88	6.11
82.32	1.11 (-8)	52.44	8.49 (-7)
80.81	1.46	50.38	1.06 (-6)
77.97	2.48	47.40	1.58
75.85	3.30	44.92	2.19
73.80	4.74	42.41	3.11
71.15	7.17 (-8)	40.00	4.34
68.44	1.15 (-7)	38.10	5.76
67.13	1.46	36.35	7.58
64.42	1.90		

TABLE 3.12 DENSITY DATA, ROCKET 3

Density, ρ (gm/cm^3)

vs

Geometric Altitude, Z (km)

Upleg Data

Z	ρ	Z	ρ
71.24	7.07 (-8)	82.94	1.26 (-8)
73.67	5.02	85.11	8.68 (-9)
76.06	3.49	87.24	6.62
78.41	2.42	89.33	3.97
80.72	1.95	94.38	1.46 (-9)
		104.70	1.73 (-10)

Downleg Data

Z	ρ	Z	ρ
98.27	7.47 (-10)	66.72	1.29 (-7)
97.31	1.04 (-9)	64.25	1.84
92.40	1.78	61.75	2.55
89.34	3.76 (-9)	59.22	3.51
82.95	1.16 (-8)	56.65	4.94
80.74	1.64	54.06	6.87
78.49	2.41	51.44	9.52 (-7)
76.20	3.35	48.80	1.26 (-6)
73.89	4.78	46.15	1.74
71.54	6.60 (-8)	43.50	2.45
69.15	1.02 (-7)	40.86	3.71
		38.25	5.49

TABLE 3.13 DENSITY DATA, ROCKET 4

Density, ρ (gm/cm^3)
vs
Geometric Altitude, Z(km)

Upleg Data

Z	ρ	Z	ρ
67.71	1.25(-7)	78.63	2.38(-8)
68.95	1.02(-7)	80.16	2.05
70.30	8.57(-8)	81.73	1.71
71.64	7.26	83.65	1.52
72.98	5.90	85.20	1.07(-8)
74.41	5.16	87.19	8.25(-9)
76.53	3.29	90.17	3.78
77.23	2.98	92.05	2.75(-9)
		111.93	3.61(-11)

Downleg Data

Z	ρ	Z	ρ
109.87	5.53(-11)	71.45	7.41(-8)
103.35	2.64(-10)	69.99	9.00(-8)
98.38	1.18(-9)	69.38	1.03(-7)
96.19	2.27	67.40	1.35
92.40	3.81	66.03	1.61
90.63	4.85	64.02	2.03
89.78	5.87	62.74	2.41
88.06	7.17	62.10	2.60
86.43	9.18(-9)	60.82	3.07
83.68	1.50(-8)	59.40	3.70
82.11	1.64	58.10	4.33
80.51	2.02	56.79	5.07
79.14	2.32	54.83	6.18
77.75	2.84	53.51	7.19
76.22	3.41	52.32	8.29(-7)
74.11	4.76	50.32	1.04(-6)
72.77	6.22	49.64	1.12

TABLE 3.13 (cont'd)

Downleg Data (cont'd)

Z	ρ	Z	ρ
48.43	1.35(-6)	40.13	4.11
47.07	1.54	39.46	4.46
45.19	2.03	38.28	5.36
43.86	2.40	35.21	8.33
42.66	2.84	34.07	9.79(-6)
41.33	3.45	32.38	1.30(-5)

Rawinsonde Data

Z	ρ	Z	ρ
0.11	1.16(-3)	10.98	3.75(-4)
1.52	1.02(-3)	12.46	3.16
3.15	8.90(-4)	14.25	2.53
4.43	7.54	16.64	1.77
5.89	6.47	18.73	1.18(-4)
7.61	5.42	20.79	8.25(-5)
9.71	4.32	23.99	4.81

TABLE 3.14 DENSITY DATA, ROCKET 5

Density, ρ (gm/cm^3)
vs
Geometric Altitude, Z (km)

Upleg Data

Z	ρ	Z	ρ
66.8	1.34(-7)	86.6	5.99(-9)
69.4	9.16(-8)	88.9	4.03
72.0	6.33	91.1	2.68
74.5	4.75	94.5	1.56
77.0	3.06	96.6	1.15(-9)
79.4	2.11	98.8	8.55(-10)
81.9	1.35(-8)	100.9	6.75
84.2	9.05(-9)	103.9	4.65
		106.9	2.66

Downleg Data

Z	ρ	Z	ρ
108.9	1.62(-10)	61.5	2.69(-7)
102.9	6.00(-10)	58.8	3.80
93.4	2.27(-9)	57.5	4.43
86.4	8.49(-9)	53.3	7.39(-7)
83.1	1.31(-8)	50.6	1.04(-6)
80.7	1.85	47.8	1.44
78.3	2.74	45.0	2.06
75.8	4.35	42.2	2.90
73.3	6.21	39.4	4.23
70.7	8.68(-8)	36.7	6.26
68.1	1.21(-7)	34.0	9.56(-6)
64.2	1.96	31.5	1.55(-5)

Rawinsonde Data

Z	ρ	Z	ρ
0.12	1.17(-3)	10.9	3.82(-4)
1.52	1.03(-3)	12.4	3.18
3.15	8.68(-4)	14.2	2.52
4.41	7.57	16.5	1.78
5.86	6.55	18.6	1.21(-4)
7.57	5.46	20.6	8.26(-5)
9.65	4.37	23.9	4.82

TABLE 3.15 DENSITY DATA ROCKET 6

Density, ρ (gm/cm^3)
vs
Geometric Altitude, Z (km)

Upleg Data

Z	ρ	Z	ρ
64.40	1.70(-7)	86.30	7.22(-9)
66.99	1.23(-7)	89.66	4.02
69.54	8.98(-8)	91.85	2.77
72.05	6.02	94.00	1.91
74.52	4.43	96.11	1.30(-9)
76.95	3.02	99.20	7.20(-10)
79.34	2.14	101.21	4.93
80.51	1.79	106.08	2.02(-10)
84.01	1.05(-8)	108.90	8.14(-11)
		111.63	8.63

Downleg Data

Z	ρ	Z	ρ
107.04	1.86(-10)	72.06	6.86(-8)
104.16	3.38	70.81	8.07(-8)
101.22	6.46	68.28	1.17(-7)
99.21	8.91(-10)	65.72	1.68
98.19	1.20(-9)	63.13	2.21
96.12	1.62	60.50	3.11
92.94	2.33	57.84	4.26
90.77	3.38	55.15	5.87
88.56	4.95	52.44	8.37(-7)
85.17	9.31(-9)	49.70	1.15(-6)
81.70	1.61(-8)	46.96	1.57
80.53	1.93	44.20	2.32
78.16	2.81	41.46	3.21
74.53	4.88	38.75	4.60
		36.09	6.46

Rawinsonde Data

Z	ρ	Z	ρ
0.13	1.17(-3)	10.9	3.80(-4)
1.57	1.02(-3)	12.4	3.18
3.21	8.40(-4)	14.2	2.52
4.46	7.60	16.6	1.76
5.91	6.55	18.7	1.21(-4)
7.61	5.49	20.7	8.26(-5)
9.68	4.41	23.9	4.82

TABLE 3.16 DENSITY DATA, ROCKET 7

Density, ρ (gm/cm^3)
vs
Geometric Altitude, Z (km)

Upleg Data

Z	ρ	Z	ρ
64.96	1.66(-7)	77.07	3.74(-8)
67.30	1.54	78.77	3.04
68.07	1.37(-7)	80.44	2.30
70.50	9.87(-8)	82.22	1.69
71.25	8.76	83.03	1.37(-8)
72.88	6.98	85.81	7.41(-9)
75.37	4.69	87.86	5.56
		93.60	2.20

Downleg Data

Z	ρ	Z	ρ
109.64	1.43(-10)	66.29	1.59(-7)
103.43	5.07	63.16	2.31
100.44	7.36(-10)	60.91	2.81
97.66	1.21(-9)	59.99	3.47
95.20	1.88	58.39	4.23
92.98	2.77	56.76	5.19
90.80	2.85	55.28	6.11
88.70	4.31	52.97	7.99
86.69	5.85	52.14	8.68(-7)
84.72	9.02(-9)	50.49	1.06(-6)
82.87	1.31(-8)	48.98	1.27
81.10	1.90	47.48	1.53
79.34	2.63	45.80	1.83
77.68	3.38	44.28	2.22
75.94	4.53	42.77	2.80
73.49	5.47	41.25	3.44
71.13	8.63(-8)	38.94	4.84
69.47	1.07(-7)	38.10	5.33
67.94	1.31	36.65	6.75

Rawinsonde Data

Z	ρ	Z	ρ
0.11	1.16(-3)	10.98	3.85(-4)
1.52	1.04(-3)	12.46	3.22
3.16	8.79(-4)	14.25	2.59
4.43	7.70	16.64	1.73
5.89	6.61	18.74	1.15(-4)
7.61	5.45	20.79	8.02(-5)
9.71	4.39	23.99	4.51

TABLE 3.17 DENSITY DATA, ROCKET 8

Density, ρ (gm/cm^3)
vs
(Corrected) Geometric Altitude, Z (km)

Upleg Data

Z	ρ	Z	ρ
68.24	8.23 (-8)	83.59	7.71 (-9)
70.71	5.93	85.82	5.40
73.14	4.14	88.01	3.60
75.53	2.83	90.16	2.42 (-9)
77.88	1.99	95.36	9.85 (-10)
80.19	1.34	102.22	4.63

Downleg Data

Z	ρ	Z	ρ
105.02	1.02 (-10)	73.03	4.93 (-8)
100.27	4.52	70.60	7.12 (-8)
98.30	6.74 (-10)	68.13	1.03 (-7)
96.29	1.02 (-9)	65.62	1.41
93.23	1.81	63.09	2.02
91.12	2.56	59.22	3.10
89.09	3.68	56.60	4.53
86.82	5.34	52.62	7.51
84.61	8.02 (-9)	51.28	8.94 (-7)
82.36	1.18 (-8)	48.58	1.25 (-6)
80.08	1.68	45.88	1.78
77.77	2.43	41.83	3.02
75.42	3.48 (-8)	40.47	3.72
		37.82	5.53

Rawinsonde Data

Z	ρ	Z	ρ
0.13	1.17 (-3)	10.95	3.78 (-4)
1.54	1.03 (-3)	12.42	3.19
3.18	8.61 (-4)	14.20	2.53
4.44	7.60	16.59	1.77
5.90	6.50	18.66	1.22 (-4)
7.61	5.44	20.71	8.21 (-5)
9.70	4.39	23.92	4.79

TABLE 3.18 DENSITY DATA, ROCKET 9

Density, ρ (gm/cm^3)
vs
Geometric Altitude, Z (km)

Upleg Data

Z	ρ	Z	ρ
21.49	7.80 (-5)	21.71	8.49 (-5)
21.63	8.25	21.74	9.47 (-5)

Downleg Data

Z	ρ	Z	ρ
11.04	2.61 (-3)	17.52	1.35 (-4)
11.37	2.00	17.83	1.16
12.04	1.50	19.06	1.00 (-4)
12.37	1.44 (-3)	19.54	9.12 (-5)
13.27	9.91 (-4)	19.99	8.76
14.37	4.22	20.49	8.00
14.83	3.17	20.92	7.49
15.69	2.11	21.45	6.96
16.84	1.57	21.74	8.74

Rawinsonde Data

Z	ρ	Z	ρ
0.13	4.86 (-5)	10.93	4.61 (-5)
1.53	8.48 (-5)	12.39	5.52
3.16	1.23 (-4)	14.17	6.60
4.42	1.80	16.54	7.67
5.88	2.56	18.59	8.72 (-4)
7.58	3.25	20.66	1.04 (-3)
9.67	3.84	23.77	1.18

TABLE 3.19 TEMPERATURE, 0 THROUGH 115 km, U.S. STANDARD ATMOSPHERE, 1962

Molecular Temperature, T_M(Degrees K)
vs
Geometric Altitude, Z(km)

Z	T_M	Z	T_M
0	288.150	60	255.772
5	255.676	65	239.282
10	223.252	70	219.700
15	216.650	75	200.15
20	216.650	80	180.65
25	221.552	85	180.65
30	226.509	90	180.65
35	236.513	95	195.65
40	250.350	100	210.65
45	264.164	105	235.65
50	270.650	110	260.65
55	265.594	115	310.65

TABLE 3.20 TEMPERATURE, 0 THROUGH 90 km, TROPICAL ATMOSPHERE (15° N)

Z	T_M	Z	T_M
0.000	299.65	60.673	250.65
4.009	276.90	64.761	236.65
10.032	236.70	70.898	215.65
14.054	209.90	75.000	201.65
20.096	207.15	80.131	184.15
26.150	223.95	85.272	184.15
30.192	232.75	90.000	184.15
34.242	241.55		
40.320	254.75		
46.416	267.95		
50.480	270.15		
54.556	264.15		

TABLE 3.21 TEMPERATURE DATA, ROCKET 1

Molecular Temperature, T_M(Degrees K)
vs
Geometric Altitude, Z(km)

Upleg Data

Z	T_M	Z	T_M
64	240.10	88	186.88
68	223.98	92	179.72
72	218.68	96	171.41
76	212.01	100	174.59
80	199.00	104	186.60
84	200.52	108	250.65

Downleg Data

Z	T_M	Z	T_M
108	250.65	72	226.08
104	192.33	68	242.78
100	182.87	64	249.01
96	181.07	60	251.25
92	185.00	56	255.94
88	187.88	52	258.42
84	203.53	48	263.02
80	204.32	44	264.55
76	215.42	40	264.26

Rawinsonde Data

Z	T_M	Z	T_M
0.09	298.15	10.91	229.15
1.50	288.15	12.37	218.15
3.13	281.15	14.15	204.15
4.39	274.15	16.50	199.15
5.84	266.15	18.61	208.15
7.55	256.15	20.70	214.15
9.65	240.15	23.96	224.15

TABLE 3.22 TEMPERATURE DATA, ROCKET 2

Molecular Temperature, T_M(Degrees K)
vs
Geometric Altitude, Z(km)

Mean Data		Upleg / Downleg	
Z	T_M	Z	T_M
35.4	245.77	71.4	202.78
39.4	245.80	75.4	192.27
43.4	252.78	79.4	188.06
47.4	263.23	83.4	187.18
51.4	265.42	87.4	182.25
55.4	258.85	91.4	179.52
59.4	246.96	95.4	183.07
63.4	231.28	99.4	191.21
67.4	214.43	103.4	230.65

TABLE 3.23 TEMPERATURE DATA, ROCKET 3

Molecular Temperature, T_M(Degrees K)
vs
Geometric Altitude, Z(km)

Mean Data		Upleg / Downleg	
Z	T_M	Z	T_M
38	248.54	70	216.90
42	254.73	74	209.80
46	269.31	78	197.80
50	259.32	82	185.34
54	255.12	86	186.37
58	249.48	90	185.37
62	237.30	94	192.15
66	227.35	98	210.65

TABLE 3.24 TEMPERATURE DATA, ROCKET 4

Molecular Temperature, T_M(Degrees K)
vs
Geometric Altitude, Z (km)

Mean Data		Upleg / Downleg	
Z	T_M	Z	T_M
32	234.06	72	217.37
36	242.81	76	207.39
40	256.53	80	199.78
44	264.30	84	189.71
48	267.79	88	174.82
52	269.25	92	169.30
56	262.26	96	164.95
60	255.89	100	169.19
64	247.81	104	184.20
68	229.68	108	250.65

Rawinsonde Data

Z	T_M	Z	T_M
0.11	300.15	10.98	232.15
1.52	291.15	12.46	220.15
3.15	285.15	14.25	206.15
4.43	277.15	16.64	197.15
5.89	269.15	18.73	207.15
7.61	257.15	20.79	211.15
9.71	242.15	23.99	217.15

TABLE 3.25 TEMPERATURE DATA, ROCKET 5

Molecular Temperature, T_M (Degrees K)
vs
Geometric Altitude, Z (km)

Upleg Data

Z	T_M	Z	T_M
66	226.28	90	223.18
70	219.20	94	246.72
74	207.39	98	252.16
78	196.45	102	265.01
82	198.47	106	272.62
86	199.35	110	285.65

Downleg Data

Z	T_M	Z	T_M
110	260.65	70	226.18
106	225.53	66	243.81
102	211.05	62	250.72
98	206.41	58	266.47
94	210.83	54	271.99
90	212.66	50	267.74
86	198.97	46	269.88
82	192.40	42	266.49
78	196.14	38	260.85
74	209.40	34	238.99

Rawinsonde Data

Z	T_M	Z	T_M
0.12	299	10.9	228
1.52	288	12.4	219
3.15	281	14.2	207
4.41	276	16.5	196
5.86	266	18.6	202
7.57	255	20.6	211
9.65	239	23.9	217

TABLE 3.26 TEMPERATURE DATA, ROCKET 6

Molecular Temperature, T_M (Degrees K)
vs
Geometric Altitude, Z (km)

Upleg Data

Z	T_M	Z	T_M
63	249.1	87	191.9
67	235.6	91	190.7
71	223.1	95	189.3
75	215.6	99	188.4
79	210.0	103	196.1
83	203.6	107	220.0
		111	270.0

Downleg Data

Z	T_M	Z	T_M
111	270.0	71	222.0
107	220.0	67	230.0
103	196.1	63	246.4
99	188.4	59	252.7
95	189.3	55	261.4
91	190.7	51	271.0
87	191.9	47	277.6
83	191.4	43	270.4
79	200.7	39	268.7
75	209.7	35	256.1

Rawinsonde Data

Z	T_M	Z	T_M
0.13	298.15	10.9	229.15
1.57	290.15	12.4	219.15
3.21	282.15	14.2	207.15
4.46	275.15	16.6	198.15
5.91	266.15	18.7	202.15
7.61	254.15	20.7	211.15
9.68	237.15	23.9	217.15

TABLE 3.27 TEMPERATURE DATA, ROCKET 7

Molecular Temperature, T_M (Degrees K)
vs
Geometric Altitude, Z (km)

Mean Data

Z	T_M
40	256.30
44	267.96
48	268.36
52	272.51
56	268.02
60	266.93
64	250.66
68	233.59
72	209.16

Upleg
Downleg

Z	T_M
76	200.77
80	194.12
84	187.99
88	196.97
92	197.21
96	202.43
100	214.39
104	229.31
108	250.65

Rawinsonde Data

Z	T_M
0.11	300
1.52	291
3.16	285
4.43	277
5.89	269
7.61	257
9.71	242

Z	T_M
10.98	232
12.46	220
14.25	206
16.64	197
18.74	205
20.79	211
23.99	217

TABLE 3.28 TEMPERATURE DATA, ROCKET 8

Molecular Temperature, T_M (Degrees K)
vs
Geometric Altitude, Z(km)

Upleg Data

Z	T_M	Z	T_M
66.5	218.69	86.5	192.81
70.5	213.95	90.5	199.21
74.5	208.92	94.5	195.23
78.5	196.05	98.5	200.49
82.5	192.09	102.5	220.65

Downleg Data

Z	T_M	Z	T_M
102.5	220.65	70.5	215.16
98.5	184.35	66.5	228.97
94.5	175.77	62.5	242.53
90.5	181.28	58.5	253.41
86.5	182.42	54.5	262.18
82.5	188.58	50.5	259.45
78.5	195.78	46.5	253.57
74.5	204.19	42.5	251.71
		36.5	256.71

Rawinsonde Data

Z	T_M	Z	T_M
0.13	298.15	10.95	230.15
1.54	288.15	12.42	218.15
3.18	283.15	14.20	206.15
4.44	275.15	16.59	197.15
5.90	268.15	18.66	200.15
7.61	256.15	20.71	212.15
9.70	238.15	23.92	218.15

TABLE 3.29 TEMPERATURE DATA, ROCKET 9

Molecular Temperature, T_M (Degrees K)
vs
Geometric Altitude, Z(km)

Downleg Data

Z	T_M	Z	T_M
21.6	350.00	21.6	450.00
19.6	376.43	19.6	467.58
17.6	320.28	17.6	384.15
15.6	275.86	15.6	319.61

Rawinsonde Data

Z	T_M	Z	T_M
0.13	298.36	10.93	229.66
1.53	287.36	12.39	216.96
3.16	283.36	14.17	206.66
4.42	276.06	16.54	196.16
5.88	267.36	18.59	200.16
7.58	255.66	20.66	208.16
9.67	229.96	23.77	217.96

TABLE 3.30 PRESSURE, 0 THROUGH 115 km, U.S. STANDARD ATMOSPHERE, 1962

Pressure, P(mm Hg)
vs
Geometric Altitude, Z (km)

Z	P	Z	P
0	7.60000(+2)	60	1.68649(-1)
5	4.05395	65	8.58545(-2)
10	1.98765(+2)	70	4.14069
15	9.08460(+1)	75	1.8679 (-2)
20	4.14732	80	7.7752 (-3)
25	1.91207(+1)	85	3.0940
30	8.97846(+0)	90	1.2329 (-3)
35	4.30980	95	5.1013 (-4)
40	2.15375	100	2.2558
45	1.11835(+0)	105	1.0739 (-4)
50	5.98392(-1)	110	5.5163 (-5)
55	3.20664	115	3.0921

TABLE 3.31 PRESSURE, 0 THROUGH 90 km, TROPICAL ATMOSPHERE (15° N)

Z	P	Z	P
0.000	7.6000(+2)	60.673	1.6612(-1)
4.009	4.7481	64.761	9.4920(-2)
10.032	2.1389	70.898	3.8402
14.054	1.1606(+2)	75.000	1.9974(-2)
20.096	4.1882(+1)	80.131	8.2514(-3)
26.150	1.6296(+1)	85.272	3.2705
30.192	8.9692(+0)	90.000	1.3966(-3)
34.242	5.0472		
40.320	2.2134		
46.416	1.0120(+0)		
50.480	6.1059(-1)		
54.556	3.6704		

Note: The bracketed number gives the power of ten by which the initial number is to be multiplied.

TABLE 3.32 PRESSURE DATA, ROCKET 1

Pressure, P(mm Hg)
vs
Geometric Altitude, Z (km)

Upleg Data

Z	P
64	1.241(-1)
68	6.944(-2)
72	3.814
76	2.054
80	1.071(-2)
84	5.526(-3)
88	2.535(-3)
92	1.238(-3)
96	5.831(-4)
100	2.706
104	1.306(-4)
108	7.447(-5)

Downleg Data

Z	P
108	7.825(-5)
104	1.449(-4)
100	2.992
96	6.159(-4)
92	1.255(-3)
88	2.548
84	5.477(-3)
80	1.047(-2)
76	1.971(-2)
72	3.602(-2)
68	6.534(-2)
64	1.126(-1)
60	1.920
56	3.251
52	5.452
48	9.060(-1)
44	1.509(+0)
40	2.503

Rawinsonde Data

Z	P
0.09	7.50(+2)
1.50	6.38
3.13	5.25
4.39	4.50
5.84	3.75
7.55	3.00
9.65	2.25
10.91	1.875(+2)
12.37	1.500
14.15	1.125(+2)
16.50	7.500(+1)
18.61	5.250
20.70	3.750
23.96	2.250

TABLE 3.33 PRESSURE DATA, ROCKET 2

Pressure, P (mm Hg)
vs
Geometric Altitude, Z(km)

Mean Data		Upleg / Downleg	
Z	P	Z	P
35.4	4.445(+0)	71.4	3.143(-2)
39.4	2.567	75.4	1.594(-2)
43.4	1.497(+0)	79.4	7.936(-3)
47.4	8.898(-1)	83.4	3.909
51.4	5.372	87.4	1.844(-3)
55.4	3.232	91.4	8.890(-4)
59.4	1.914	95.4	4.336
63.4	1.096(-1)	99.4	2.141
67.4	6.002(-2)	103.4	1.142

TABLE 3.34 PRESSURE DATA, ROCKET 3

Pressure, P (mm Hg)
vs
Geometric Altitude, Z(km)

Mean Data		Upleg / Downleg	
Z	P	Z	P
38	2.997(+0)	70	3.969(-2)
42	1.755	74	2.123
46	1.055(+0)	78	1.107(-2)
50	6.365(-1)	82	5.586(-3)
54	3.790	86	2.729
58	2.203	90	1.337(-3)
62	1.277(-1)	94	6.619(-4)
66	7.244(-2)	98	3.401(-4)

TABLE 3.35 PRESSURE DATA, ROCKET 4

Pressure, P (mm Hg)
vs
Geometric Altitude, Z (km)

Mean Data

Z	P
32	6.954(+0)
36	3.973
40	2.320
44	1.377(+0)
48	8.302(-1)
52	5.043
56	3.049
60	1.818
64	1.067(-1)
68	5.983(-2)

Upleg / Downleg

Z	P
72	3.276(-2)
76	1.741(-2)
80	9.033(-3)
84	4.534
88	2.183(-3)
92	9.987(-4)
96	4.510
100	2.040(-4)
104	9.518(-5)
108	5.073(-5)

Rawinsonde Data

Z	P
0.11	7.50(+2)
1.52	6.38
3.15	5.25
4.43	4.50
5.89	3.75
7.61	3.00
9.71	2.25
10.98	1.875(+2)
12.46	1.500
14.25	1.125(+2)
16.64	7.500(+1)
18.73	5.250
20.79	3.750
23.99	2.250

TABLE 3.36 PRESSURE DATA, ROCKET 5

Pressure, P (mm Hg)
vs
Geometric Altitude, Z(km)

Upleg Data

Z	P	Z	P
66	7.304(-2)	90	1.538(-3)
70	4.011	94	8.764(-4)
74	2.143	98	5.157
78	1.100(-2)	102	3.081
82	5.555(-3)	106	1.878
86	2.833	110	1.168

Downleg Data

Z	P	Z	P
110	8.418(-5)	70	4.675(-2)
106	1.457(-4)	66	8.241(2)
102	2.681	62	1.404(-1)
98	5.066	58	2.410
94	9.532(-4)	54	3.982(+2)
90	1.763(-3)	50	6.341(-1)
86	3.341	46	1.046(+0)
82	6.628(-3)	42	1.721
78	1.309(-2)	38	2.864
74	2.525	34	4.888

Rawinsonde Data

Z	P	Z	P
0.12	7.50(+2)	10.9	1.875(+2)
1.52	6.38	12.4	1.500
3.15	5.25	14.2	1.125
4.41	4.50	16.5	7.500(+1)
5.86	3.75	18.6	5.250
7.57	3.00	20.6	3.750
9.65	2.25	23.9	2.250

TABLE 3.37 PRESSURE DATA, ROCKET 6

Pressure, P (mm Hg)
vs
Geometric Altitude, Z(km)

Upleg Data

Z	P	Z	P
63	1.073(-1)	87	2.685(-3)
67	6.188(-2)	91	1.347(-3)
71	3.458	95	6.725(-4)
75	1.880	99	3.326
79	1.004(-2)	103	1.668(-4)
83	5.260(-3)	107	8.763(-5)
		111	5.057

Downleg Data

Z	P	Z	P
111	5.057(-5)	71	3.776(-2)
107	8.763(-5)	67	6.784(-2)
103	1.668(-4)	63	1.169(-1)
99	3.326	59	2.040
95	6.725(-4)	55	3.433
91	1.347(-3)	51	5.776
87	2.685	47	9.443(-1)
83	5.357(-3)	43	1.543(+0)
79	1.059(-2)	39	2.545
75	2.032	35	4.246

Rawinsonde Data

Z	P	Z	P
0.13	7.50(+2)	10.9	1.875(+2)
1.57	6.38	12.4	1.500
3.21	5.25	14.2	1.125(+2)
4.46	4.50	16.6	7.500(+1)
5.91	3.75	18.7	5.250
7.61	3.00	20.7	3.750
9.68	2.25	23.9	2.250

TABLE 3.38 PRESSURE DATA, ROCKET 7

Pressure, P (mm Hg)
vs
Geometric Altitude, Z (km)

Mean Data

Z	P
40	2.318(+0)
44	1.385(+0)
48	8.378(-1)
52	5.104
56	3.116
60	1.897
64	1.133
68	6.538(-2)
72	3.558

Upleg
Downleg

Z	P
76	1.859(-2)
80	9.404(-3)
84	4.655
88	2.332
92	1.189(-3)
96	6.102(-4)
100	3.231
104	1.777
108	1.025

Rawinsonde Data

Z	P
0.11	7.50(+2)
1.52	6.38
3.16	5.25
4.43	4.50
5.89	3.75
7.61	3.00
9.71	2.25

Z	P
10.98	1.875(+2)
12.46	1.500
14.25	1.125(+2)
16.64	7.500(+1)
18.74	5.250
20.79	3.750
23.99	2.250

TABLE 3.39 PRESSURE DATA, ROCKET 8

Pressure, P (mm Hg)
vs
Geometric Altitude, Z(km)

Upleg Data

Z	P	Z	P
66.5	5.179(-2)	86.5	1.951(-3)
70.5	2.810	90.5	9.864(-4)
74.5	1.493(-2)	94.5	5.044
78.5	7.767(-3)	98.5	2.590
82.5	3.908	102.5	1.378

Downleg Data

Z	P	Z	P
102.5	1.283(-4)	70.5	3.405(-2)
98.5	2.501	66.5	6.211(-2)
94.5	5.222(-4)	62.5	1.096(-1)
90.5	1.093(-3)	58.5	1.882
86.5	2.278	54.5	3.161
82.5	4.669	50.5	5.307
78.5	9.273(-3)	46.5	8.735(-1)
74.5	1.802(-2)	42.5	1.490(+0)
		38.5	2.542

Rawinsonde Data

Z	P	Z	P
0.13	7.50(+2)	10.95	1.875(+2)
1.54	6.38	12.42	1.500
3.18	5.25	14.20	1.125(+2)
4.44	4.50	16.59	7.500(+1)
5.90	3.75	18.66	5.250
7.61	3.00	20.71	3.750
9.70	2.25	23.92	2.250

TABLE 3.40 PRESSURE DATA, ROCKET 9

Pressure, P (mm Hg)
vs
Geometric Altitude, Z (km)

Downleg Data

(T_{M_r} = 350°K) Z	P	(T_{M_r} = 450°K) Z	P
21.6	6.58(+1)	21.6	8.46(+1)
19.6	7.79	19.6	9.68(+1)
17.6	9.45(+1)	17.6	1.13(+2)
15.6	1.19(+2)	15.6	1.38

Rawinsonde Data

Z	P	Z	P
0.13	7.60(+2)	10.93	1.90(+2)
1.53	6.46	12.39	1.52
3.16	5.32	14.17	1.14
4.42	4.56	16.54	7.60(+1)
5.88	3.80	18.59	5.32
7.58	3.04	20.66	3.80
9.67	2.28	23.77	2.28

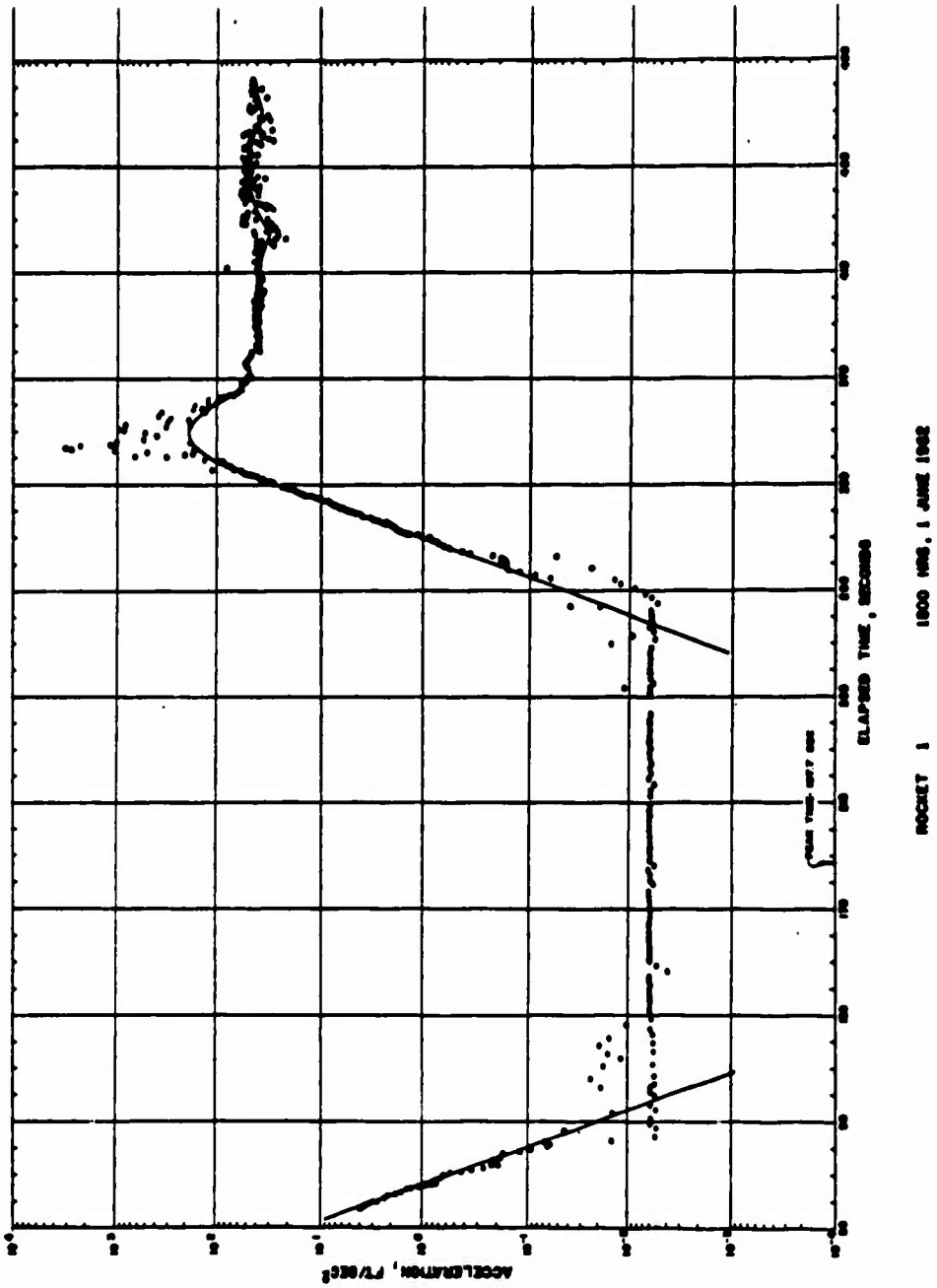

Figure 3.1 Curve of drag acceleration versus elapsed time, Rocket 1.

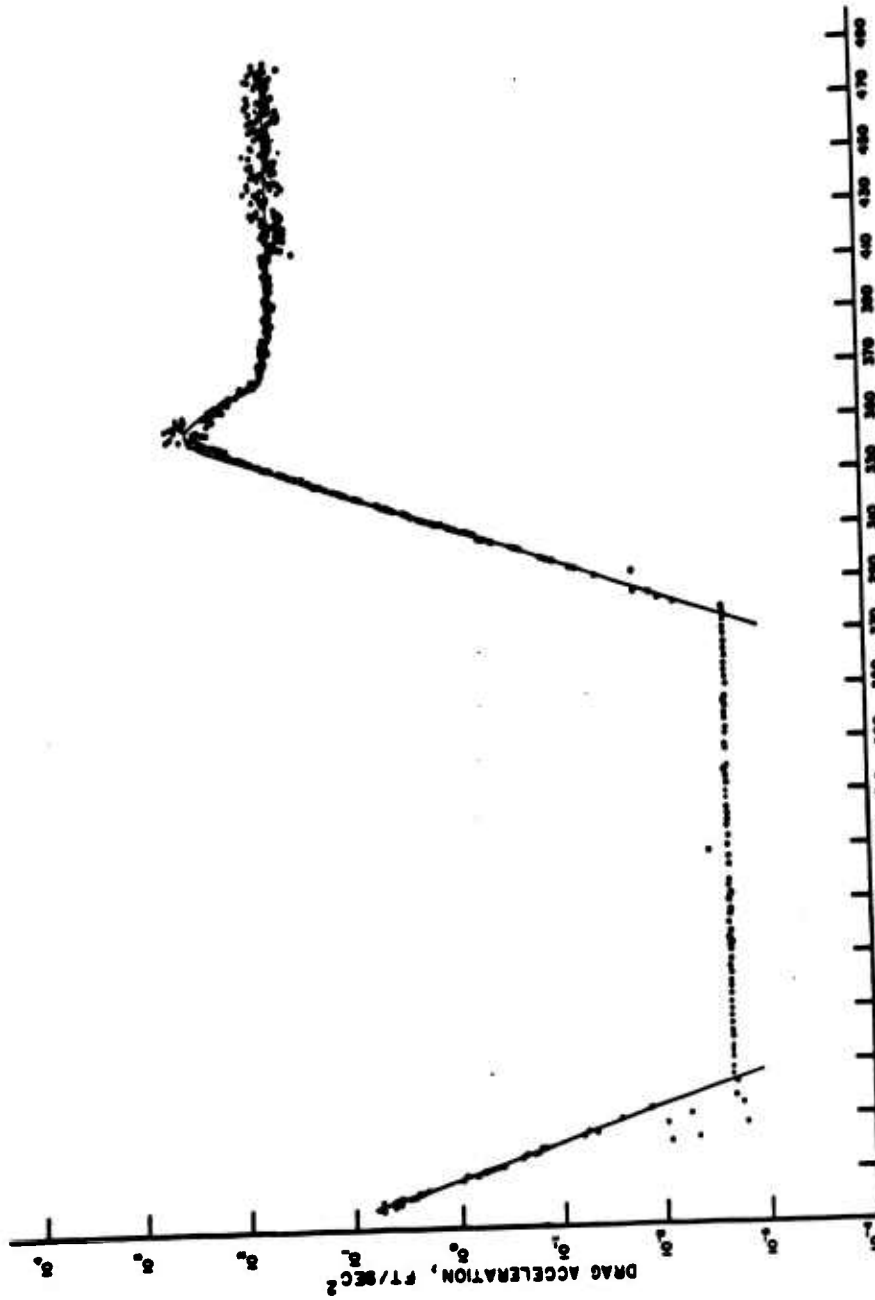

Figure 3.2 Curve of drag acceleration versus elapsed time, Rocket 2.

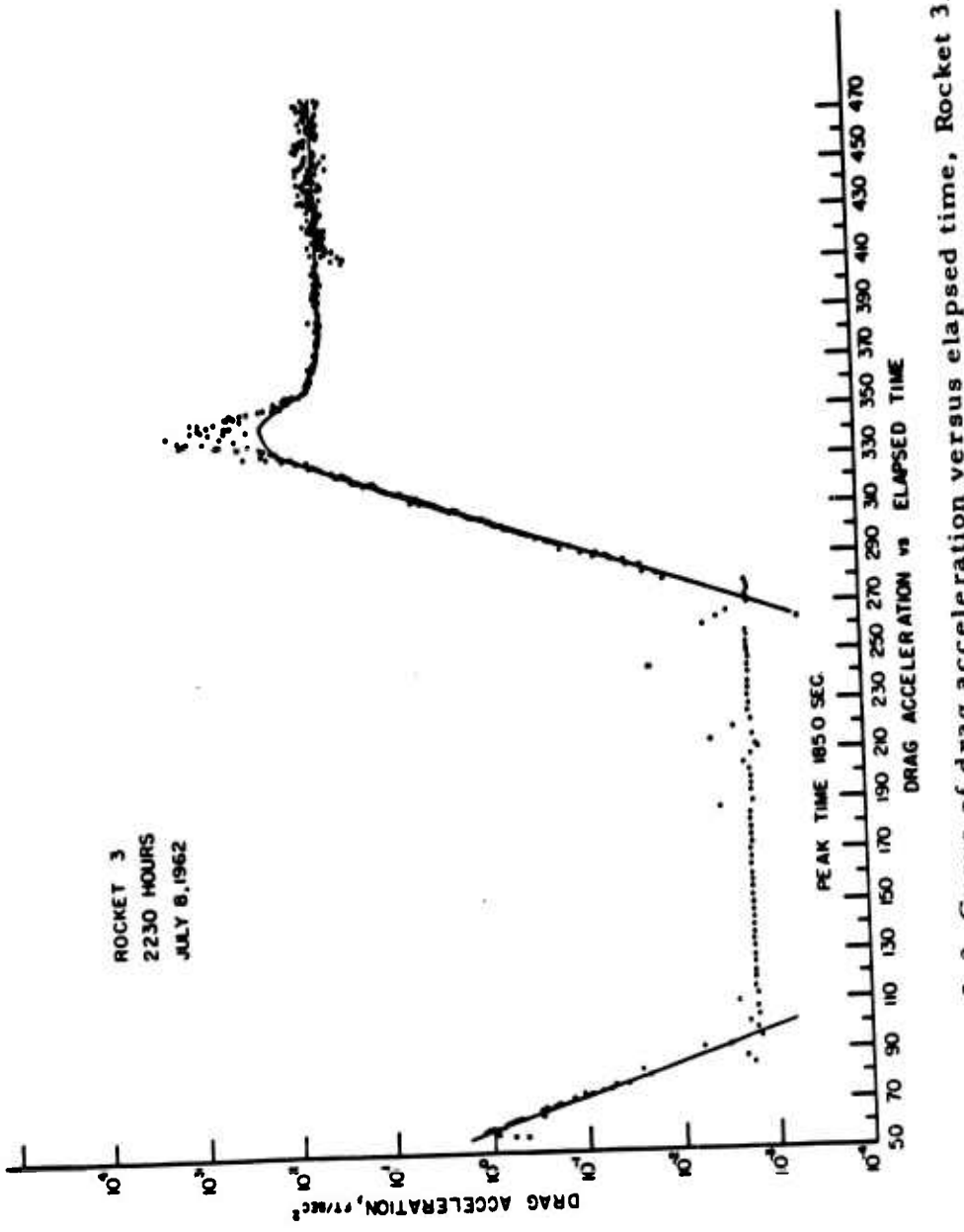

Figure 3.3 Curve of drag acceleration versus elapsed time, Rocket 3.

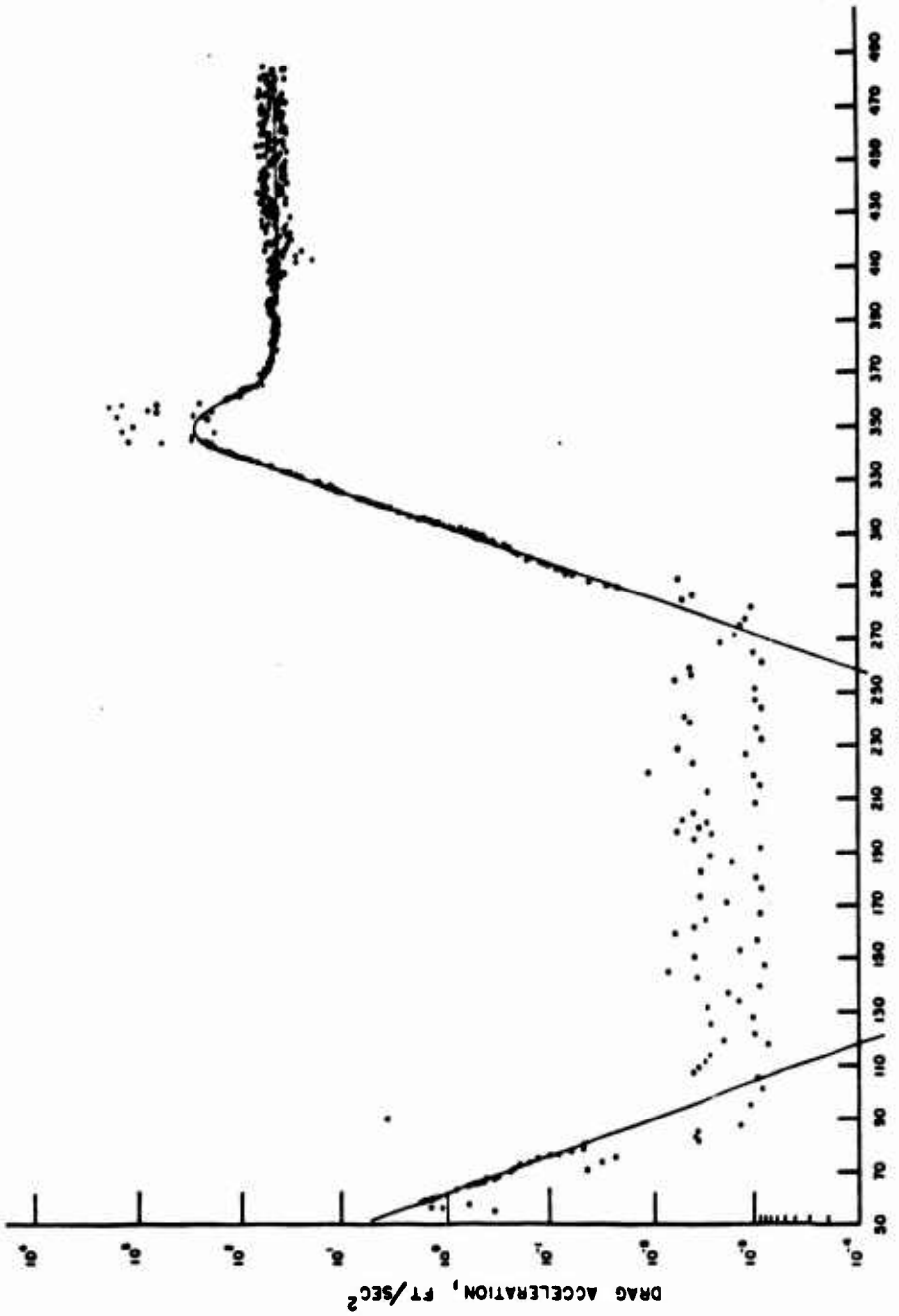

Figure 3.4 Curve of drag acceleration versus elapsed time, Rocket 4.

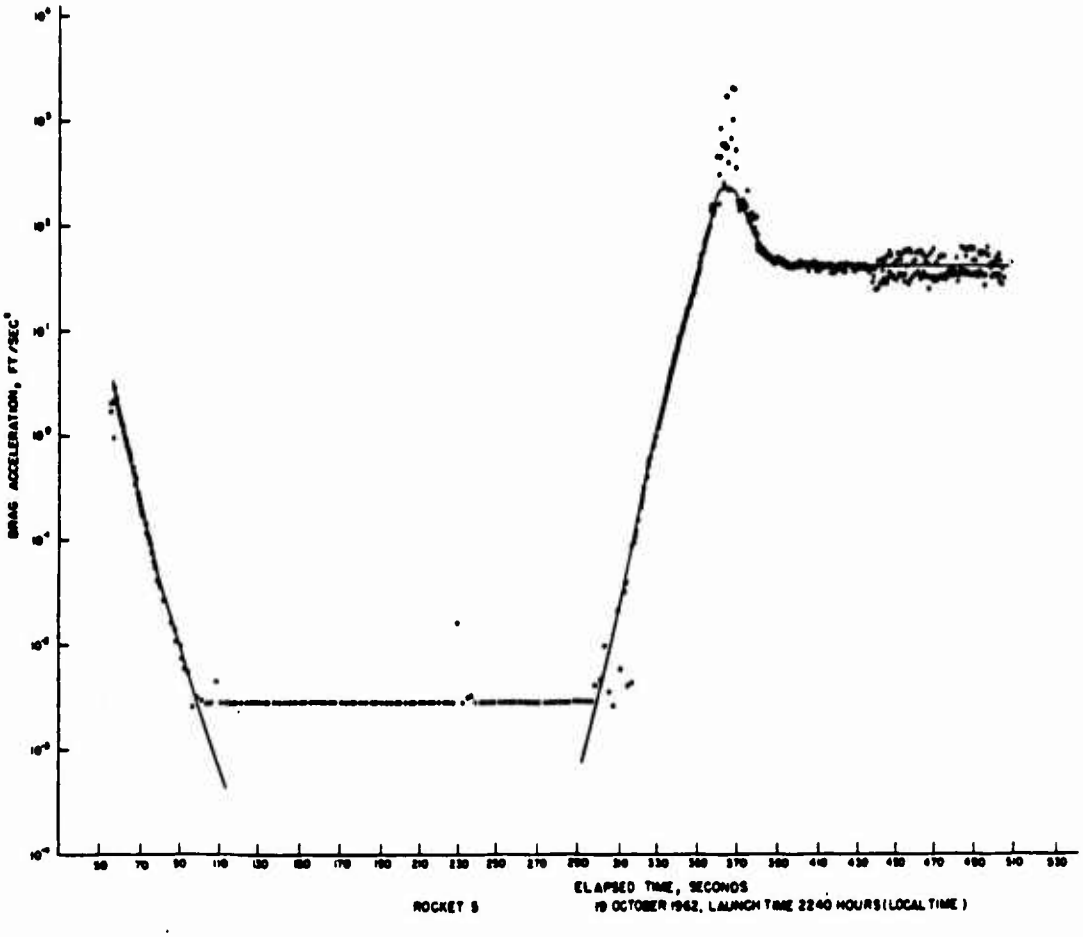

Figure 3.5 Curve of drag acceleration versus elapsed time, Rocket 5.

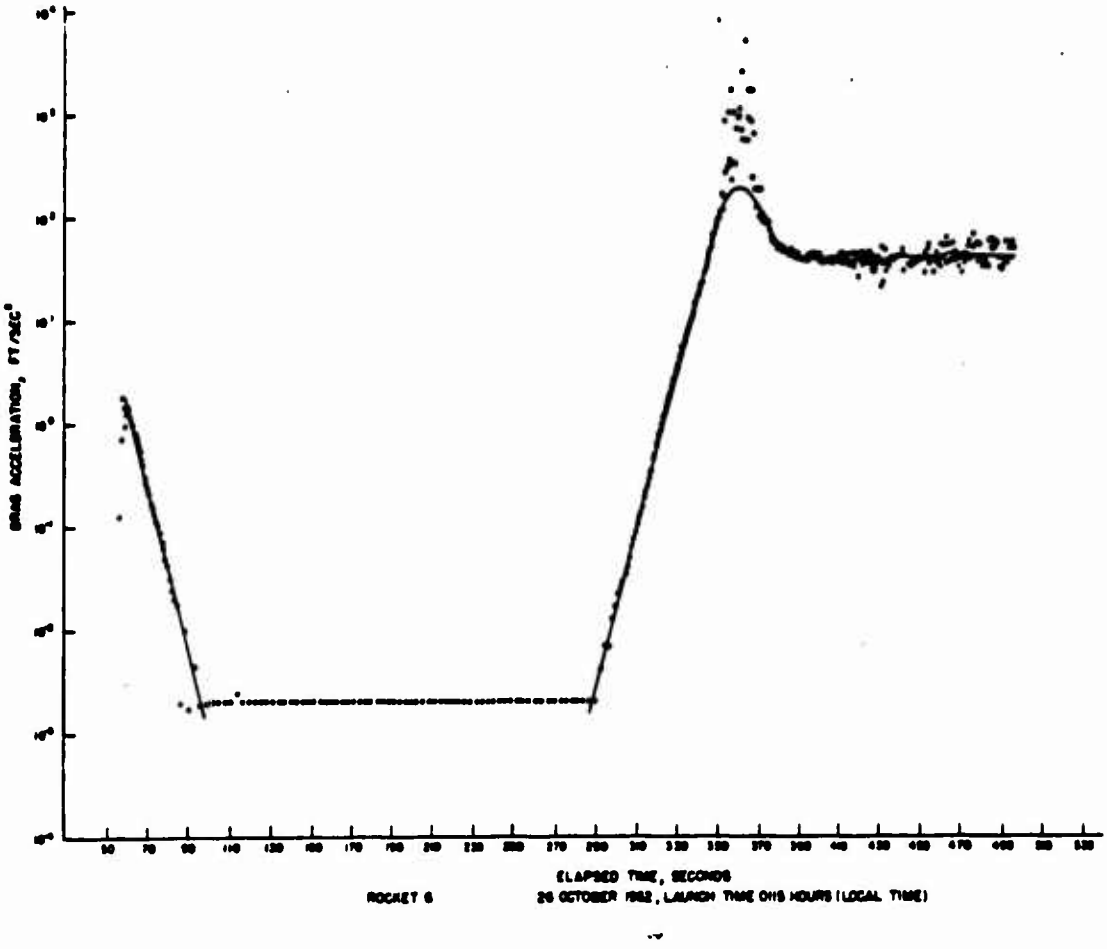

Figure 3.6 Curve of drag acceleration versus elapsed time, Rocket 6.

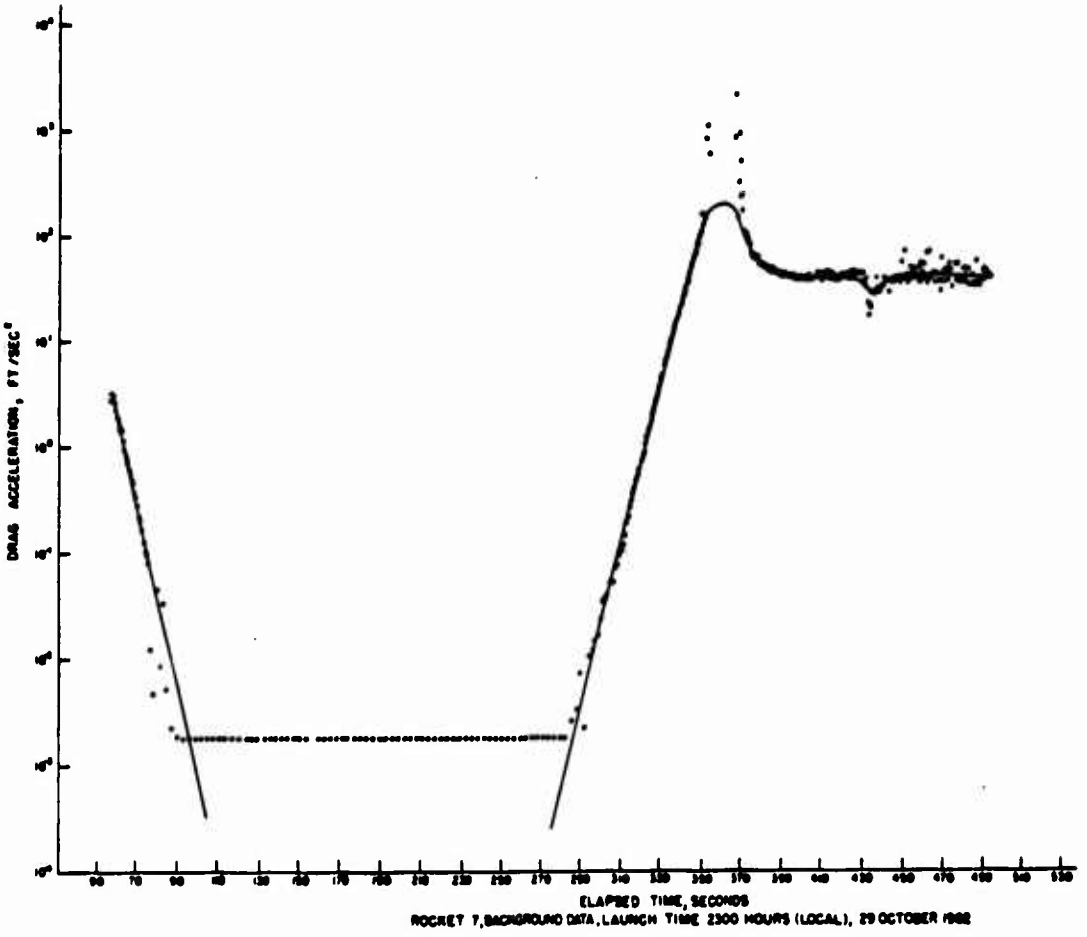

Figure 3.7 Curve of drag acceleration versus elapsed time, Rocket 7.

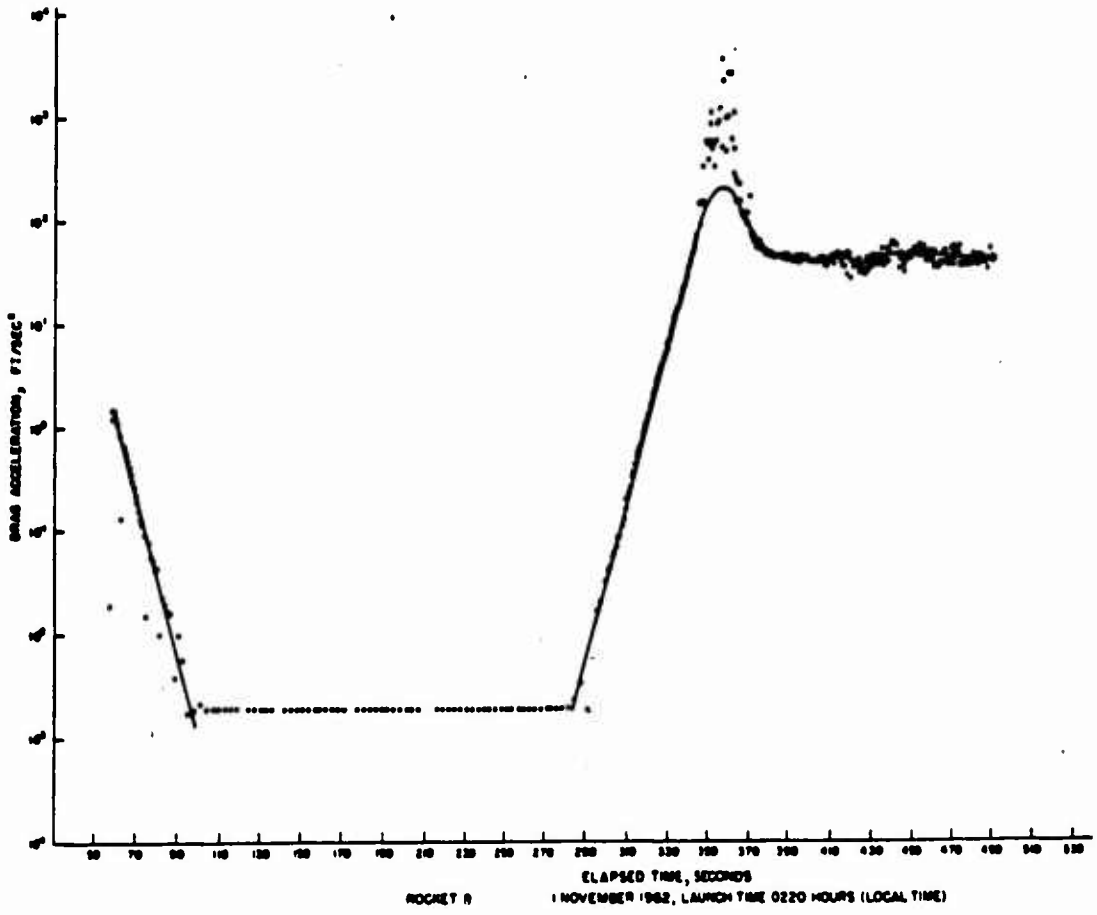

Figure 3.8 Curve of drag acceleration versus elapsed time, Rocket 8.

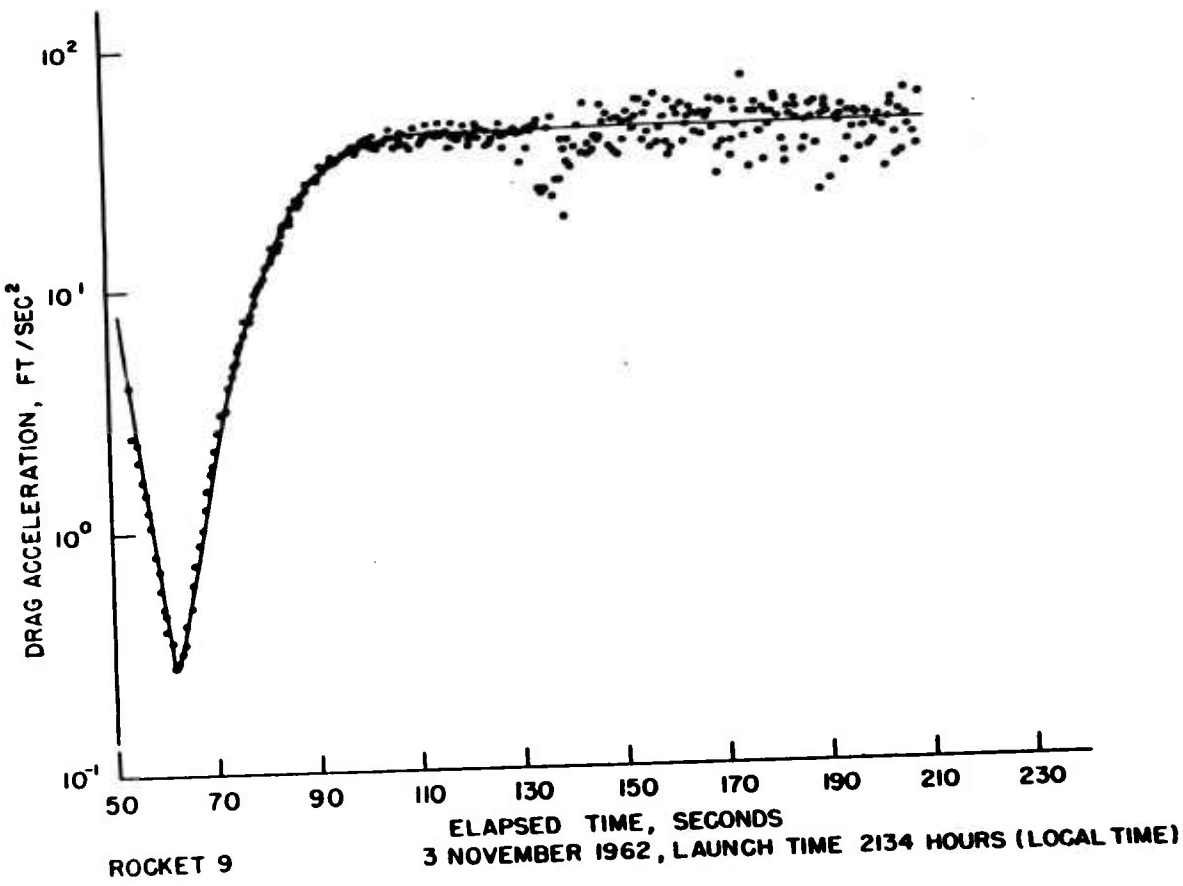

Figure 3.9 Curve of drag acceleration versus elapsed time, Rocket 9.

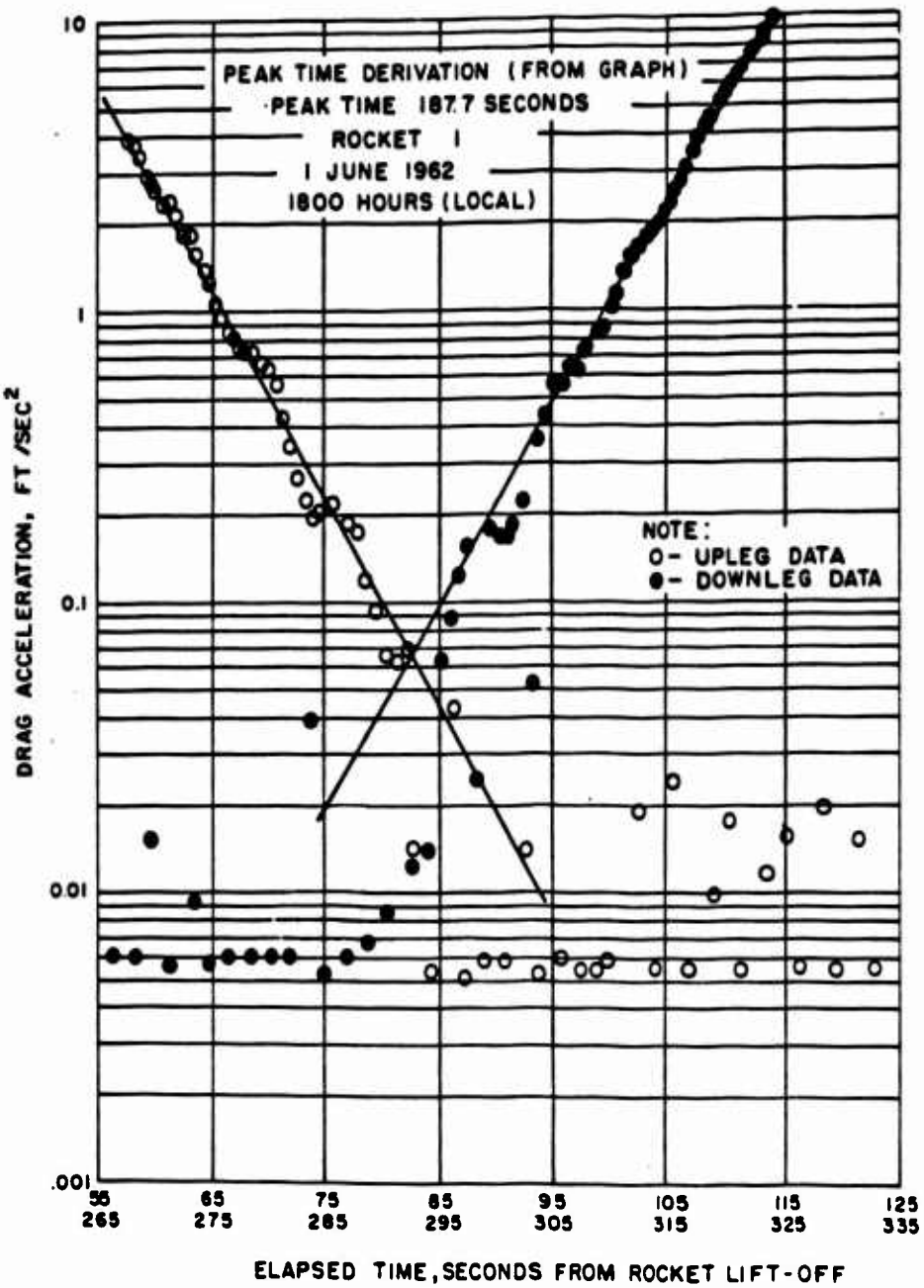

Figure 3.10 Graph for deriving peak time, Rocket 1.

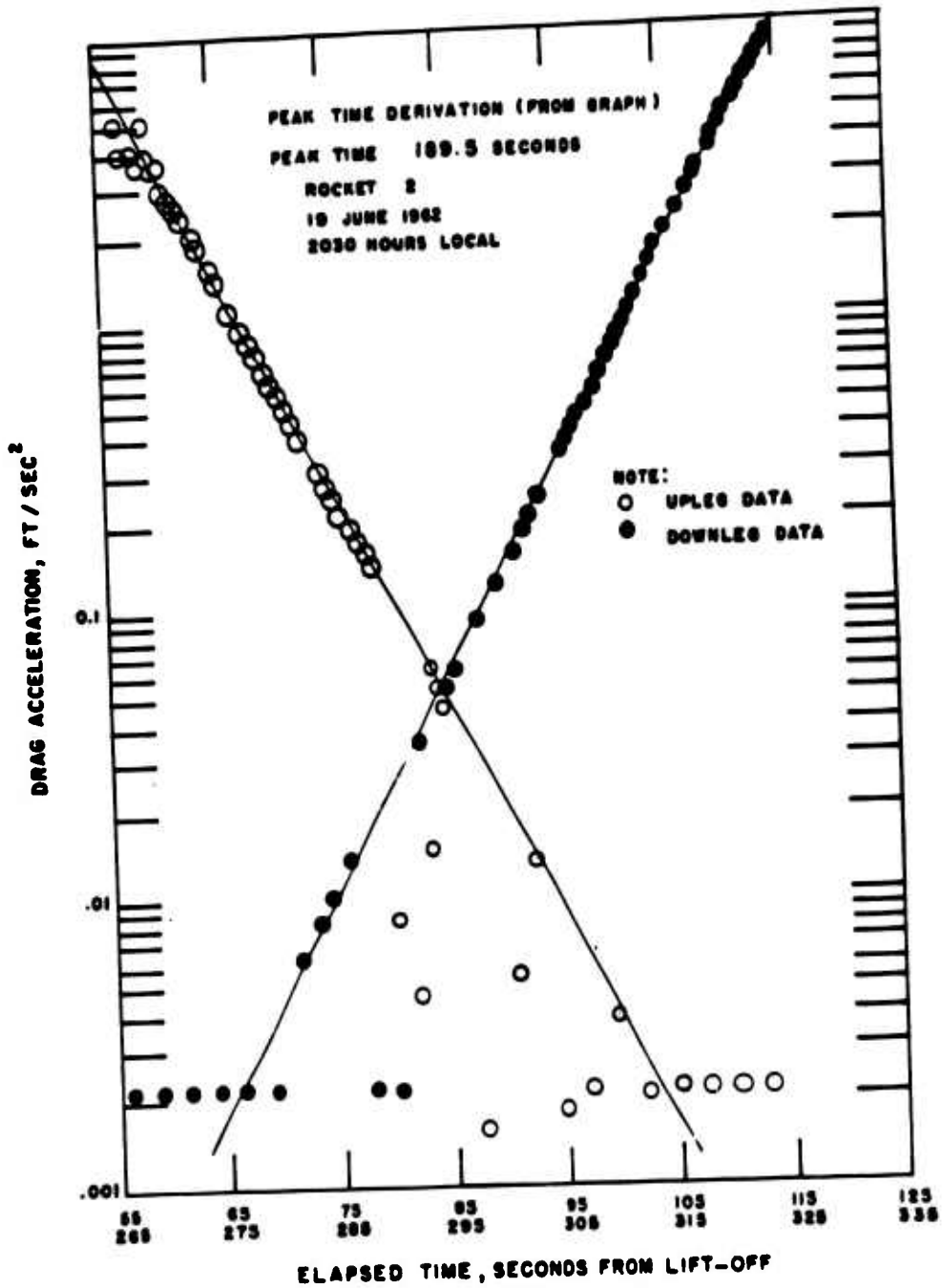

Figure 3.11 Graph for deriving peak time, Rocket 2.

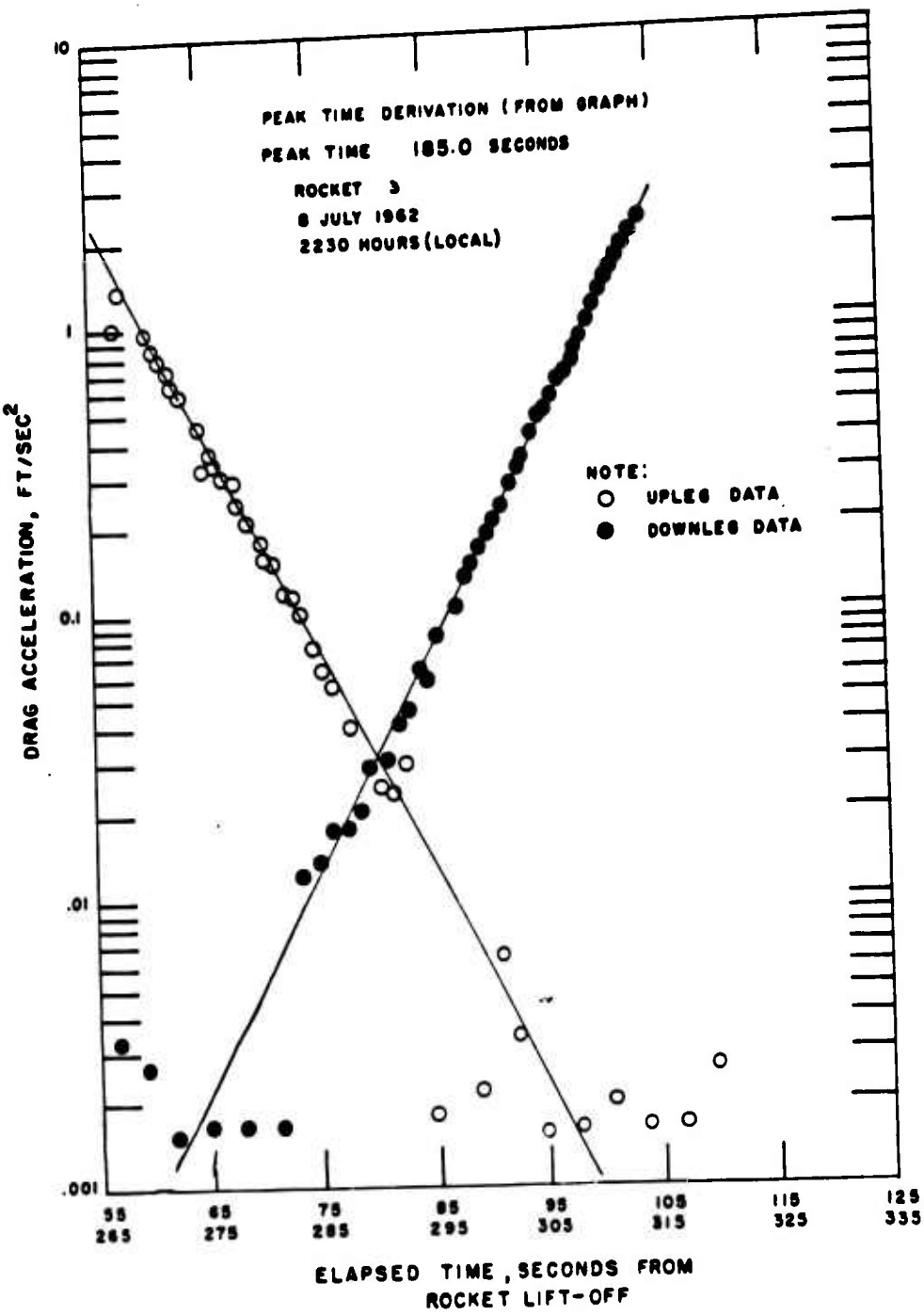

Figure 3.12 Graph for deriving peak time, Rocket 3.

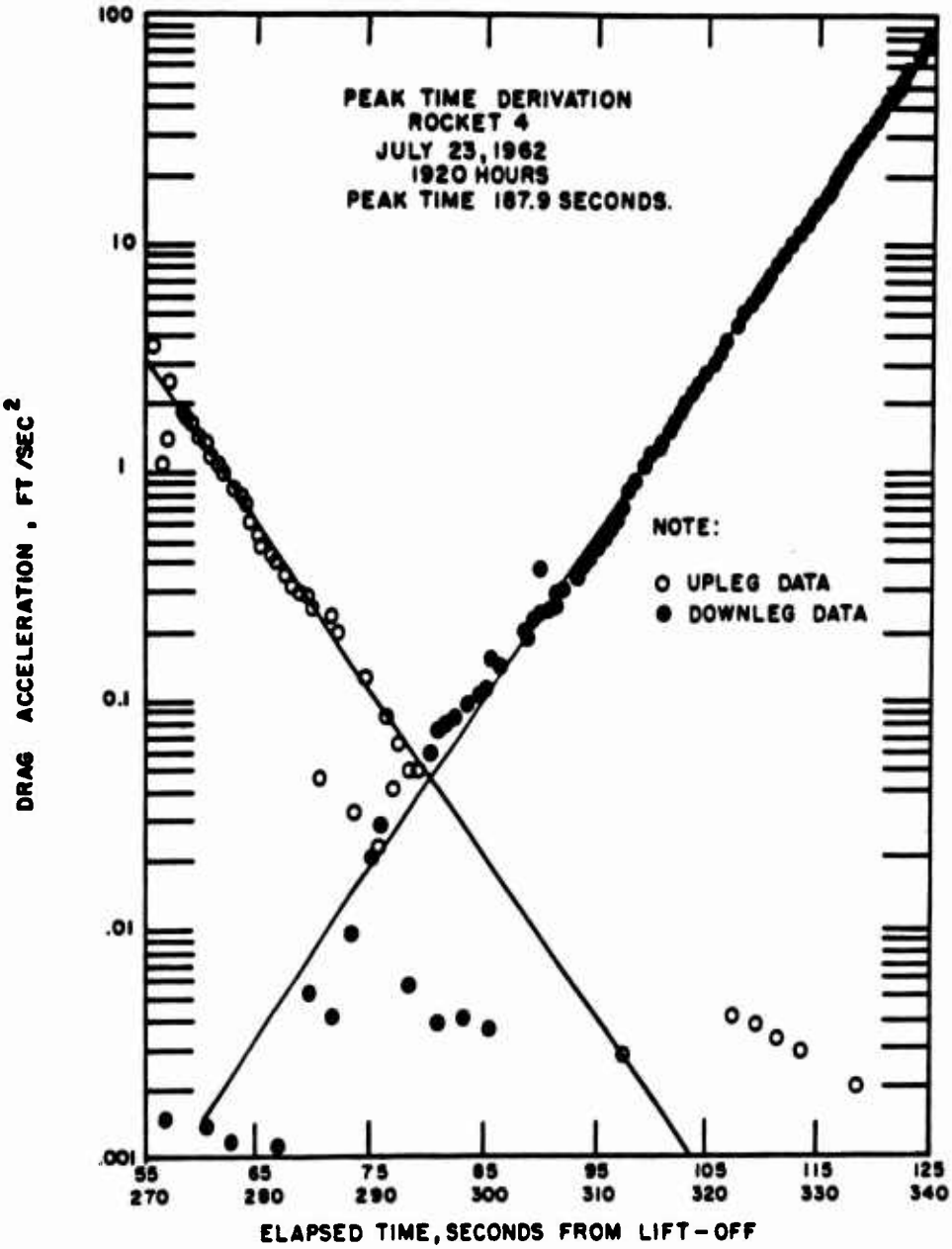

Figure 3.13 Graph for deriving peak time, Rocket 4.

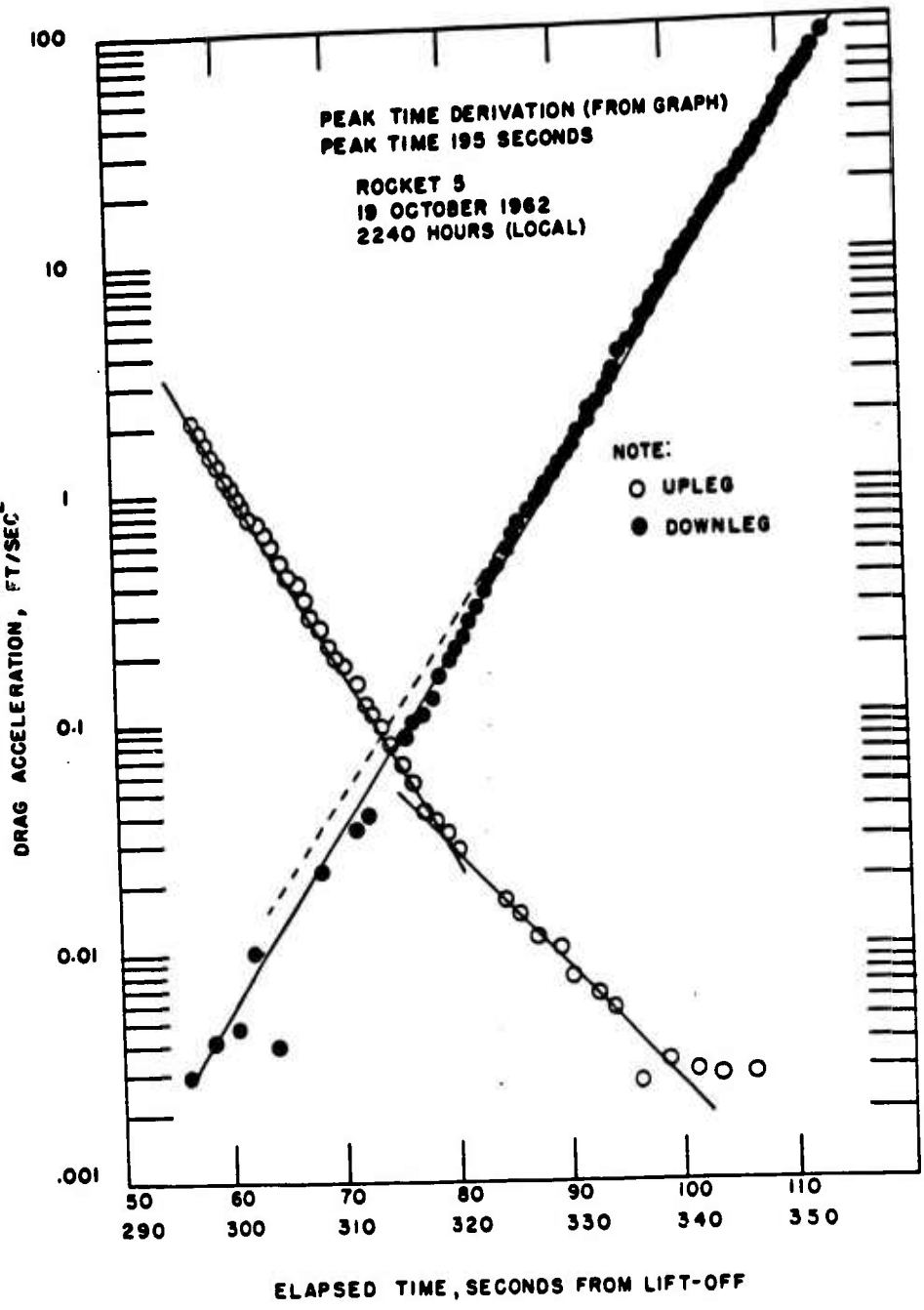

Figure 3.14 Graph for deriving peak time, Rocket 5.

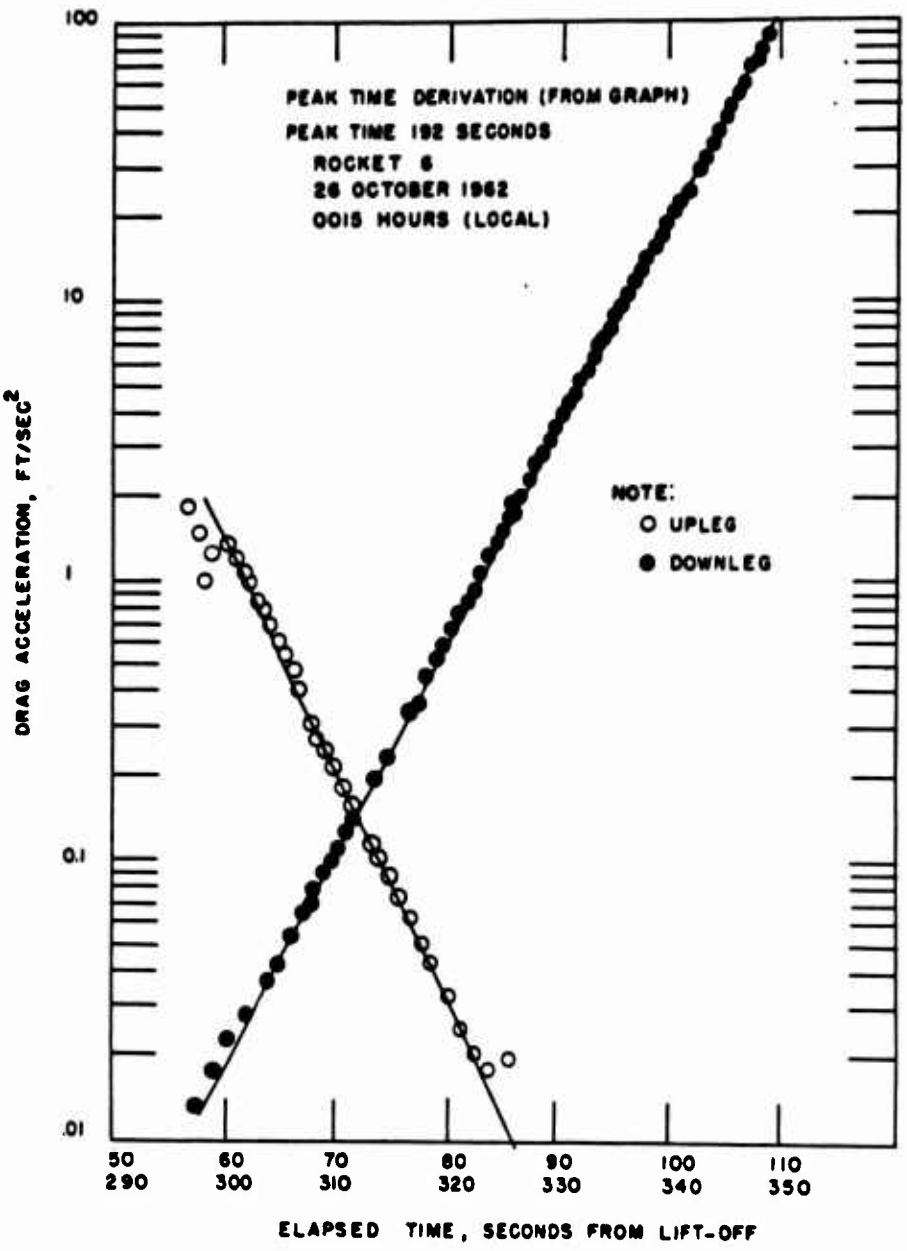

Figure 3.15 Graph for deriving peak time, Rocket 6.

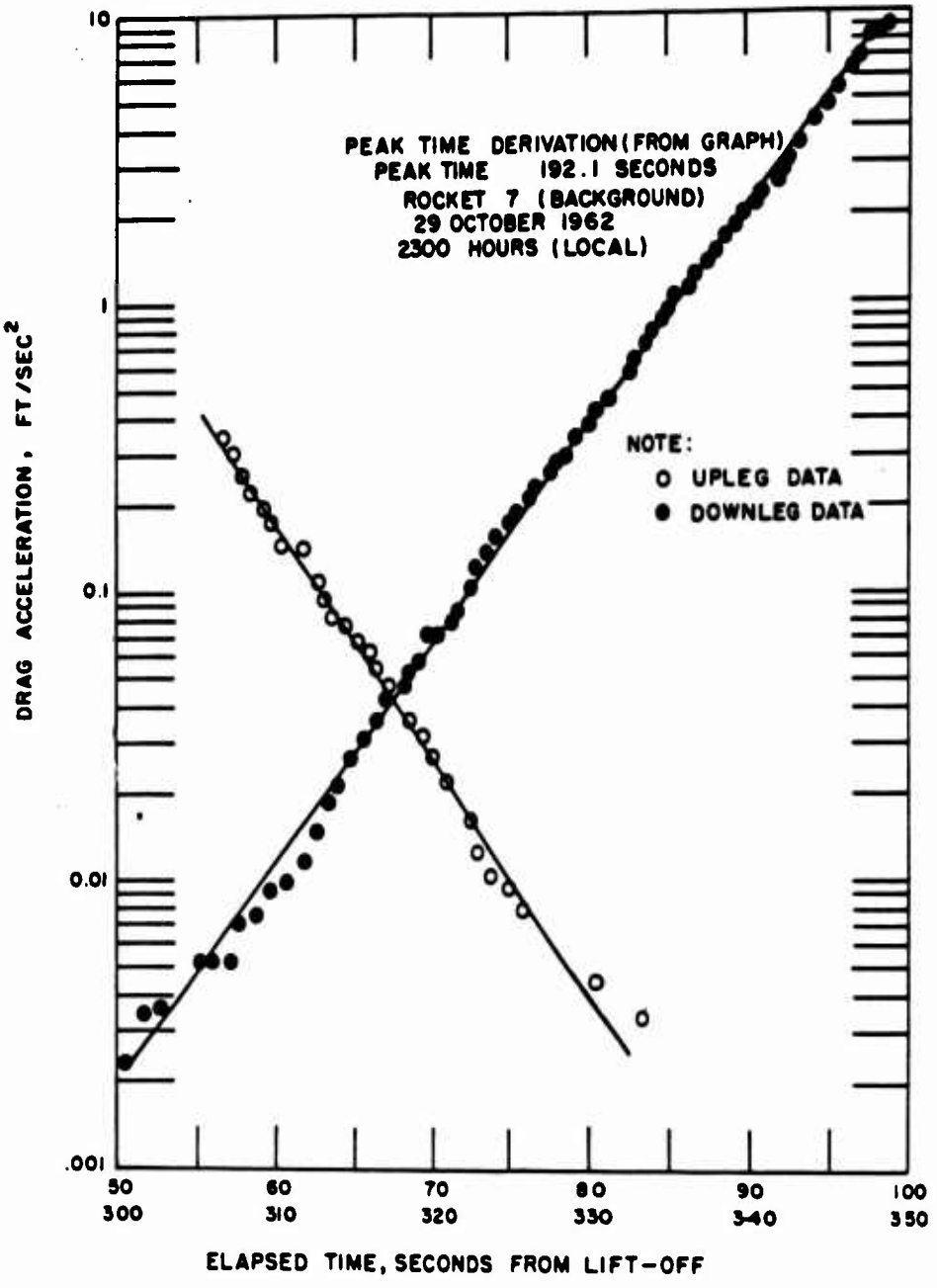

Figure 3.16 Graph for deriving peak time, Rocket 7.

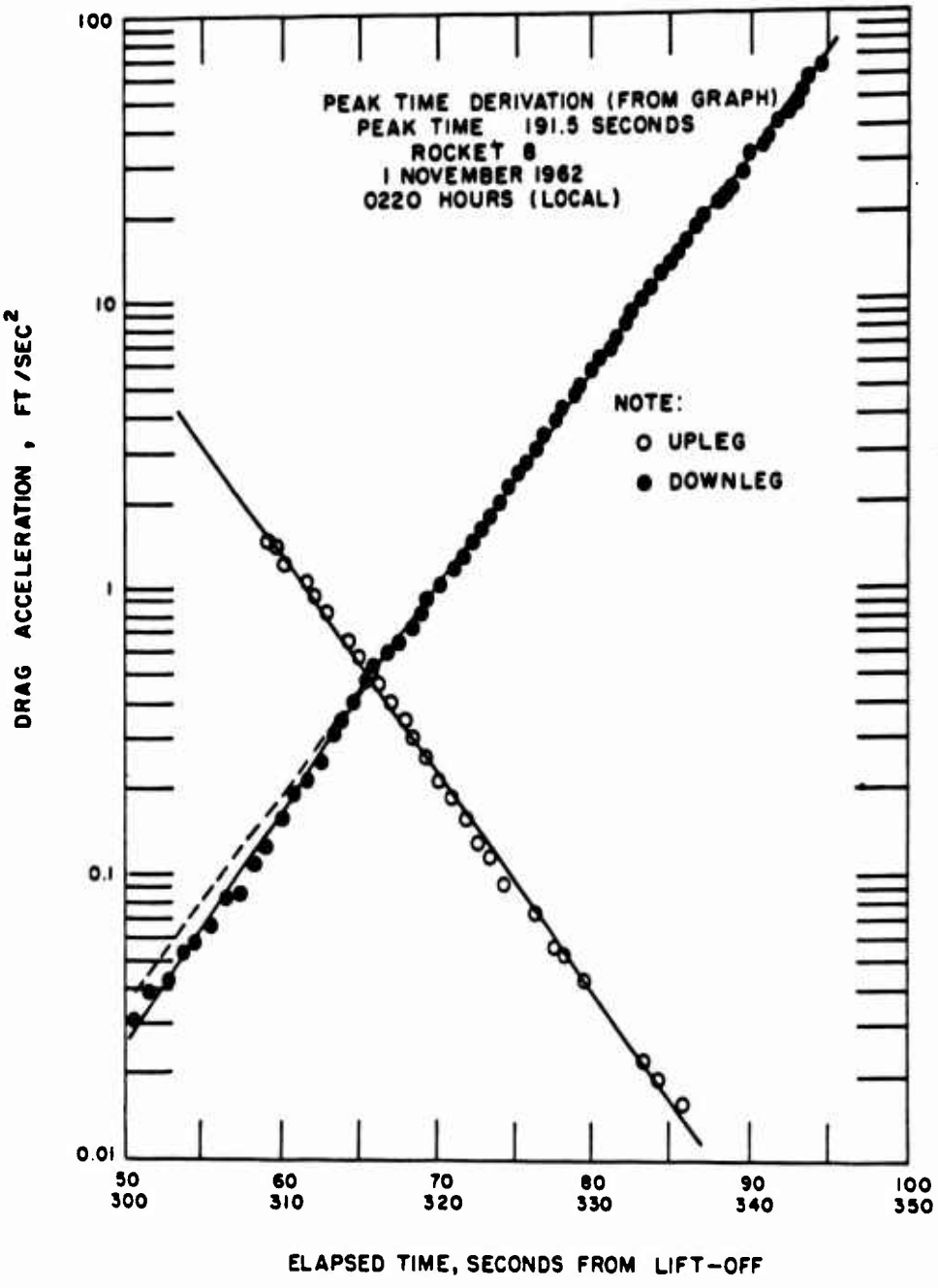

Figure 3.17 Graph for deriving peak time, Rocket 8.

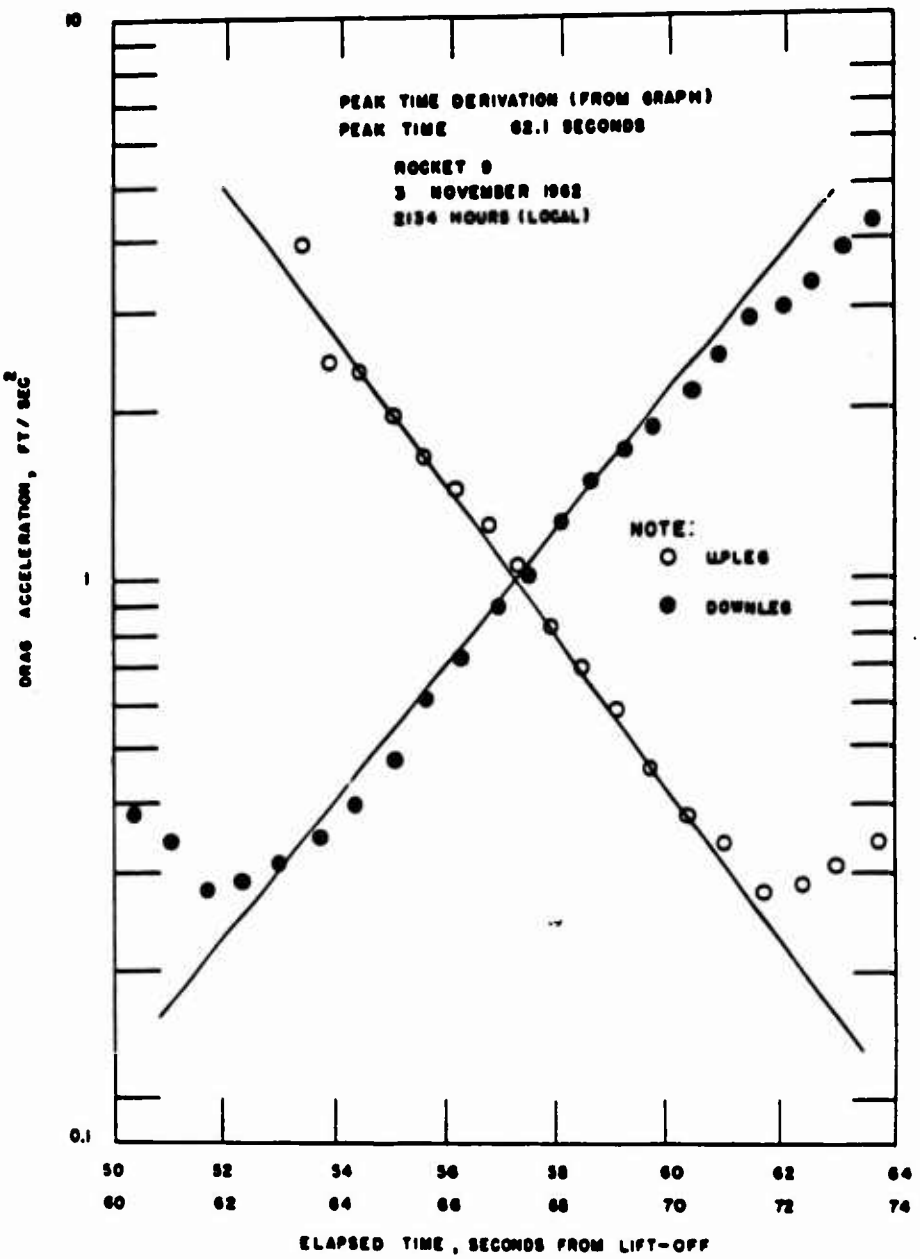

Figure 3.18 Graph for deriving peak time, Rocket 9.

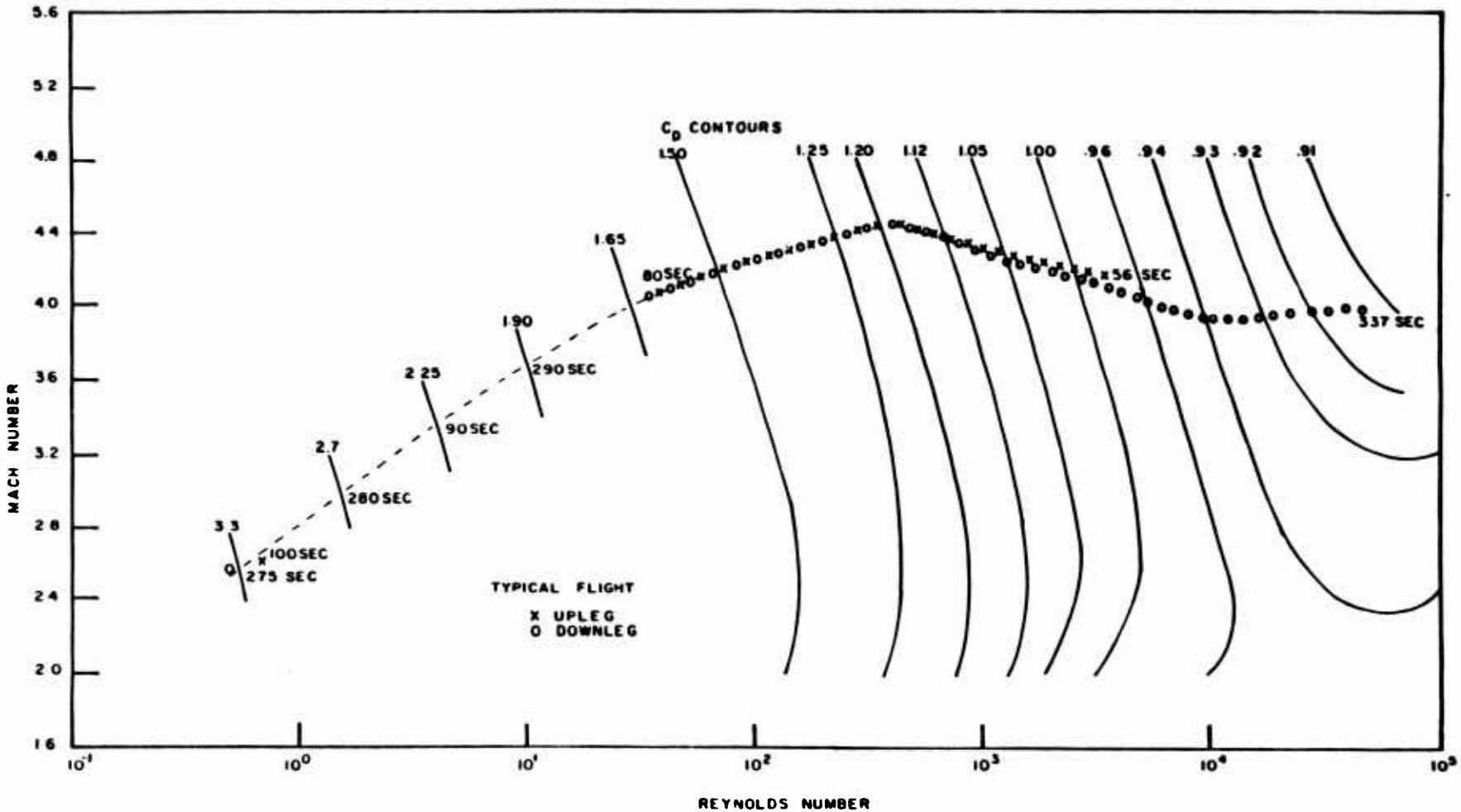

Figure 3.19 Curve of drag coefficient versus Mach and Reynolds numbers.

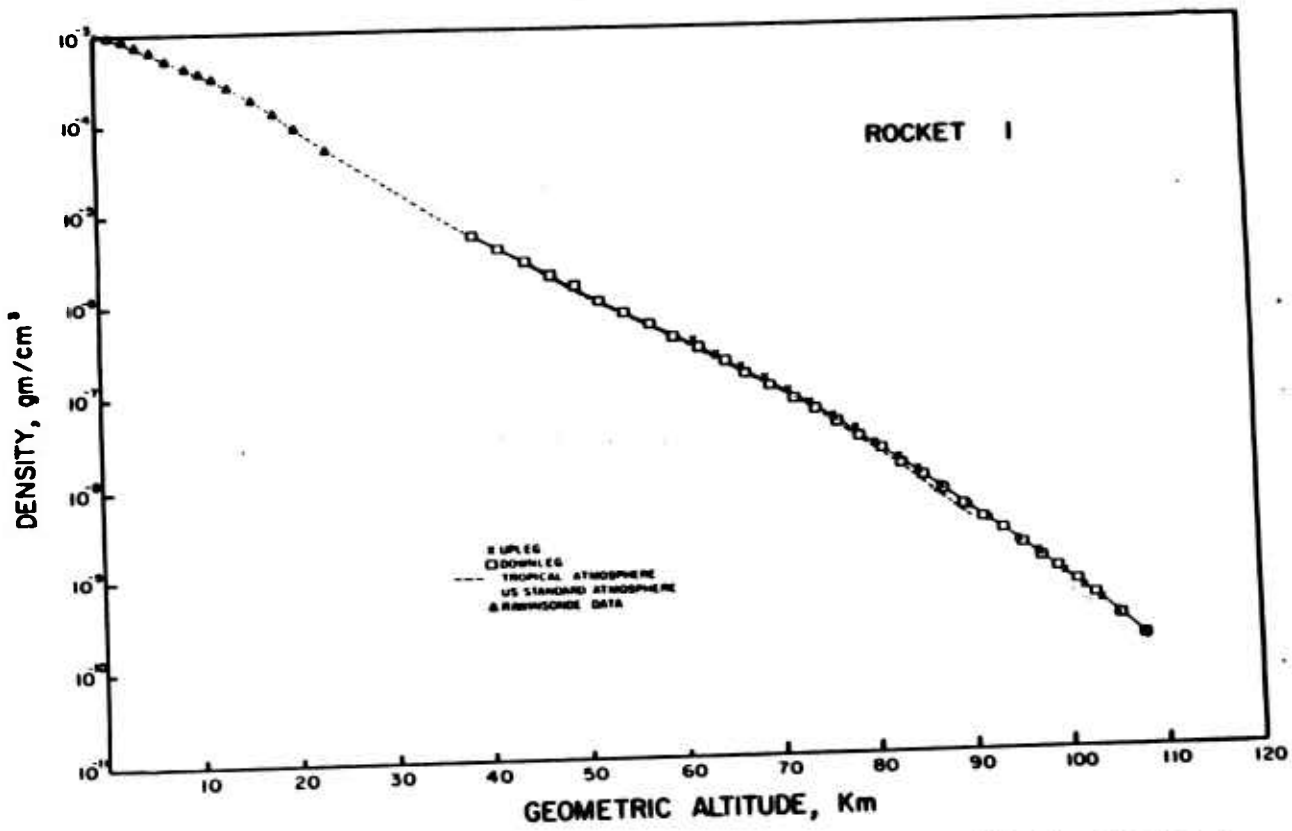

Figure 3.20 Curve of atmospheric density versus altitude, Rocket 1.

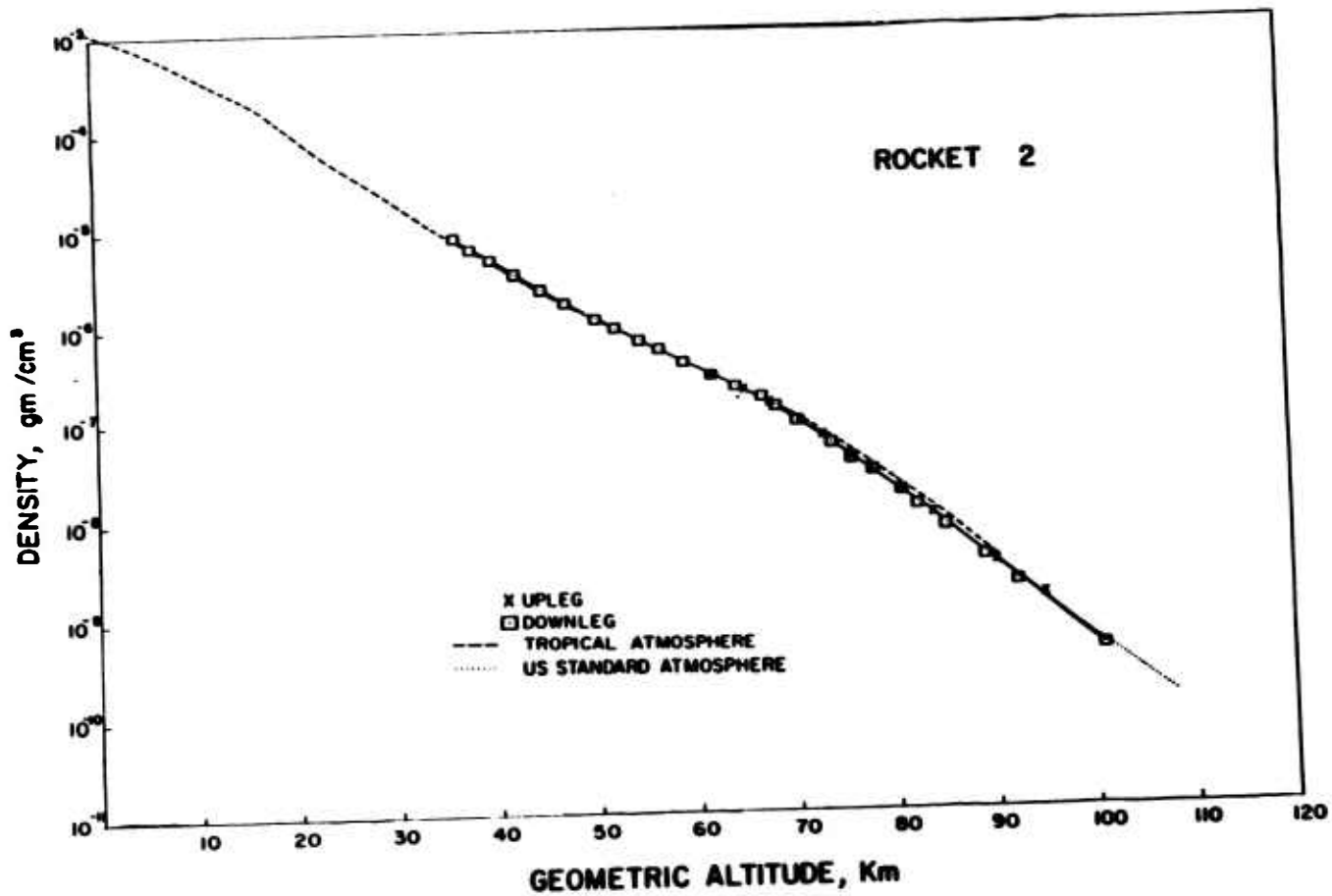

Figure 3.21 Curve of atmospheric density versus altitude, Rocket 2.

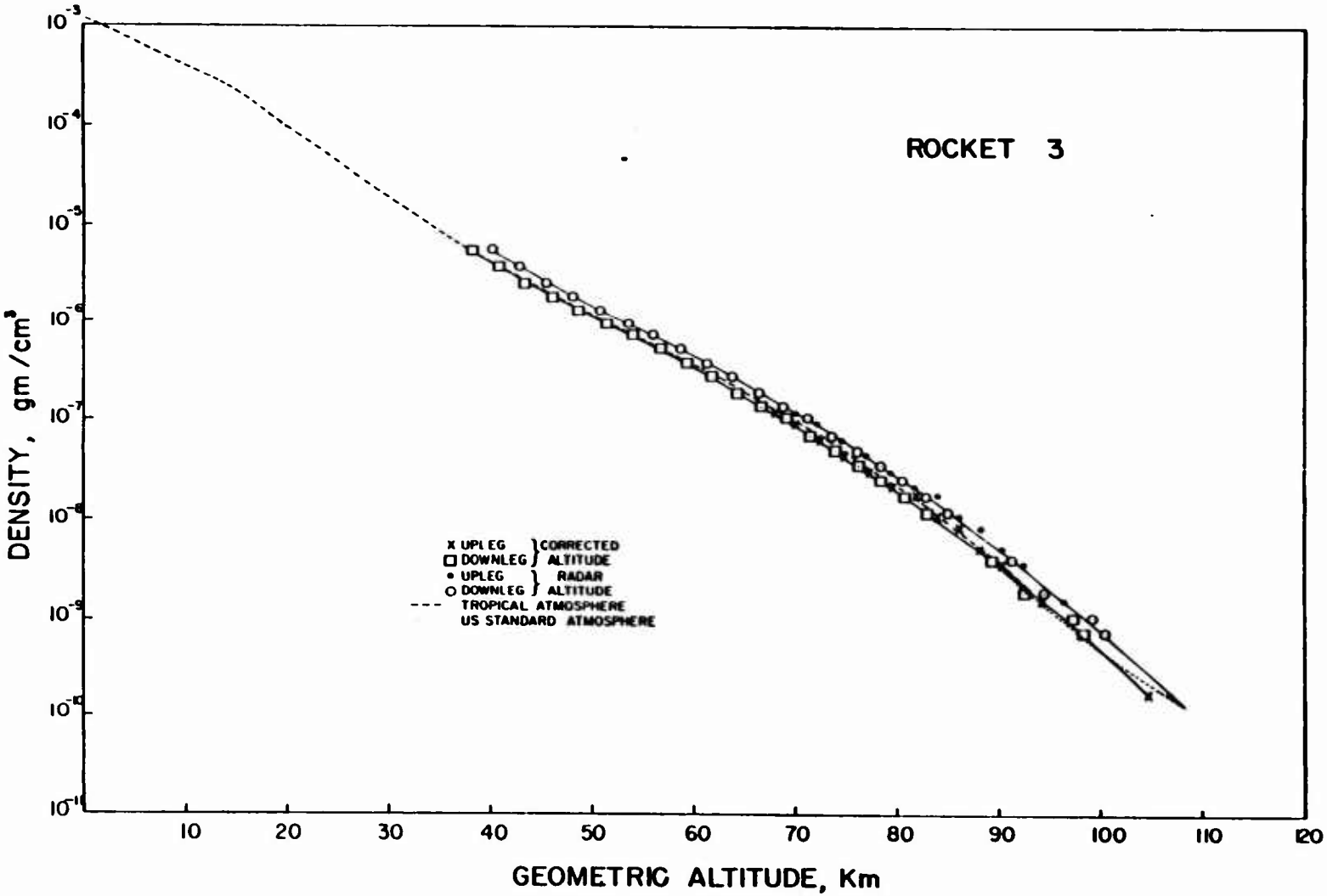

Figure 3.22 Curve of atmospheric density versus altitude, Rocket 3.

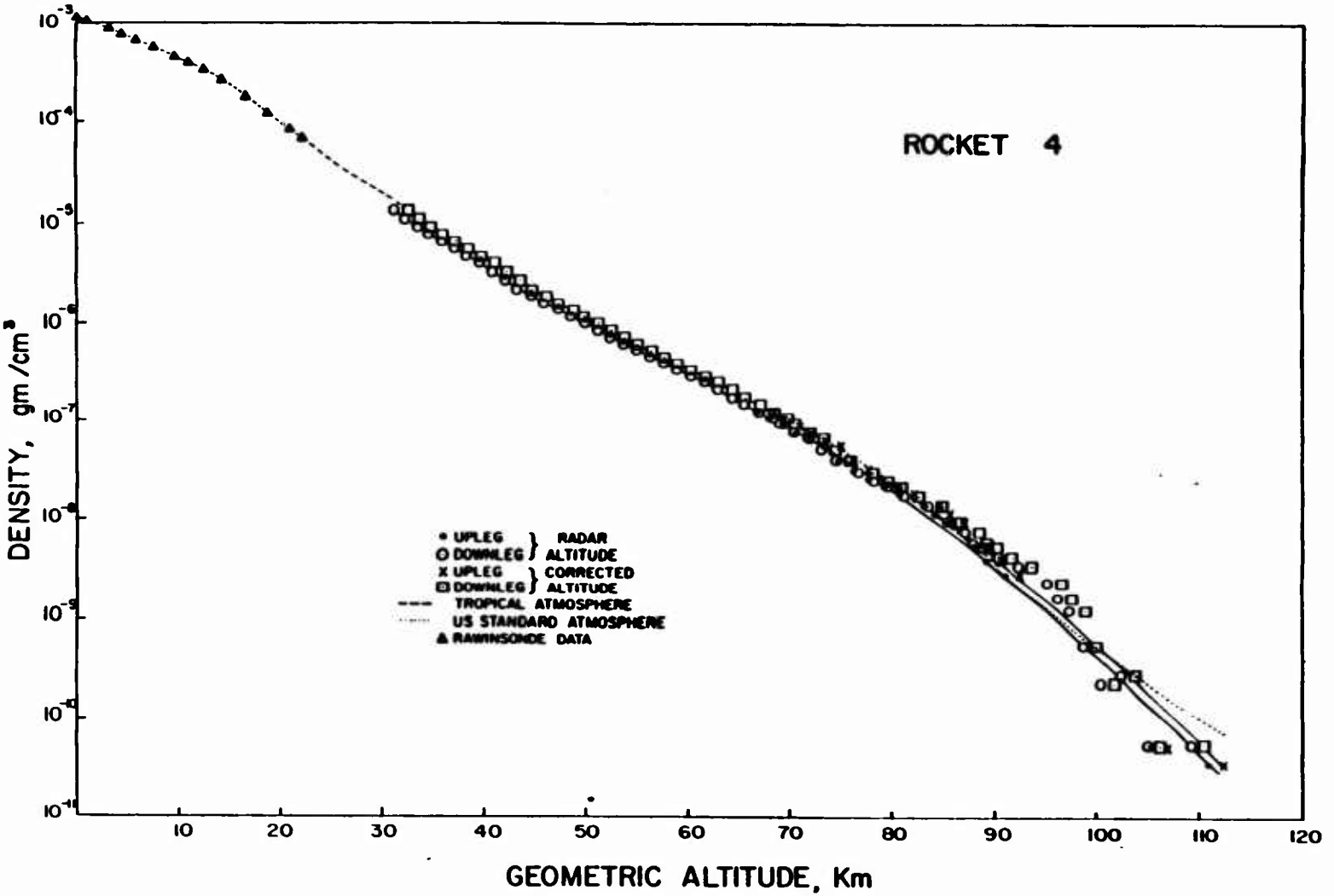

Figure 3.23 Curve of atmospheric density versus altitude, Rocket 4.

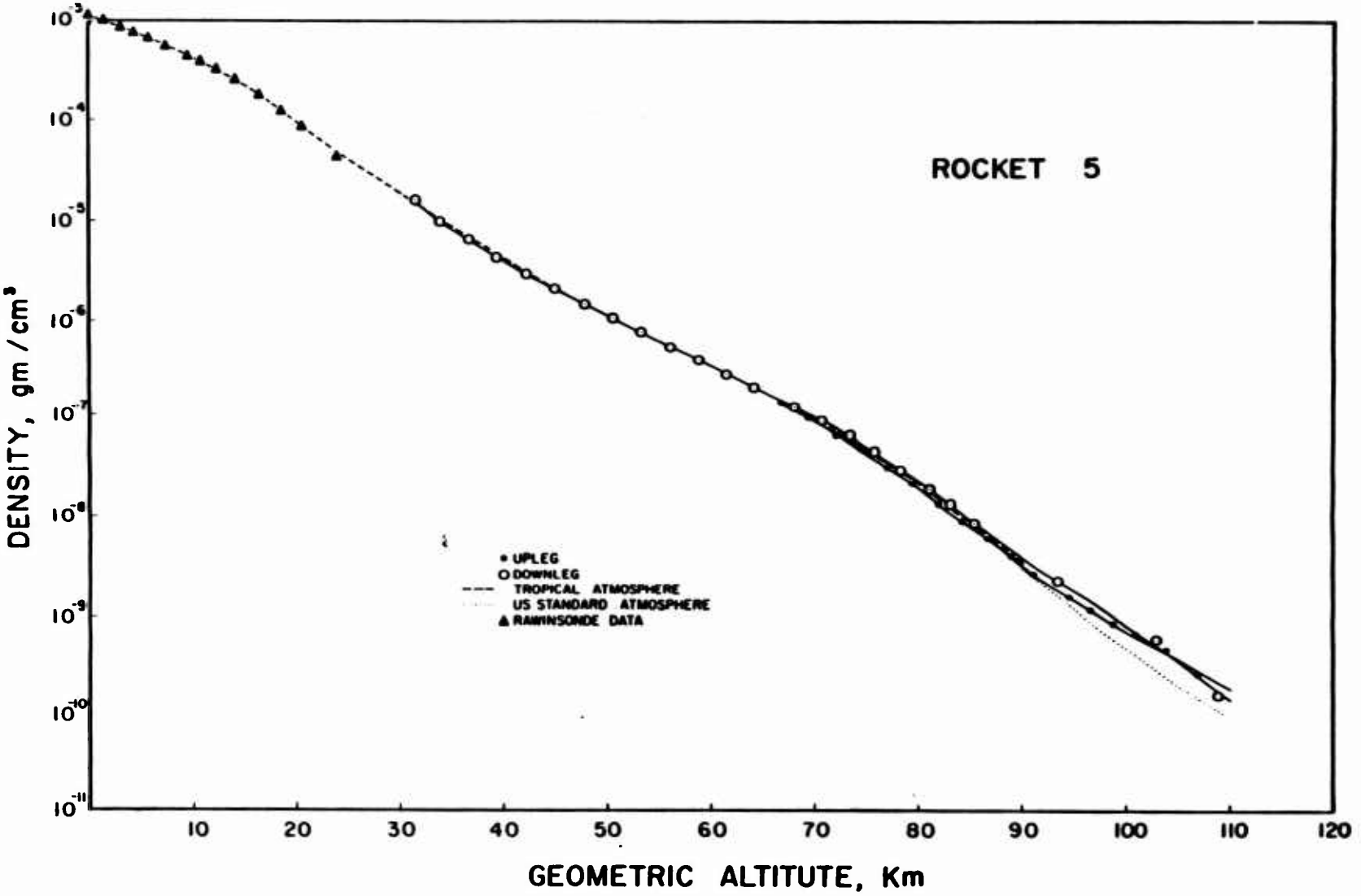

Figure 3.24 Curve of atmospheric density versus altitude, Rocket 5.

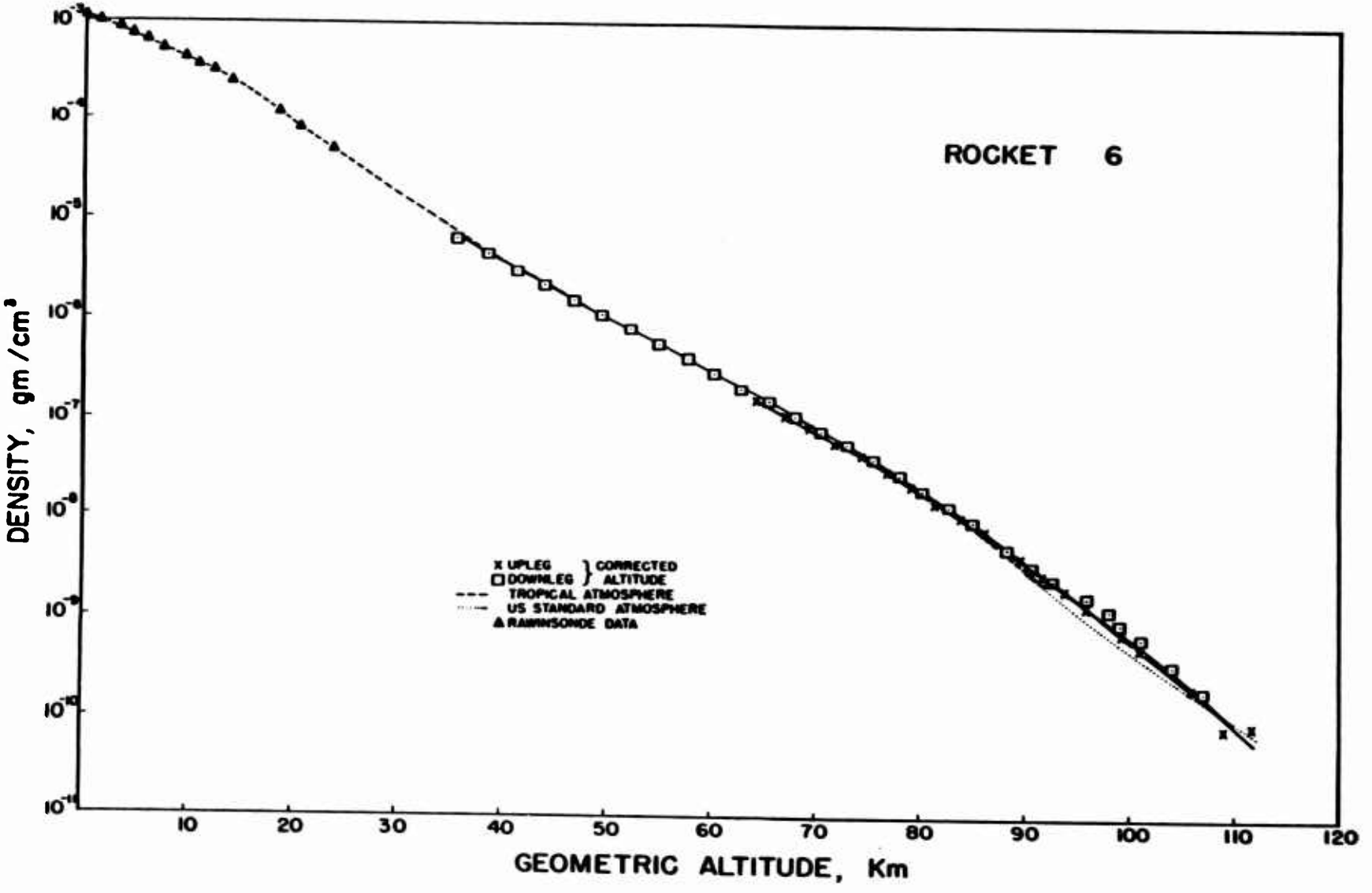

Figure 3.25 Curve of atmospheric density versus altitude, Rocket 6.

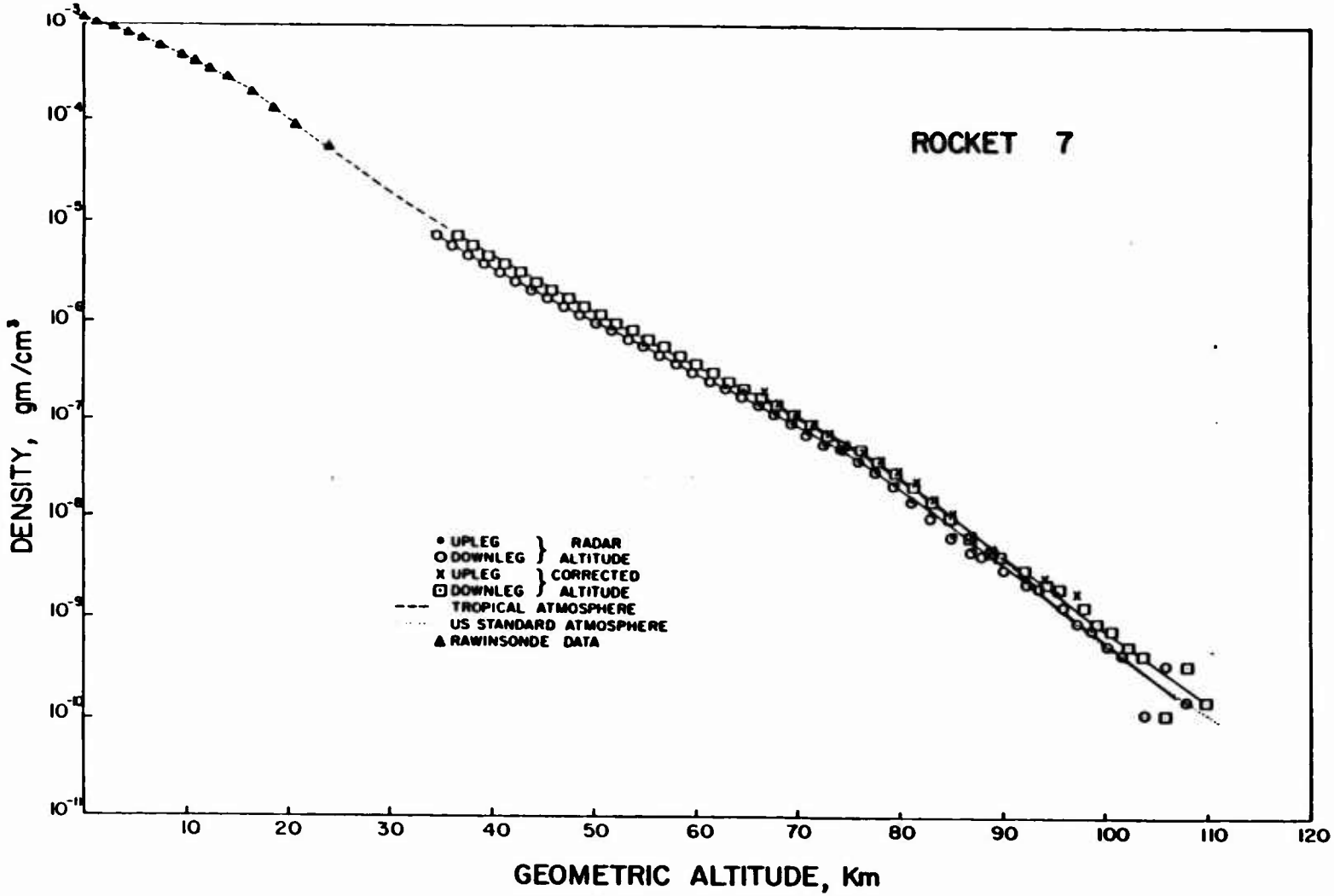

Figure 3.26 Curve of atmospheric density versus altitude, Rocket 7.

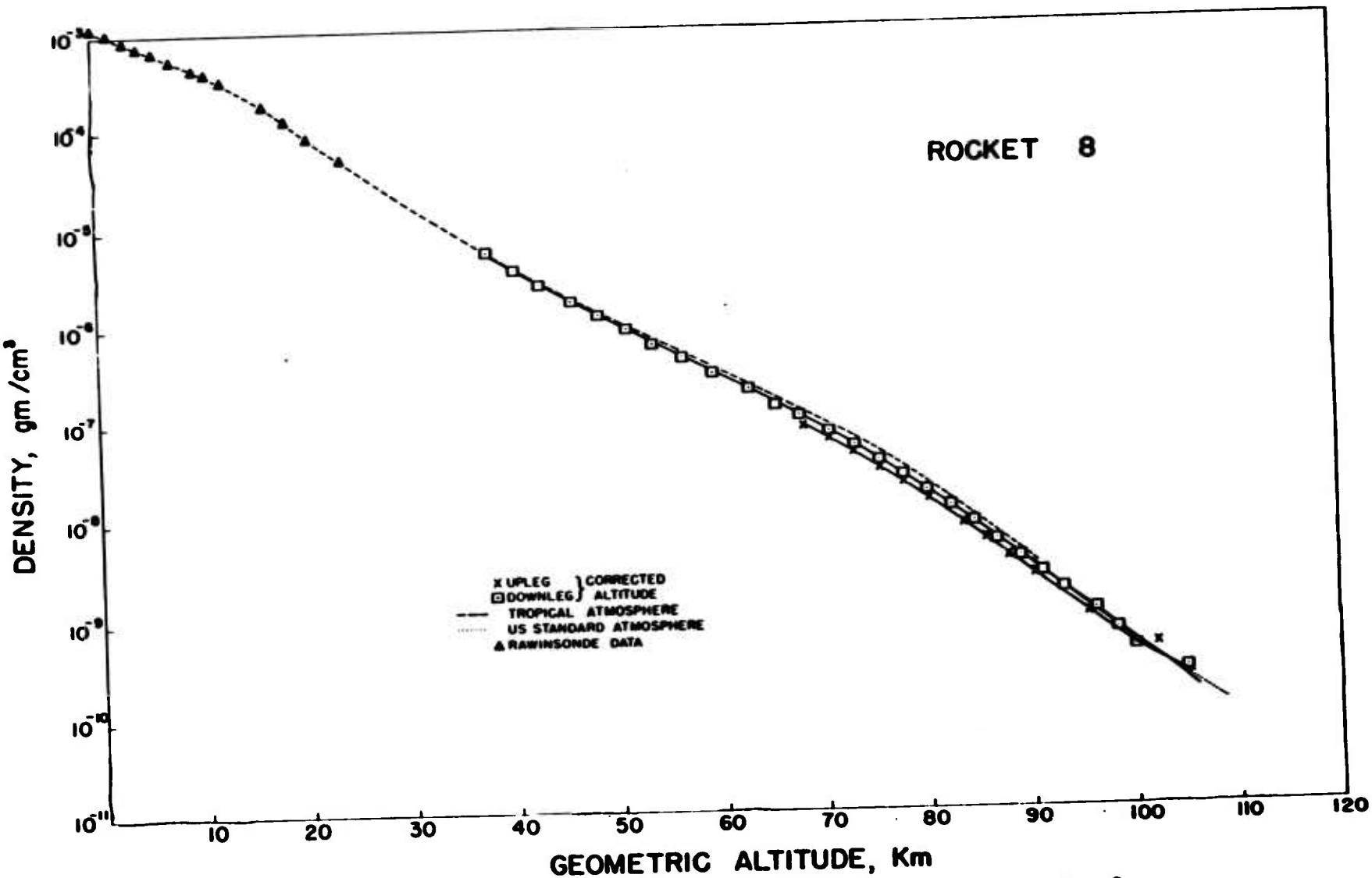

Figure 3.27 Curve of atmospheric density versus altitude, Rocket 8.

Page 207 deleted.

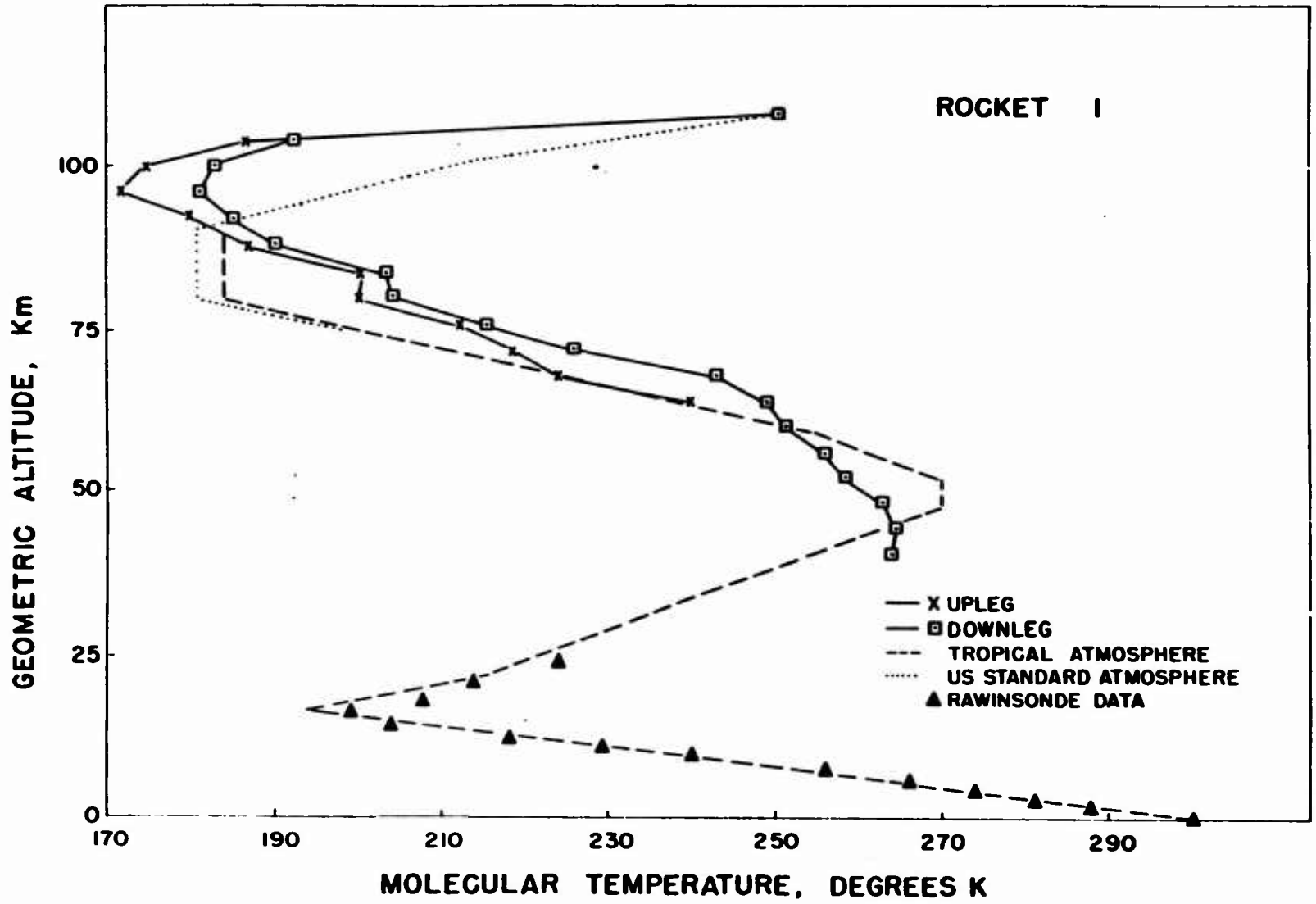

Figure 3.29 Curve of atmospheric temperature versus altitude, Rocket 1.

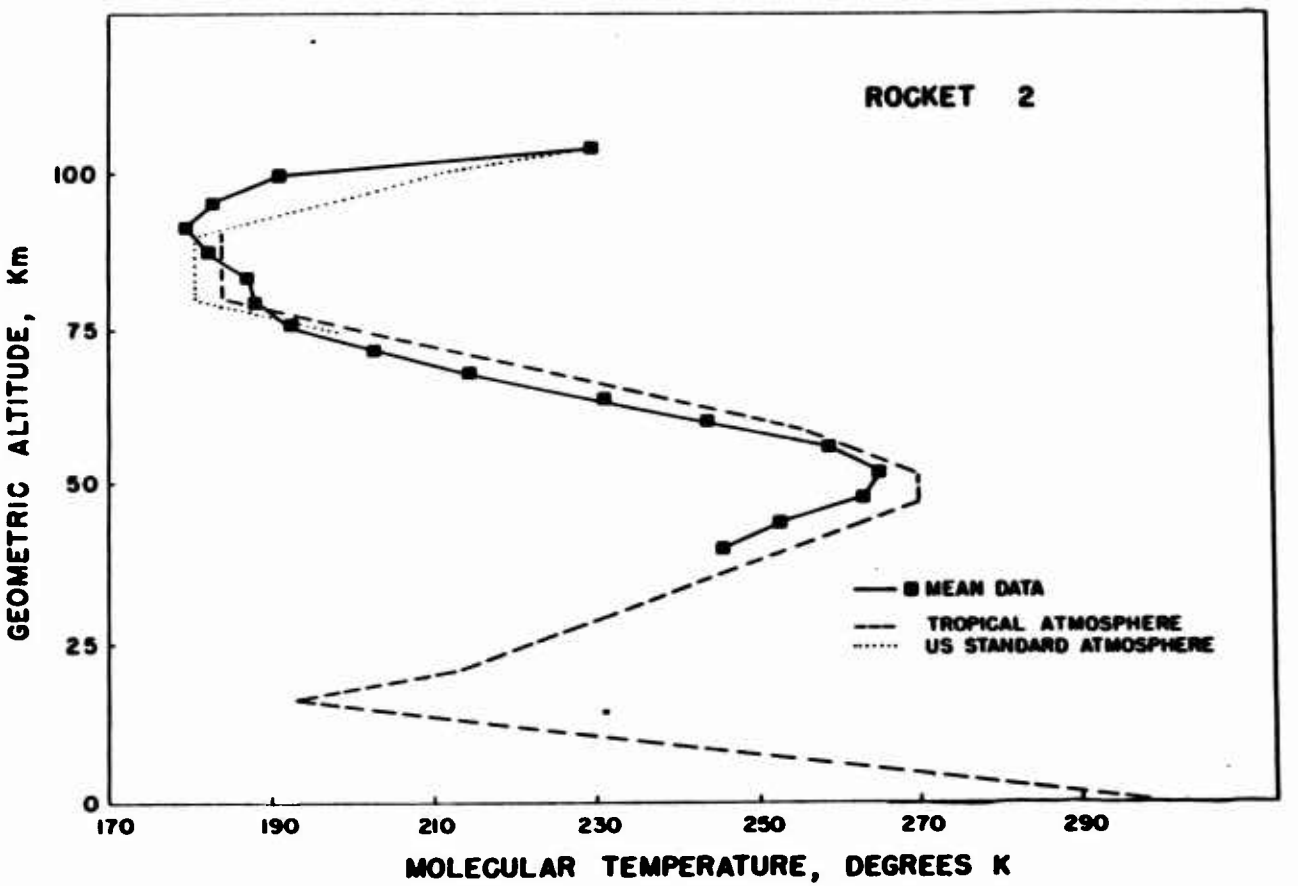

Figure 3.30 Curve of atmospheric temperature versus altitude, Rocket 2.

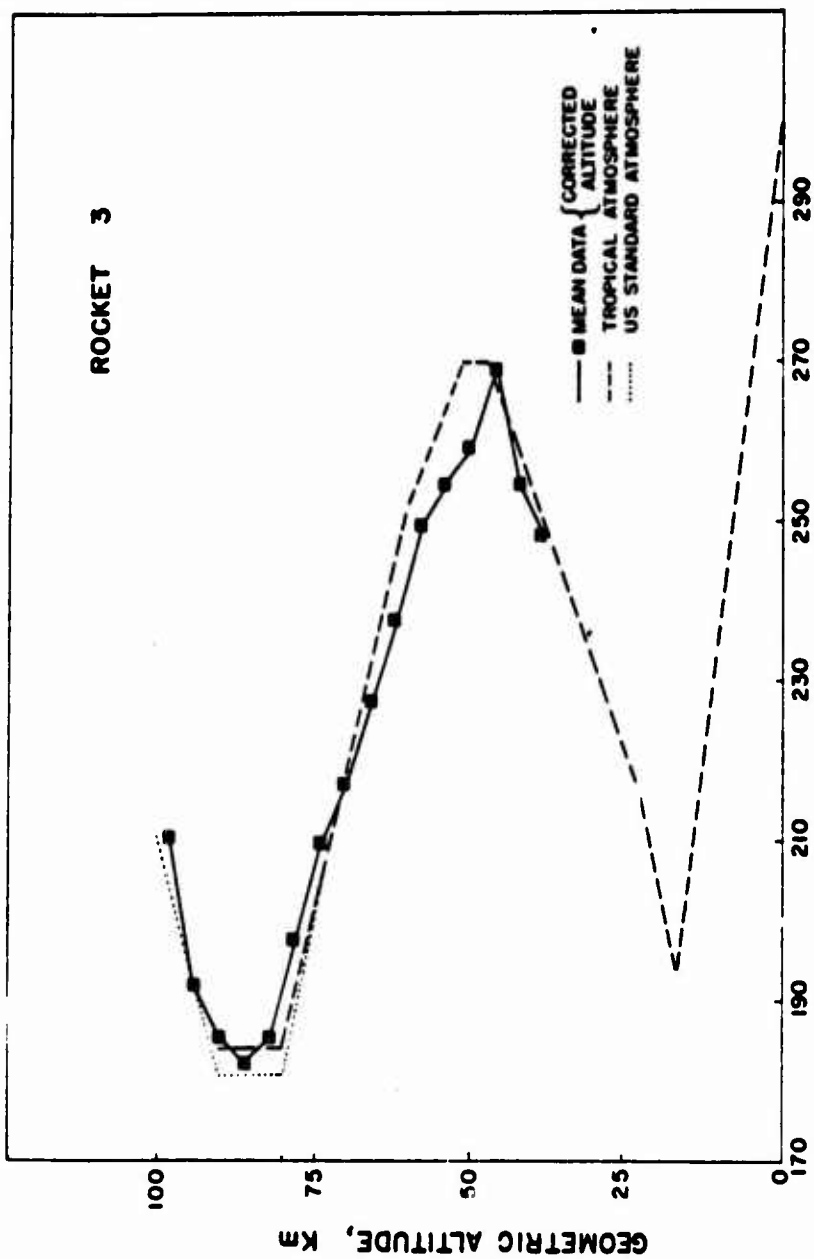

Figure 3.31 Curve of atmospheric temperature versus altitude, Rocket 3.

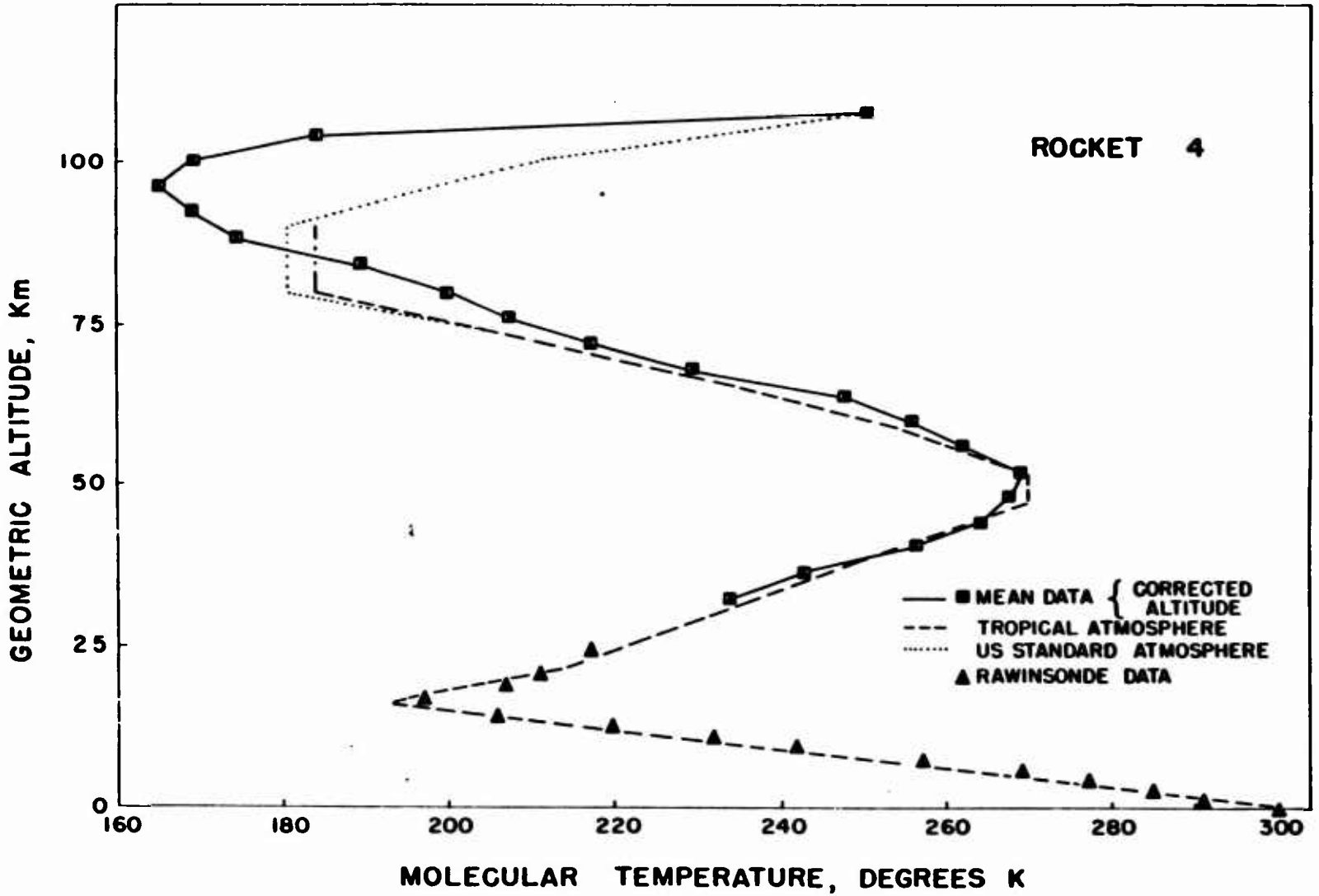

Figure 3.32 Curve of atmospheric temperature versus altitude, Rocket 4.

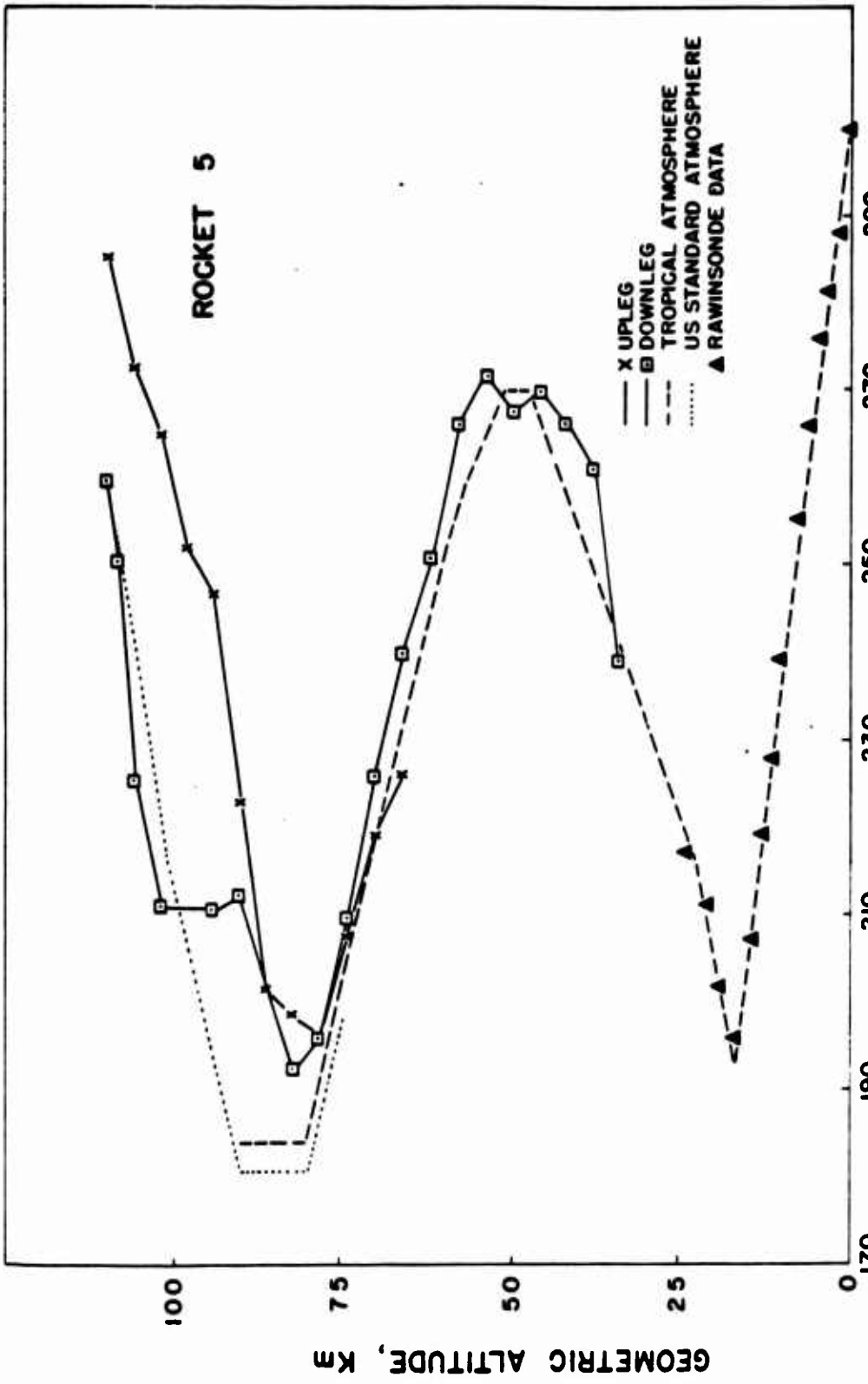

Figure 3.33 Curve of atmospheric temperature versus altitude, Rocket 5.

Page 213 deleted.

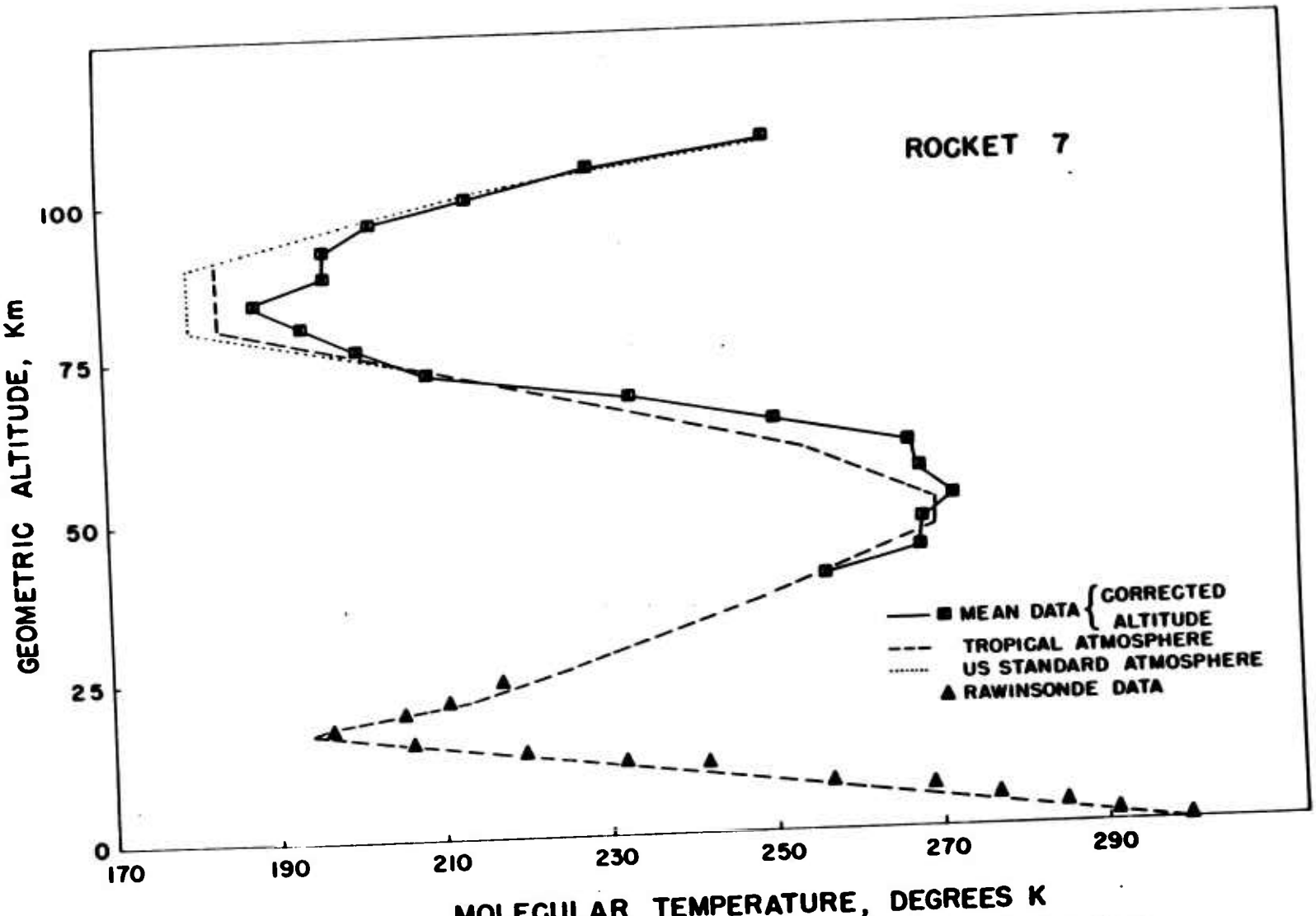

Figure 3.35 Curve of atmospheric temperature versus altitude, Rocket 7.

Pages 215 and 216 deleted.

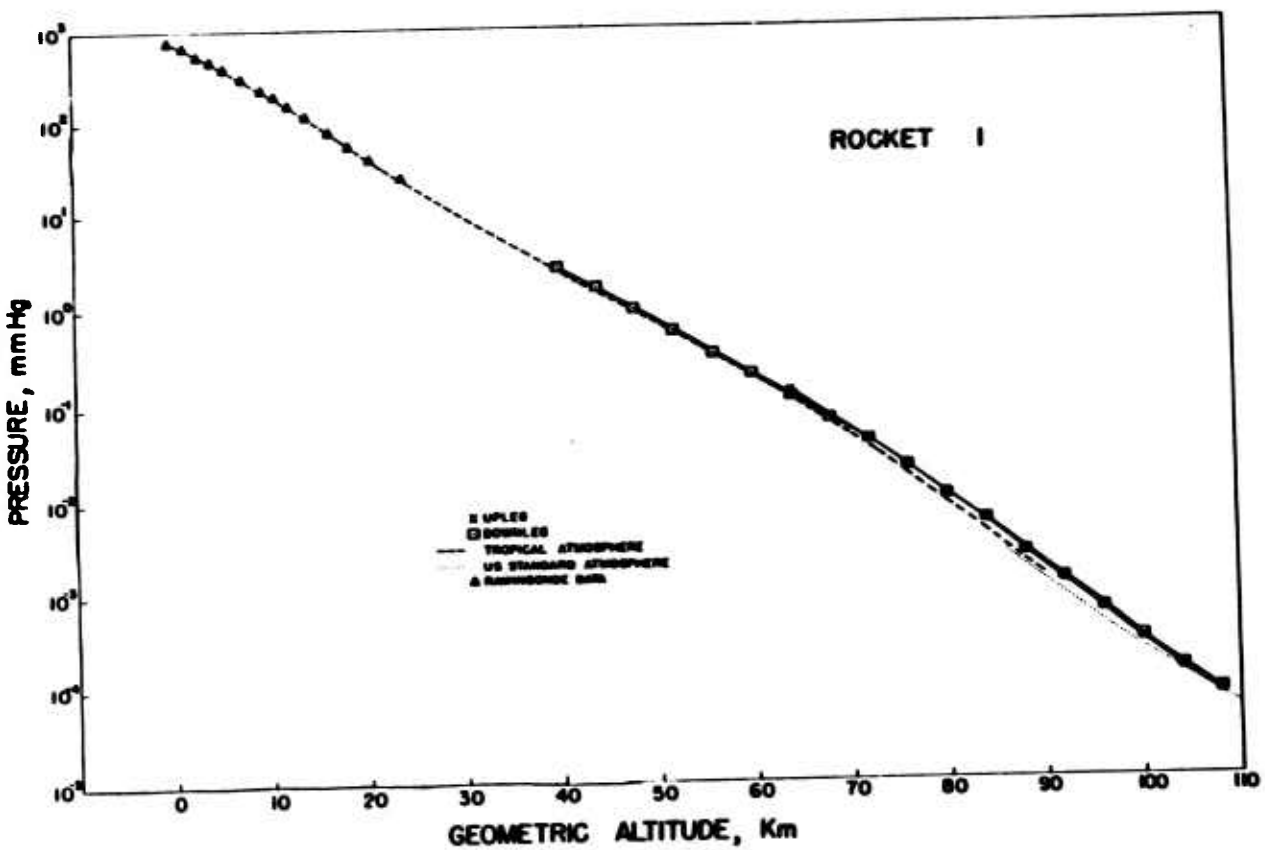

Figure 3.38 Curve of atmospheric pressure versus altitude, Rocket 1.

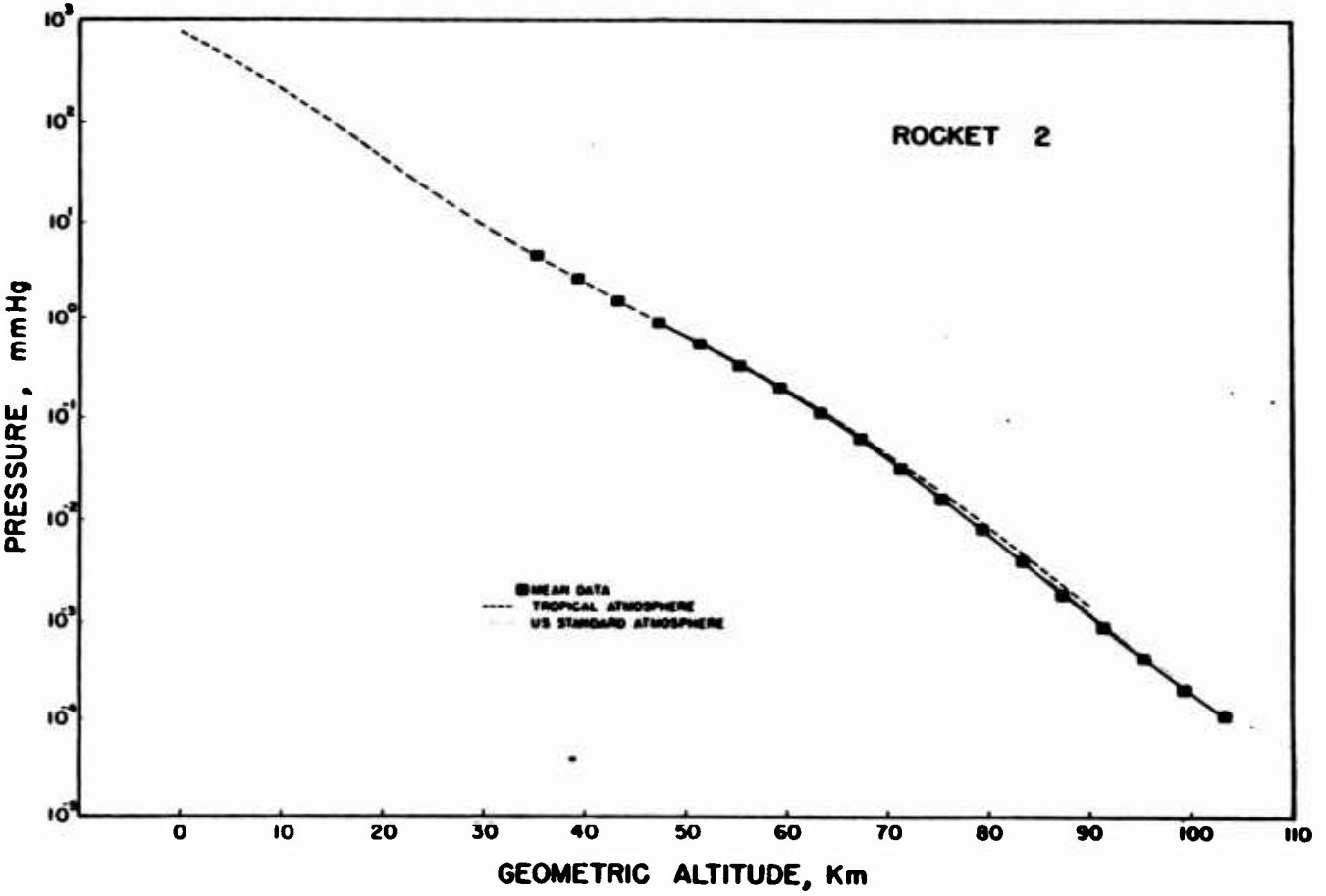

Figure 3.39 Curve of atmospheric pressure versus altitude, Rocket 2.

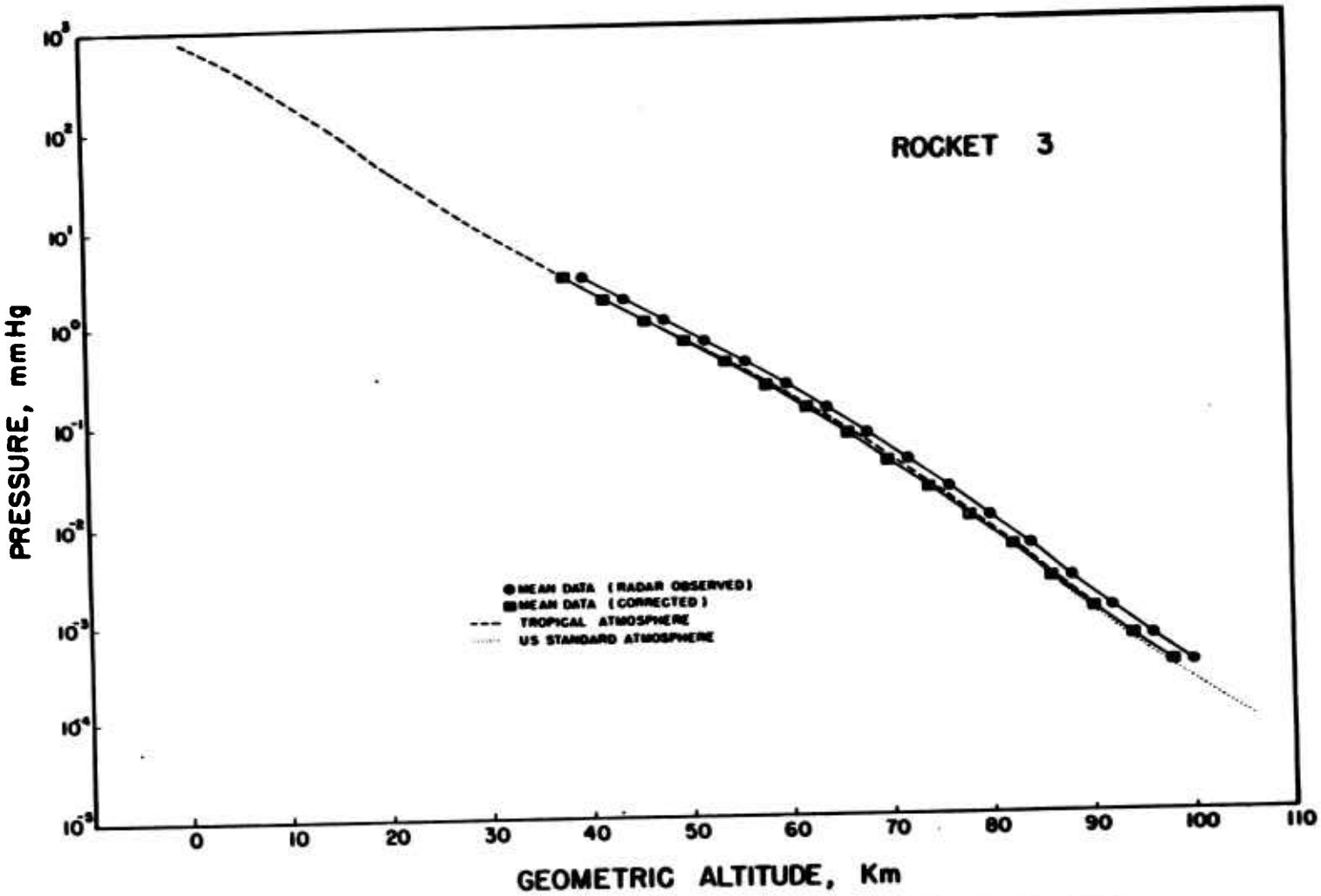

Figure 3.40 Curve of atmospheric pressure versus altitude, Rocket 3.

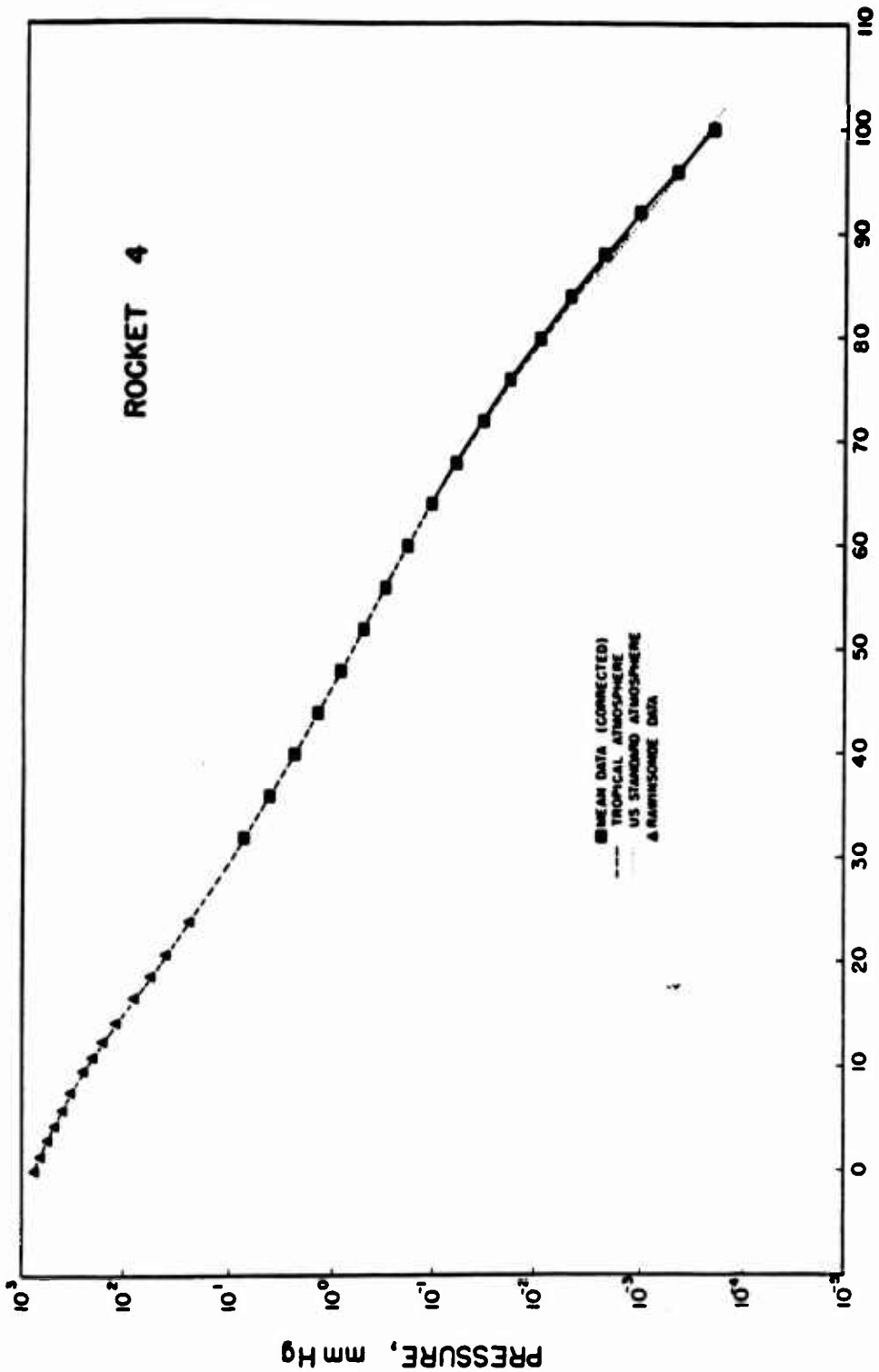

Figure 3.41 Curve of atmospheric pressure versus altitude, Rocket 4.

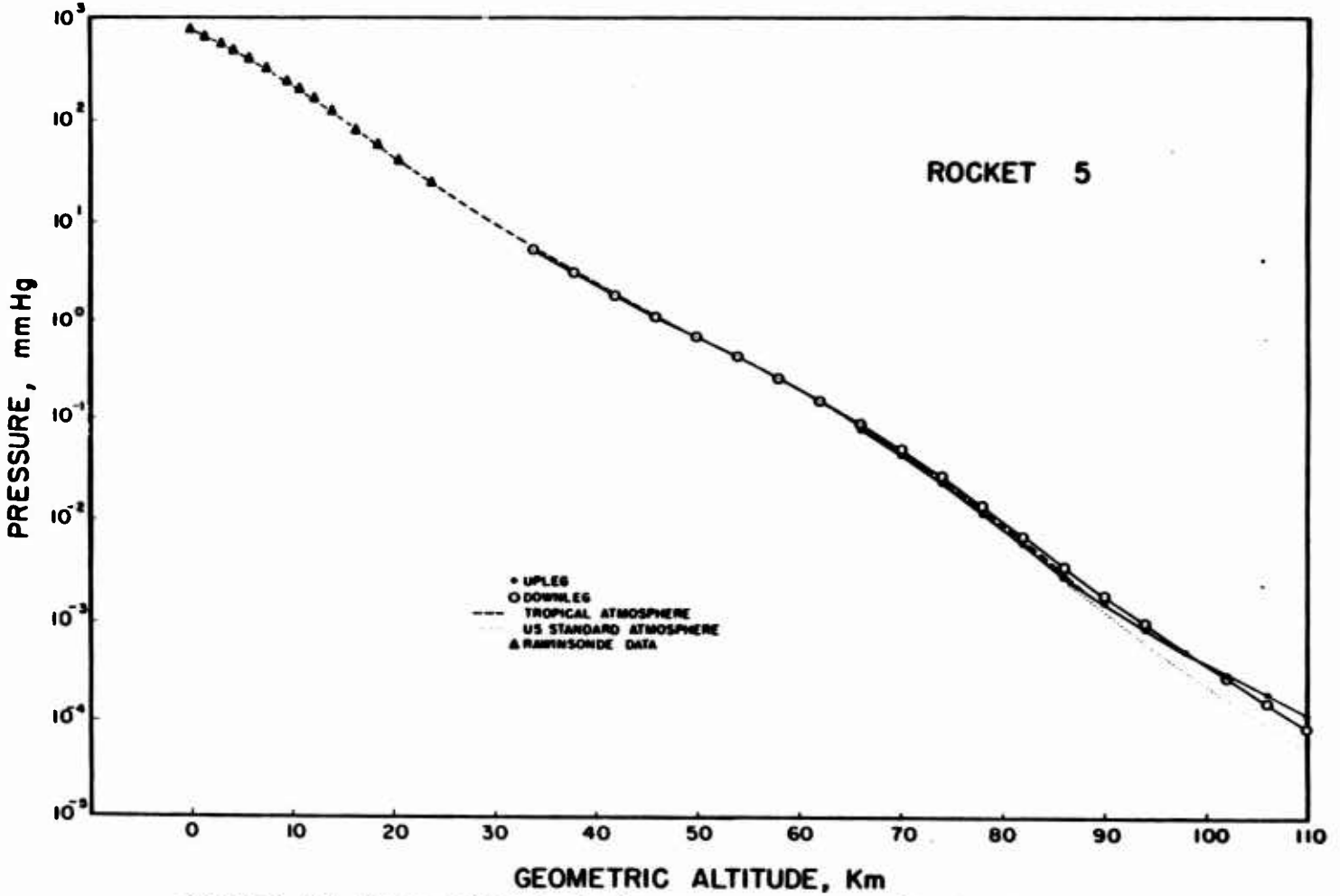

Figure 3.42 Curve of atmospheric pressure versus altitude, Rocket 5.

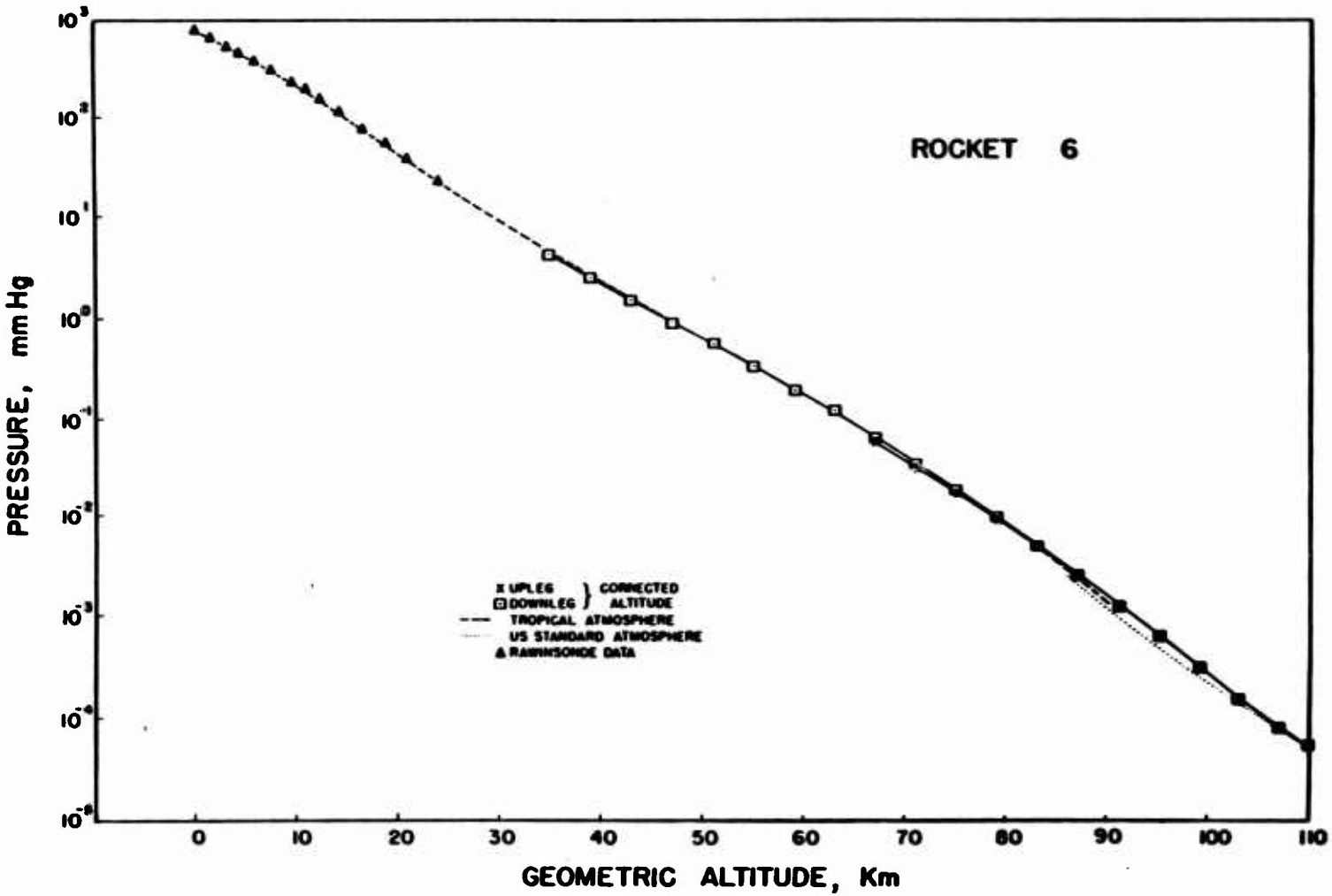

Figure 3.43 Curve of atmospheric pressure versus altitude, Rocket 6.

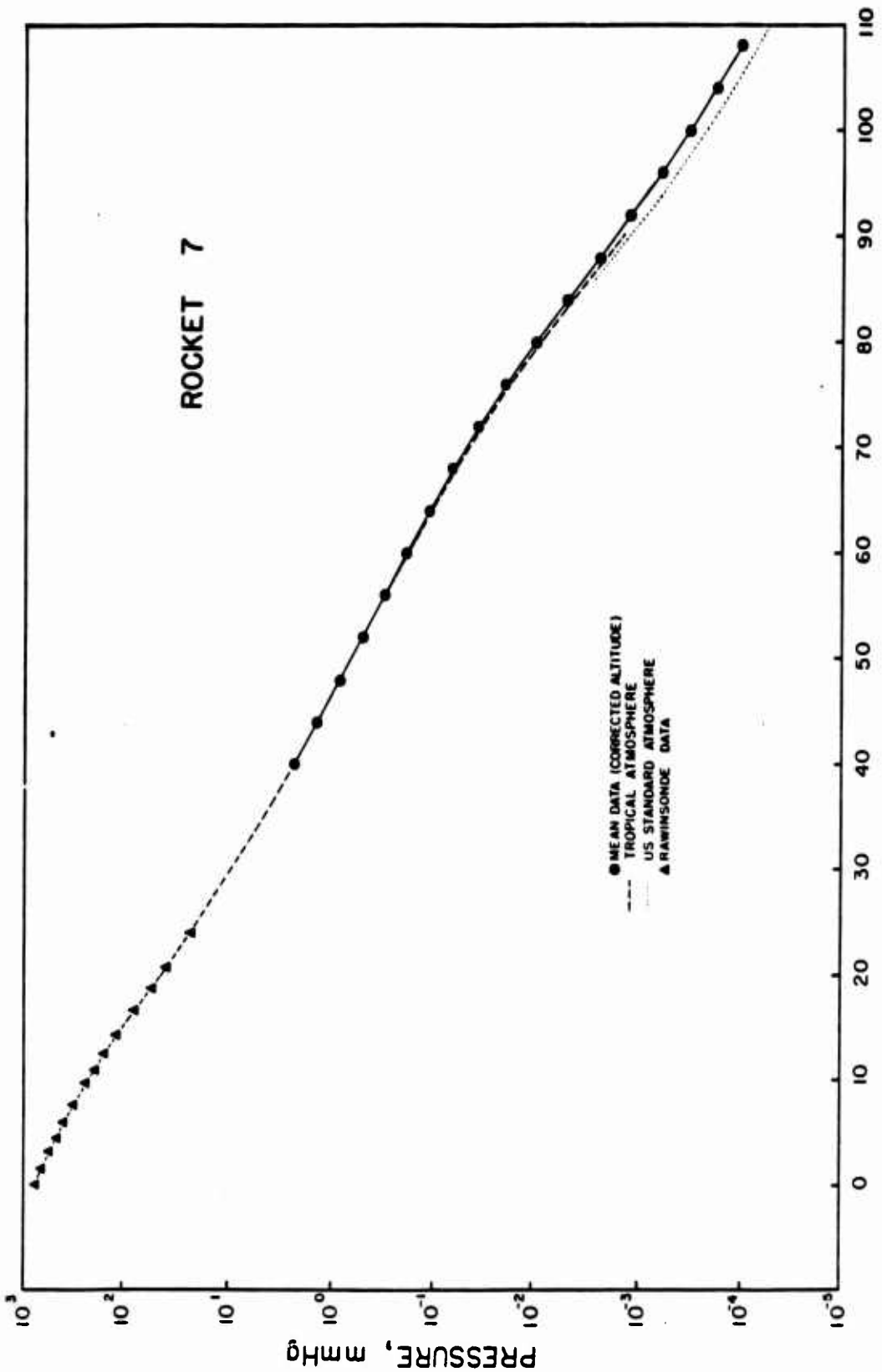

Figure 3.44 Curve of atmospheric pressure versus altitude, Rocket 7.

Pages 224 and 225
deleted.

CHAPTER 4

DISCUSSION

4.1 DENSITY MEASUREMENTS

The results obtained by the five rockets (Rockets 1, 2, 3, 4, and 7) measuring the density of the normal atmosphere will be discussed first. The data are compared with the special Tropical Atmosphere developed for a latitude of 15°. However, this model terminates at 90 km. Above that altitude the data are compared with the U.S. Standard Atmosphere, 1962, which was developed for a latitude of 45°, with the realization that at the latitude of Johnston Island there will be some deviation from this model.

The agreement of the experimental data with the models is, in general, good. However, there are some important differences. The density measured by Rocket 1 (1800 hours, 1 June 1962) agrees well with the Tropical Atmosphere below 60 km (Figure 3.20). Above that altitude the measured density is higher, and between 90 and 100 km the difference with the U.S. Standard is more than fifty per cent.

On Rocket 2 (2230 hours, 19 June 1962) the measured density is slightly higher than the Tropical Atmosphere near 40 km, but lower (by as much as twenty per cent) between 70 and 90 km

(Figure 3.21). Some of the higher altitude measured points were omitted from the figure. The highest altitude at which a measurement was made during the upleg of the flight was 104.4 km, where the density was 1.68×10^{-10} gm/cm^3.

The density on Rocket 3 (2230 hours, 8 July 1962) is close to that of the Tropical Atmosphere below 60 km, but lower (by as much as fifteen per cent) between 60 and 90 km (Figure 3.22). The densities measured by Rockets 2 and 3, at the same time of day nineteen days apart, are surprisingly similar.

The density measured by Rocket 4 (1920 hours, 23 July 1962) is close to that of the Tropical Atmosphere at all altitudes up to 80 km (Figure 3.23). Between 80 and 90 km, it is higher than this model. The measured values are higher than the U.S. Standard Atmosphere up to 103 km. They cross the Standard at that altitude and then become lower.

The results of the above four measurements made during June and July indicate good agreement with the Tropical Atmosphere up to about 60 km. At higher altitudes, in the late afternoon (1800-1920 hours), the densities are higher than the models up to about 105 km but cross to lower values above that altitude. The evening measurements (2230 hours) indicate lower densities than the Tropical

Atmosphere between 60 and 90 km, with values near the U. S. Standard between that altitude and about 96 km above which altitude the measured values become lower than the Standard.

The only other measurement of the normal atmosphere, Rocket 7, was made at 2300 hours, 29 October 1962. Up to 70 km the measured density is very close to that of the Tropical Atmosphere (Figure 3.26). Above that altitude the density is higher than the model. Between 90 and 110 km the density is about twenty-five per cent higher than the U.S. Standard. The observed densities above 70 km are different from those measured at the same time of day in June and July but, with only one measurement, it is not possible to state that this is due to a variation with season.

The results obtained with Rockets 5, 6, 8, and 9 fired shortly after nuclear detonations will now be discussed. First, there was a significant difference between the upleg and downleg data in each case. This is not surprising, since perturbations were induced in the atmosphere, and these were a function both of position and time, each of which varied during the flight of the sphere.

Rocket 5 was fired at H + 10 minutes (2240 hours, 19 October 1962) following Check Mate. On the upleg of the flight, measurements were made between approximately H + 11 and H + 12 minutes

and on the downleg between approximately H + 15 and H + 16 minutes. Figure 4.1 shows the horizontal trajectory of the rocket.

Rocket 6 was fired at H + 15 minutes (0015 hours, 26 October 1962) on Blue Gill Triple Prime. On the upleg of the flight, measurements were made between approximately H + 16 and H + 17 minutes and on the downleg between approximately H + 20 and H +

21 minutes. Figure 4.2 shows the horizontal trajectory of the rocket.

At the altitude of ejection (64 km) the density was fifteen per cent less than the Tropical Atmosphere model. This deviation gradually became less at higher altitudes until it was zero near 84 km (Figure 3.25). Between that altitude and 108 km the measured densities were higher than the models. The increase over the U.S. Standard Atmosphere between 90 and 100 km was approximately thirty per cent. The downleg density was likewise higher than the models between 108 and 80 km. Below 80 km the density was quite close to that of the Tropical Atmosphere.

Rocket 8 was fired at H + 10 minutes (0220 hours, 1 November 1962) on King Fish. Measurements were made on the upleg of the flight between approximately H + 11 and H + 12 minutes and on the downleg between approximately H + 15 and H + 16 minutes.

The horizontal trajectory of the rocket is shown in Figure 4.3. Because of the large horizontal distance of the King Fish detonation from Johnston Island (70.91 km), it was not possible to approach it very closely without sacrificing unduly the altitude reached by the rocket. A slight compromise was made by reducing the launch elevation angle to 83°. Nevertheless, the horizontal distance of the peak of the rocket flight from the detonation point was 49.0 km. It should be noted that in the case of all firings following nuclear detonations the azimuth of the Falling Sphere rocket was less than that of the detonation (about 193° true). This was the result of a structural limit on the launcher, plus the effect of prevailing winds during launch. Each of the Rockets 5, 6, 8, and 9 were fired at as large an azimuth as possible with the available launch equipment.

The density measured between the altitude of ejection (68 km) and 90 km was thirty per cent less than the Tropical Atmosphere model. The deviation, compared with the U.S. Standard Atmosphere, became zero at 103 km (Figure 3.27). The density measured on the downleg agreed with the U.S. Standard between 105 and 90 km. In the range 90 to 65 km the density was approximately fifteen per cent below the Tropical Atmosphere. Between 65 and 38 km the de-

viation steadily diminished to zero.

Rocket 9 was fired at H + 4 minutes (2134 hours, 3 November 1962) after the Tight Rope detonation. It was planned to be a normal Nike-Cajun flight. However, the Cajun motor did not ignite. This resulted in a normal ballistic flight, but with considerably reduced velocity and peak altitude. Because of the low detonation altitude of Tight Rope this was a fortunate occurrence, and the data obtained is probably more interesting than would have been obtained with a flight to the normal peak altitude. Measurements were made between H + 4 min 52 sec and H + 6 min 20 sec. The horizontal trajectory of the rocket is shown in Figure 4.4

Note the sharp deviation caused in the sphere trajectory as it passed near the location of the fireball. This is a conspicuous effect of the detonation. Figure 4.5 contains a plot of the sphere altitude as a function of time after launch of the rocket.

Figure 3.28 shows the measured densities compared with the Tropical Atmosphere and Rawinsonde measurements made shortly before the nuclear test.

Devia-

tions of this type have been observed at very low altitudes with previous flights by the University of Michigan. On the other hand, it is possible that the apparently large densities are due to additional accelerations received by the sphere due to air motions induced by the fireball. Note that these spurious values occurred in the region where the sphere trajectory was sharply deviated.

4.2 ATMOSPHERIC TEMPERATURE

Atmospheric temperatures deduced from density data for Rockets 1, 2, 3, 4, and 7 are plotted in Figures 3.29, 3.30, 3.31, 3.32, and 3.35, respectively. These constitute the measurements of the temperature of the normal atmosphere. The temperatures deduced from the upleg and downleg data for Rocket 1 are slightly different. Presumably, the mean of these data gives the best measurement of the ambient at the time. Note that the temperature minimum, which lies between 80 and 90 km in the models, is found to be higher in altitude, lying between 90 and 100 km, and lower in value, approximately 176.5 °K. This also results in changes in the temperature gradients above and below the tempera-

ture gradients above and below the temperature minimum. In addition, there are differences between the observed temperatures and models near the temperature maximum at 50 km. The observed Rawinsonde temperatures were relatively close to those of the Tropical Atmosphere model.

The measurements of Rocket 4 were made at approximately the same time of day (late afternoon) and year (June-July) as those of Rocket 1, and the temperatures are surprisingly similar. The high-altitude minimum again occurs between 90 and 100 km, with a value of 165°K. The temperature maximum at 51 km is very close to the value of the Tropical Atmosphere.

The measurements of Rockets 2 and 3 were also made during June-July, but later in the evening (2230 hours). The upper three temperatures of Rocket 3 should be corrected as follows. The temperatures at 98 km should be lowered by 6°K to 204.7°K, at 94 km by 1.3°K to 190.9°K, and at 90 km by 0.3°K. The temperature profiles from the two measurements are very similar to each other and the Tropical Atmosphere. The low temperatures between 90 and 100 km observed in the late afternoon have disappeared. However, the temperatures below 85 km tend to be lower in the evening than in the late afternoon.

The other measurement of the normal atmosphere was Rocket 7 (2300 hours, 29 October). The temperatures are similar to those of Rockets 2 and 3 measured at the same time of day but in June-July. However, in the range of measurement the temperature varied from 5 to 15°K warmer.

The temperatures measured after nuclear detonations are shown in Figures 3.33, 3.34, 3.36, and 3.37. The deviations of the temperatures from the U.S. Standard Atmosphere and the Tropical Atmosphere, respectively, are shown in Tables 4.1, 4.2, 4.3, and 4.4.

Below 80 km the temperatures measured by Rocket 5 are almost identical with those of Rocket 7, which is used for comparison. However, above that altitude, there was a temperature increase ranging from 5° to 50°K at early times after the detonation. At later times (downleg) this temperature increase had largely disappeared. That the perturbation is restricted to above is reasonable when it is remembered that the detonation took place at an altitude of

The temperatures measured by Rocket 6 show an increase in temperature between 35 and 50 km and indicate the atmosphere above 70 km appeared to have been raised by the detonation.

Some settling of the atmosphere back toward normal between the time of the upleg and downleg curves can be seen in Figure 3.34.

Relatively little change in the temperature was detected by Rocket 8. This is probably due to the comparatively large distance that this rocket was away from the detonation point.

Rocket 9 passed very close to the Tight Rope detonation point. Thus, large perturbations would be expected and were observed. It is difficult to be sure what the actual temperature was near the fireball.

Taking into account the trajectory of the sphere, relative to the fireball, it is believed that the temperature distribution obtained with T_{M_r} equal to 450°K is the most accurate solution.

4.3 PRESSURE RESULTS

The pressure measurements of the normal atmosphere are shown in Figures 3.38, 3.39, 3.40, 3.41, and 3.44. The data are compared with the Tropical Atmosphere to 90 km and with the U.S. Standard Atmosphere between approximately 85 and 110 km.

The pressures measured by Rocket 1 are slightly higher than the models throughout the range of measurement. The biggest differences occur between 80 and 95 km where the increase lies between thirty and forty per cent. The shape of the pressure curve determined by Rocket 4 is similar to that of Rocket 1, but the pressures are lower. The pressures of Rocket 4 agree closely with those of the models except for a small increase ranging from five to fifteen per cent, between 75 and 95 km.

The pressure curves obtained from Rockets 2 and 3 are similar to each other, but different in shape from those of Rockets 1 and 4. The pressures of Rockets 2 and 3 are the same as the Tropical Atmosphere at low altitudes (up to about 55 km) but become less at

higher altitudes. The reduction is fifteen per cent for Rocket 2 at 90 km and eight per cent for Rocket 3 at 70 km.

The final measurement of the natural atmosphere was made by Rocket 7, at approximately the same time of day as Rockets 2 and 3 but later in the year. The Rocket 7 pressure curve is similar in shape to those of Rockets 2 and 3, but there are differences in the numerical values. Again, at altitudes up to 55 km the pressures agree with the Tropical Atmosphere, but above that altitude the pressure becomes relatively higher with increasing altitude. The increase, relative to the U.S. Standard Atmosphere, is forty per cent at 108 km.

Rocket 5 measured the atmospheric pressure a short time after the Check Mate detonation.

The pressures measured after Blue Gill Triple Prime are shown in Figure 3.43. At the altitude of ejection the pressure was less than the Tropical Atmosphere. The reduction became

less until it was zero at 84 km. Between that altitude and 110 km the measured pressures were higher than the models. The downleg data was similar to the upleg data down to 80 km. Between that altitude and 40 km it was close to the Tropical Atmosphere. Below 45 km the measured pressures were slightly lower than the model. Any perturbations produced by the nuclear detonation were small in this case, but it should be remembered that the measurements were made at relatively late times (16 to 21 minutes) after the nuclear detonation.

Rocket 8 measured the atmospheric pressure following King Fish (Figure 3.45). The pressure at the altitude of ejection was about forty per cent less than the Tropical Atmosphere. This reduction slowly became less at higher altitudes until it was about ten per cent (compared with the U. S. Standard Atmosphere) at 103 km. The pressure measured on the downleg was the same as on the upleg at 103 km. It increased relatively until it was the same as the U. S. Standard at 90 km. Between 90 and 35 km the pressure varied from ten to twenty per cent below the Tropical Atmosphere. These pressure deviations are similar to those in the density.

It is interesting to note that for Rocket 6 little change was

observed in the pressure, but significant temperature changes were detected. On the other hand, for Rocket 8 important pressure changes were detected, but little change in the temperature was observed. For Rocket 5 significant changes in both temperature and pressure were measured.

The pressures measured by Rocket 9 following Tight Rope, are shown in Figure 3.46.

TABLE 4.1 TEMPERATURE DEVIATIONS, ROCKET 5

Temperature Deviations

Z, km	T_M, °K	ΔT_{MS}, °K *	ΔT_{MT}, °K **
	Upleg Data		
110.0	285.7	+25.0	
106.0	272.7	+32.0	
98.0	252.2	+47.5	
90.0	223.3	+42.6	+39.1
86.0	199.4	+18.7	+15.2
74.0	207.4	+ 3.3	+ 2.2
66.0	226.2	- 9.2	- 6.3
	Downleg Data		
110.0	260.7	0.0	
106.0	255.5	-15.2	
94.0	210.8	+18.1	
90.0	212.7	+32.0	+28.5
86.0	199.0	+18.3	+14.8
74.0	209.4	+ 5.3	+ 4.2
66.0	243.8	+ 8.4	+11.3
54.0	272.0	+ 4.4	+ 6.8
34.0	239.0	- 5.3	- 2.1

* ΔT_{MS} is the temperature deviation from the U.S. Standard Atmosphere, 1962

** ΔT_{MT} is the temperature deviation from the Tropical Atmosphere model.

TABLE 4.2 TEMPERATURE DEVIATIONS, ROCKET 6

Temperature Deviations

Z, km	T_M, °K	ΔT_{MS}, °K	ΔT_{MT}, °K
	Upleg Data		
111.0	270.0	0.0	
107.0	220.0	-25.7	
103.0	196.1	-29.6	
95.0	189.3	- 6.4	
90.0	191.0	+10.3	+ 6.8
83.0	203.6	+22.9	+19.4
75.0	215.6	+15.4	+13.9
71.0	223.1	+ 7.3	+ 7.8
63.0	249.1	+ 2.0	+ 6.4
	Downleg Data		
111.0	270.0	0.0	
107.0	220.0	-25.7	
103.0	196.1	-29.6	
95.0	189.3	- 6.4	
90.0	191.0	+10.3	+ 6.8
83.0	191.4	+10.7	+ 7.2
75.0	209.7	+ 9.5	+ 8.0
71.0	222.0	+ 6.2	+ 6.7
63.0	246.4	- 0.7	+ 3.7
47.0	277.6	+ 7.9	+ 7.4
35.0	256.1	+19.6	+12.8

TABLE 4.3 TEMPERATURE DEVIATIONS, ROCKET 8

Temperature Deviations

Z, km	T_M, °K	ΔT_{MS}, °K	ΔT_{MT}, °K
	Upleg Data		
102.5	220.7	- 3.2	
98.5	200.5	- 6.1	
94.5	195.2	+ 0.6	
90.5	199.2	+18.5	
86.5	192.8	+12.1	+ 8.6
78.5	196.1	+ 9.6	+ 6.4
74.5	208.9	+ 6.8	+ 5.5
66.5	218.7	+14.7	-12.0
	Downleg Data		
102.5	220.7	- 3.2	
98.5	184.4	-22.2	
94.5	175.8	-18.8	
90.5	181.3	+ 0.6	
86.5	182.4	+ 1.7	- 1.8
78.5	195.8	+ 9.3	+ 6.1
74.5	204.2	+ 2.1	+ 0.8
66.5	229.0	- 4.4	- 1.7
62.5	242.5	- 6.6	- 1.9
54.5	262.2	- 4.4	- 2.1
46.5	253.6	-14.7	-14.2
36.5	256.7	+16.1	+10.2

TABLE 4.4 TEMPERATURE DEVIATIONS, ROCKET 9

Temperature Deviations

Z, km	T_M, °K	ΔT_{MS}, °K	ΔT_{MT}, °K
	Downleg Data (T_{M_r} = 350.0 °K)		
21.6	350.0	+131.8	+136.4
19.6	376.4	+159.7	+171.2
17.6	320.3	+103.6	+119.1
15.6	275.9	+59.2	+76.0
	Downleg Data (T_{M_r} = 450°K)		
21.6	450.0	+231.8	+236.4
19.6	467.6	+250.9	+262.4
17.6	384.2	+167.5	+183.0
15.6	319.7	+103.0	+119.8

Pages 245 through 249
deleted.

CHAPTER 5

CONCLUSIONS AND RECOMMENDATIONS

The four measurements of the properties of the normal atmosphere (density, temperature, and pressure) made during June and July indicate a diurnal variation, within the altitude range 35 to 110 km. One measurement of the normal atmosphere made in October suggests that there is a seasonal variation, but more measurements are required to confirm this. The preceding results are of considerable value for the accurate analysis of shock propagation, X-ray deposition,and other data obtained during Fish Bowl.

Measurements were made shortly after four high-altitude nuclear detonations. Large changes in the atmospheric properties were detected after Check Mate and very large changes after Tight Rope. Smaller perturbations were detected after Blue Gill and King Fish. Although the changes were complicated, they are primarily due to heating of the atmosphere. Most of the variation in the effects was due to differences in the time of measurement and location of the rocket relative to the fireball. These are summarized in the following table.

Event	Time of Measurement (minutes)	Approx. Distance from Detonation (km)
Check Mate	H + 11 → 12, H + 15 → 16	75
Blue Gill	H + 16 → 17, H + 20 → 21	45
King Fish	H + 11 → 12, H + 15 → 16	50
Tight Rope	H + 5 → 6	0.6

The reason for the very large deviation after Tight Rope was obviously due to the measurement being made very close to the fireball at an early time after the detonation. The reason for the large perturbation measured after Check Mate is less obvious. However, it is believed that the persistent perturbation was due to the large amount of debris that was formed in this test and deposited in the altitude region

It is recommended that in future high-altitude tests a more complete measurement of the post-detonation properties of the atmosphere be obtained by firing Falling Sphere rockets at approximately the following times:

H - 60 minutes

H - 1 minute

H + 5 minutes

H + 15 minutes

REFERENCES

1. L. M. Jones and F. L. Bartman; "A Simplified Falling Sphere Method for Upper Air Density"; Engrng. Rsch. Inst., Univ. of Mich., Ann Arbor, Mich.; AFCRC-TN-56-497, Jun 56. (Uncl.)
2. John W. Peterson; "Analytical Study of the Falling Sphere Experiment for Upper Air Density Measurement"; Engrng. Rsch. Inst., Univ. of Mich., Ann Arbor, Mich.; AFCRC-TN-56-870, Nov 56. (Uncl.)
3. J. W. Peterson, H. F. Schulte and E. J. Schaefer; I. "A Simplified Falling Sphere Method for Upper Air Density". II. "Density and Temperature Results from Eight Flights"; Engrng. Inst. Univ. of Mich., Ann Arbor, Mich.; AFCRC-TN-59-263 May 59. (Uncl.)
4. J. W. Peterson, D. A. Robinson and H. F. Schulte; "Falling Sphere Instrumentation Development"; Univ. of Mich. Rsch. Inst., Ann Arbor, Mich.; AFCRC-TR-60-247, Feb 60. (Uncl.)
5. L. M. Jones and J. W. Peterson; "Upper Air Densities and Temperatures Measured by the Falling Sphere Method"; Univ. of Mich. Rsch. Inst., Ann Arbor, Mich.; AFCRL-803, Feb 61. (Uncl.)
6. Obed C. Haycock; "Improvements in the Falling Sphere Instrumentation"; Sc. Rpt. No. 1, Upper Air Rsch. Lab. Univ. of

Utah, Salt Lake City, Utah; AFCRC-TR-60-233, Feb 60.(Uncl.)

7. John Bickford; "Development of a Transit-Time Accelerometer"; Final Engrng. Rpt., Raymond Engrng. Lab., Inc., Middletown, Conn.; Cont. No. AF19(604)-7370, Apr. 61.(Uncl.)

8. V. C. Liu; "On the Aerodynamic Drag of Sphere"; Sc. Rpt. No. 1; ORA Project 02885; Oct 61, Cont. AF 19(604)-5477; Dept. of Aeronautical and Astronautical Eng., Univ. of Mich., Ann Arbor, Mich.(Uncl.)

9. Jerome Aroesty; "Sphere Drag in the Low Density Supersonic Flow"; Tech. Rpt. No. HE-150-192, Jan 62; Inst. of Engrng. Rsch., Univ. of Calif., Berkeley, Calif.(Uncl.)

10. A. Court, A. J. Kantor, A. E. Cole; "Supplemental Atmospheres"; Rsch Note, AFCRL-62-899, Sept. 62; ARCRL, Bedford, Mass.(Uncl.)

11. "U. S. Standard Atmosphere, 1962" K. S. W. Champion, W. J. O'Sullivan and S. Teweles, Editors; U. S. Govt. Printing Office, Wash., D. C.(Uncl.)

12. K. S. W. Champion and R. A. Minzner; "Revision of United States Standard Atmosphere, 90 to 700 Kilometers", Reviews of Geophysics, Vol. 1, No. 1, pages 57-84, February, 1963. (Uncl.)

Pages 255 through 256
deleted.